



Physique formelle de spin diagrammatique

Richard East

► To cite this version:

Richard East. Physique formelle de spin diagrammatique. Physique mathématique [math-ph]. Université Grenoble Alpes [2020-..], 2022. Français. NNT: 2022GRALM004 . tel-03719945

HAL Id: tel-03719945

<https://tel.archives-ouvertes.fr/tel-03719945>

Submitted on 11 Jul 2022

HAL is a multi-disciplinary open access archive for the deposit and dissemination of scientific research documents, whether they are published or not. The documents may come from teaching and research institutions in France or abroad, or from public or private research centers.

L'archive ouverte pluridisciplinaire **HAL**, est destinée au dépôt et à la diffusion de documents scientifiques de niveau recherche, publiés ou non, émanant des établissements d'enseignement et de recherche français ou étrangers, des laboratoires publics ou privés.

THÈSE

Pour obtenir le grade de

DOCTEUR DE L'UNIVERSITÉ GRENOBLE ALPES

Spécialité : Mathématiques et Informatique

Arrêté ministériel : 25 mai 2016

Présentée par

Richard EAST

Thèse dirigée par **Rachid ECHAHED**, Chercheur
et co-encadrée par **Dominic HORSMAN**

préparée au sein du **Laboratoire Laboratoire d'Informatique de Grenoble**
dans l'**École Doctorale Mathématiques, Sciences et technologies de l'information, Informatique**

Physique formelle de spin diagrammatique

Formal diagrammatic spin physics

Thèse soutenue publiquement le **7 mars 2022**,
devant le jury composé de :

Monsieur ALEKS KISSINGER

Professeur assistant, University of Oxford, Rapporteur

Monsieur ETERA LIVINE

Directeur de recherche, CNRS DELEGATION RHONE AUVERGNE,
Rapporteur

Monsieur MNACHO ECHEMIM

Professeur des Universités, GRENOBLE INP, Président

Monsieur SIMON PERDRIX

Directeur de recherche, INRIA CENTRE NANCY-GRAND-EST,
Examinateur

Monsieur NICOLAS LAFLORENCIE

Directeur de recherche, CNRS DELEGATION OCCITANIE OUEST,
Examinateur



Formal Diagrammatic Spin Physics



Richard David Petrak East

Université Grenoble Alpes

Thèse présentée pour obtenir le grade universitaire de

Docteur

Decembre 2021

Acknowledgements

Mine has been a strange PhD, partitioned as it was by the pandemic, as was the case for many students of this generation. There has also been the additional peculiarity of my long suffering supervisor Dominic finding himself almost immediately on the diseases' spread to France struck down by long COVID and finding himself repeatedly hospitalised over the last 2 years. Before all else I would like to wish him a steadier recovery than fate seems to have dealt him so far. I would also like to thank him for his initial guidance during my first year and forgiveness for having gone so thoroughly out of scope of the initial project.

Given the difficulties of finding myself without guidance and, in terms of the field I work, academic isolation here in Grenoble I am perhaps more indebted than usual to the consideration, kindness, and above all patient email exchanges, of number of external academics. Of most note are Adolfo Grushin and Pierre Martin-Dussaud whose respective research areas form the content of this thesis. To the former I am indebted for much after those initial 10 minutes of office conversation when I first proposed what must have seemed an unlikely effort to rewrite tensor network states and his suggestion of the analysis of the AKLT state. I have since become some sort of quasi-adoptive element of his research group, dragging in bizarre diagrams like a stray-cat grateful for a splash of milk might drag in the odd mouse. I am forever bringing with me strange questions wrapped in strange techniques accompanied by scribbles. To the latter I owe the patient conversations and email exchanges stemming from what began for him as an out of the blue email query about the structure of Yutsis diagrams alongside some crumbs of a ZXH-ification of spin-networks that were technically wrong but somehow in the correct direction. In addition to these two I owe a particular debt to Nick Chancellor and John Van de Wetering who at different stages in my PhD have been very generous with their time in working with me to tackle various technical and conceptual considerations that have subsequently emerged as a diagrammatic analysis of $SU(2)$. I would also like to thank Ana Belén Sainz for those considerate Zoom conversations where she checked that in Dom's absence I was not utterly lost and was as approximate to happy and sane as one could expect during one the earths more tedious plagues. In addition I must also mention Niel de Beaudrap with whom I have discussed a number of topics that did not make it into this thesis and who has always been able to offer various bits of advice both professional and technical. I also want to mention Katee Driscoll, Marios Christodoulou, Bob Coecke, Stefano Gogioso, Fabrizio Genovese, Cole Comfort, Maria Maffei, Cristian Mariani, Rachid Echahed, Mehdi Mhalla and Ashutosh Goswami who have all contributed in some way to my academic work in one way or another. I beg forgiveness for any others I've forgotten.

Of course, in the abstract, academia makes for a cold mistress, she will not love you back: without the friends I've made along the way this PhD would barely be worth doing at all. I would like to thank all of them, those close by, and those whom, I regret to confess, I cannot see them nearly as much as I would like: Strewn as I, and they, have been, across nations and continents. I also would like to thank Mum, Dad, Tim, Nana, and Papy who I know would have welcomed me back home to Coventry should this have all gone wrong and who ensure that if all else fails I still have an actual home somewhere. I, of course, also must think of that cup, perfect for tea, which saw me through the pandemic.

I also cannot finish without acknowledging the école doctorale and associated PhD administration for their assiduous efforts to make themselves easily the most difficult aspect of obtaining a doctorate in France. Their hard work for the last few years in providing a problem for every solution has always kept me alert and on my toes to ensure that I am emotionally and financially ready for the various disasters that would not exist if not for their tireless work. You have secured a special place in my heart.

Abstract

Diagrams are ubiquitous in physics and have catalysed progress on numerous occasions. From tensor networks and quantum circuits to Feynman diagrams, there are few areas of physics that don't employ some informal pictorial reasoning. These diagrams represent the underlying mathematical operations and aid physical interpretation, but cannot generally be computed with directly. In this thesis the ZXH-calculus, a graphical language based on the ZX-calculus, is offered as a prototype for a formal diagrammatic calculational tool for theoretical physics involving spin. This extends the ZXH-calculus (and more broadly the ZX family of calculi to which it belongs) beyond its traditional domain which has largely been dominated by quantum computing. In order to do this the spin lattices taken from condensed matter physics are studied. It is also shown how spin-networks of the form often seen as the state-space of loop quantum gravity (LQG) can be diagrammatised along with operators acting on them.

To achieve this a diagrammatic form of $SU(2)$ representation theory is outlined. Following this in condensed matter a number of results are shown. The 1D AKLT state, a symmetry protected topological state, is expressed in the ZXH-calculus by developing a representation of spins higher than $1/2$ within the calculus. By exploiting the simplifying power of the ZXH-calculus rules it is shown how this representation straightforwardly recovers the AKLT matrix-product state representation, the existence of topologically protected edge states, and the non-vanishing of a string order parameter. Extending beyond these known properties, the diagrammatic approach also allows one to analytically derive that the Berry phase of any finite-length 1D AKLT chain is π . In addition, an alternative proof that the 2D AKLT state on a hexagonal lattice can be reduced to a graph state, demonstrating that it is a universal quantum computing resource. Continuing on the theme of condensed matter it is then shown how one can build 2D higher-order topological phases diagrammatically, which is used to illustrate a symmetry-breaking phase transition.

Turning to LQG the first step is the analysis of Yutsis diagrams, a standard graphical calculus used in quantum chemistry and quantum gravity, which captures the main features of $SU(2)$ representation theory. Second, it is shown how it embeds within Penrose's binor calculus. The two are then rewritten as ZXH-diagrams. In the process we show how the $SU(2)$ invariance of Wigner symbols is trivially provable in the ZXH-calculus. Additionally, we show how we can explicitly diagrammatically calculate $3jm$, $4jm$ and $6j$ symbols. It has long been thought that quantum gravity should be closely aligned to quantum information theory. In this paper, we present a way in which this connection can be made exact, by writing the spin-networks

of loop quantum gravity in the ZX-diagrammatic language of quantum computation. Finally after outlining the motivation for considering spin-networks as the quantisation of space, the geometric operators are discussed, and in specific cases diagrammatic versions of the operators are provided. More generally what is done here shows a route by which LQG can be interpreted in quantum informational terms by rewriting its kinematical states as networks of qubits in ZXH.

In total these results demonstrate that the ZXH-calculus is a powerful language for representing quantum systems and even allows for the computation on physical states entirely graphically. Within condensed matter it is hoped this will pave the way to develop more efficient many-body algorithms and giving a novel diagrammatic perspective on quantum phase transitions. In LQG it is hoped this re-imagining of its state space will spur further integration of quantum information and gravity.

Contents

1	Introduction	1
2	Introduction to diagrammatic Calculi	5
3	Diagrammatic representation theory of $SU(2)$	13
3.1	Constructing irreducible representations of $SU(2)$	13
3.2	Diagrammatic construction of spin-spaces	15
3.3	Diagrammatic Lie algebra representation theory	21
4	Diagrammatic reasoning for condensed matter physics	27
4.1	Introduction to the relevant concepts in condensed matter physics	27
4.1.1	The 1D AKLT state	32
4.2	The 1D AKLT state in the ZXH-calculus	34
4.2.1	Aside on the form of the diagrams for the 1D AKLT state	39
4.2.2	Quantized Berry phase	41
4.3	The 2D AKLT state as a universal resource for quantum computing	45
4.4	Crystal symmetries and transitions in ZXH	53
4.5	Summary of Condensed Matter Results	57
5	Diagrams for Spin-networks and Wigner symbols	59
5.1	From Yutsis diagrams to spin-networks	59
5.1.1	Recoupling theory	60
5.1.2	Yutsis diagrams	64
5.1.3	Penrose diagrams	68
5.1.4	Spin-networks	71

5.2	The translation to ZXH	73
5.2.1	Links	74
5.2.2	Trivalent nodes	76
5.2.3	Examples	80
5.2.4	Higher Wigner invariants and the question of quantum computation	88
5.2.5	The ZXH Spin-network	89
5.3	Motivating operators on spin-networks	90
5.4	Operators on spin networks	93
5.5	Diagrammatic Spin network operators	95
5.5.1	Quantised Area	95
5.5.2	Quantised Volume	97
5.6	Orderless information conception of space-time	103
5.7	Summary of Yutsis Diagram and Spin-Network Results	106

6	Conclusion	109
----------	-------------------	------------

Appendices

A	Graph states	113
B	Spin matrices and representation theory	115
C	Additional diagrammatic proofs	119
C.0.1	Additional proofs for the AKLT Berry Phase calculation	119
C.0.2	CSWAP POVM calculations	120
C.0.3	Removing π phases from a graph state	122
D	Overview of graphical rewrite rules	123
E	Sage verification code	125
F	Differentiable Manifolds	127

G A brief note on curvature and its link to the Einstein field equations	131
G.1 Einstein's field equations and the Einstein-Hilbert action	133
H ADM splitting	135
I Introduction to $SU(2)$ representation theory	141
I.1 Introduction to representation theory	141
I.1.1 Introductory concepts and Lie groups	141
I.1.2 Lie Groups and Lie Algebras	142
I.1.3 Representations	145
I.1.4 Compositions of representations	147
I.1.5 Important properties for the representation of $SU(2)$	149
I.2 Importance of $SU(2)$ in physics	150
Bibliography	153

1

Introduction

The objective of this thesis is ultimately to advocate for formal diagrammatic methods in physics. There are, in physics, a wealth of diagrammatic representations of physical systems, in the sense that there are pictures that to a greater or lesser extent seek to capture the essential nature of some underlying physical system. Examples of these will be actively discussed in this thesis like tensor network diagrams, Penrose diagrams, or Yutsis diagrams [1]. Some will not be such as Feynman diagrams[2] for example. When one writes a diagram of any of the kinds just mentioned one is engaged in a kind of linguistic activity. To speak very broadly when one draws a diagram there is a ‘thing’ out there in the world or, as is more typical in theoretical physics, that itself is a mathematical representation of a physical system, that one seeks to represent. This ‘thing’ is complex but we wish to discuss it: So we create symbols that relate to it’s attributes. We then dictate relations between these symbols that themselves enter into the symbolic structure. Before long one is discussing equivalences of things based on their representation with these symbols. In theoretical computer science and logic there are some key terms that help us specify the details of what is described here: universality, soundness, completeness. When we create symbols and define relations of equivalence between them we have created a formal language. Keeping the distinction in our minds between the thing and its representation in the language, we say that the language is universal if all the things we wish to discuss have a representation in our language. We say the language is sound if all the equivalences it proposes between representations are true in the sense that they hold for the

things represented. We say the language is complete if every true equality between the things we want to represent exists as an equality in the language. Every diagram described above can be characterised as, at best, a non-universal, sound, incomplete language.

The ZX calculus [3, 4] and the associated diagrammatic languages in the form of ZW, ZH, and ZXH which is what I work with here, are all examples of universal, sound, complete languages. These are languages for qubit quantum mechanics or more formally for all $\mathbb{C}^{2n} \mapsto \mathbb{C}^{2m}$ maps. It is in this sense I use the term formal diagrams. A universal, sound, and complete language can be used to reason mathematically in the place of its referent. Concretely with the ZX calculus instead of working with linear algebra one uses the diagrams of the calculus and manipulate them via rewrites in the language to derive equivalences. One does linear algebra graphically [5]. These methods have found application in quantum computation, with results in measurement-based quantum computation [6, 7, 8], topological quantum computation [9, 10, 11, 12], quantum error correction [13, 14] and quantum circuit compilation and optimisation [15, 16, 17, 18, 19, 20].

These calculi were first introduced in 2008 a mere 13 years prior to the writing of this thesis. This is sufficient time for some post-docs to become senior researchers, perhaps the odd professor, and their PhDs to rise the ranks getting a few PhD students of their own. Along the way perhaps they gather a few other converts in academia and in industry. Unsurprisingly however, its breadth of application is very much tied to the background of those who originated and developed the calculus: computer science. Typically the calculi are used for describing, developing, and optimising quantum algorithms and the devices that may one day run them. As will become apparent in this thesis, though computation and algorithmic perspectives are a natural way to perceive ZX diagrams, what is most of interest to me is the diagrammatic language as a means to discuss quantum information. It is through this perspective I have sought to make some of the first forays with these techniques into theoretical and mathematical physics proper, divorced of any direct ambition to think in terms of computation or algorithms which form the *raison d'être* for the computer science community. That said this connection is greatly facilitated by the languages history and practicality for such endeavours and so what is written here could easily form the bridge for one wishing to bring tools from the computer science world into theoretical and mathematical physics.

Regarding the application to physics the focus in this thesis is on describing physical systems based around the notion of spin. Spin is a primordial concept in physics which I articulate as orderless quantum information and will later advocate as being more primal than qubits even. The areas focussed on will be condensed matter physics where spin lattices are an enormous field of interest and the spin-recoupling theory as described by Yutsis, which finds application in fields as removed as quantum chemistry, or Penrose's binor calculus [21] and associated spin-networks which find use in the field of Loop Quantum Gravity (LQG). In order to facilitate description and calculation in these fields it is necessary to create a formal diagrammatic description of $SU(2)$ representation theory for both the Lie group and algebra structure. As such this is also contained in this thesis.

The structure of this thesis begins with an introduction to the ZXH calculus. There is then an introduction to representation theory with a strong focus on the elements important for the analysis of $SU(2)$. The following section then builds on the previous two introductory sections to show how we can describe spin systems in terms of ZXH diagrams. It will be shown that one can use symmetric projectors on n spin- $\frac{1}{2}$ wires, which are a basic element in ZXH, to create spin- $\frac{n}{2}$ spaces. It is then shown how one can discuss the associated Lie algebra of $SU(2)$ diagrammatically with constructions demonstrating how algebra elements acting on the spin- $\frac{1}{2}$ space can be 'raised' to acting on the space of spin- $\frac{n}{2}$. After this the diagrammatic analysis of spin is applied to condensed matter physics where a number of things are achieved. Firstly the well known 1D AKLT [22] state is represented formally as a ZXH diagram and properties such as it dilute anti-ferromagnetism are shown via diagrammatic calculation. We then show the novel result that that Berry phase [23] of the 1D AKLT state is π for all chain lengths, which was previously only known in the thermodynamic limit. Following this we show how one can construct the 2D AKLT state. From this it is demonstrated that one can diagrammatically see how the 2D honeycomb AKLT state [24] can be used as a resource for measurement based quantum computing in the sense that it can be reduced, given sufficient lattice sizes, to a cluster state. Finally it is shown how one can formally represent a lattice symmetry breaking transition as a single parametrised ZXH diagram.

The section after this then applies the diagrammatic analysis of spin in a different direction. The Yutsis diagrams of quantum chemistry (used to represent Wigner symbols [1, 25] for the

analysis of spin recoupling) and Penrose's Binor calculus are simultaneously diagrammatised and a ZXH approach to the description of Wigner symbols and $SU(2)$ invariant functions is presented. The comparison of Yutsis diagram and binor calculus is itself of some originality in the concreteness of its presentation. This ZXH analysis of Wigner symbols is in turn used to provide an articulation of spin-networks of the kind seen in loop quantum gravity (LQG)[26] in terms of ZXH as they can be seen as a tensor network generated by Wigner symbols. There is some discussion on the implications of an informational description of spin-networks taken, as they are in LQG, as the quantised spatial geometry. Finally some speculative analysis is presented on the creation and application of diagrammatic geometric algebra operators of the kind interpreted as observables of 3D space in the kinematics of LQG.

2

Introduction to diagrammatic Calculi

The ZX calculus is a diagrammatic language for qubit quantum mechanics - it represents operators as diagrams and has rules for manipulating these diagrams to equate them to other operators. To be more specific it is a sound and complete language for linear maps of the form $\mathbb{C}^{2n} \mapsto \mathbb{C}^{2m}, n, m \in \mathbb{Z}$ that is to say every equality between the diagrams represents a valid equality between the linear maps (soundness) and that every equality between the linear maps is demonstrable in the language as an equality between the diagrams that represent them (completeness). It can also be viewed as a dagger compact category, or more explicitly spelled out, it is a category which contains a symmetric monoid, is compact closed and comes equipped with a dagger map.

From a more practical angle the compositional structure of ZX diagrams is as follows: The monoidal product (tensor product for Hilbert spaces) of two diagrams is represented by placing one diagram above the other. To compose one ZX diagram followed by another one, we place the two diagrams side by side horizontally and connect the outputs of the first diagram on the left to the inputs of the second right-hand diagram. Concretely all ZX diagrams can be formed from ‘wires’ and ‘spiders’. Wires entering on the left of a diagram are inputs and those on the right are outputs.

The spiders are linear operators that have any integer number of input or output wires. They come in two varieties, the Z-spiders which are green dots and X-spiders which are red dots.

They can both be labelled by a phase $\alpha \in \mathbb{R}$:

$$\text{Diagram with green circle and } \alpha := |0 \cdots 0\rangle\langle 0 \cdots 0| + e^{i\alpha} |1 \cdots 1\rangle\langle 1 \cdots 1| \quad (2.1)$$

$$\text{Diagram with red circle and } \alpha := |+\cdots+\rangle\langle +\cdots+| + e^{i\alpha} |- \cdots -\rangle\langle -\cdots-| \quad (2.2)$$

Note that if viewed in monochrome or by those with green and red colour blindness, Z-spiders are the lighter shaded of the two. As described more abstractly above, ZX-diagrams are constructed by composing these spiders and the wires sequentially, which corresponds to the composition of linear maps, and in parallel, which corresponds to the tensor product of linear maps. As a special case of these diagrams there are those with no inputs, which represent (unnormalised) states, and diagrams with no disconnected wires, which represents complex scalars.

From these spiders we can immediately give some familiar quantum states and unitary maps in terms of the ZX-calculus

$$\text{Diagram with green circle} = |0\rangle + |1\rangle = \sqrt{2} |+\rangle \quad (2.3)$$

$$\text{Diagram with red circle} = |+\rangle + |-\rangle = \sqrt{2} |0\rangle \quad (2.4)$$

$$\text{Diagram with green circle and } \alpha = |0\rangle\langle 0| + e^{i\alpha} |1\rangle\langle 1| = Z_\alpha \quad (2.5)$$

$$\text{Diagram with red circle and } \alpha = |+\rangle\langle +| + e^{i\alpha} |- \rangle\langle -| = X_\alpha \quad (2.6)$$

Note that if there is no α in the spider as in state preparations (2.3) and (2.4) we take this to mean α is zero. With the X and Z rotations to hand if we take $\alpha = \pi$ in (2.5) and (2.6) we have the Pauli matrices:

$$\text{Diagram with red circle and } \pi = Z \quad \text{Diagram with red circle and } \pi = X \quad (2.7)$$

Recalling that by placing inputs side by side we are acting on the product space by composing spiders appropriately we can form more complicated linear maps, such as the CNOT gate that flips the bit value of the second qubit if the first qubit is $|1\rangle$:

$$\text{Diagram with green circle and red circle} = \frac{1}{\sqrt{2}} \begin{pmatrix} 1 & 0 & 0 & 0 \\ 0 & 1 & 0 & 0 \\ 0 & 0 & 0 & 1 \\ 0 & 0 & 1 & 0 \end{pmatrix} \propto \text{CNOT} \quad (2.8)$$

Where we write ‘ \propto ’ to explicitly show the diagram is only proportional to the gate, here we need to multiply by the global scalar correction $\sqrt{2}$ for them to be exactly equal. The truth of this equality is demonstrated functionally below in equation (2.13). Often a great deal of insight can be deduced from the general structure of the diagrams which are only proportional to the linear map one might initially want to work with.

To make a connection with other better known mathematical constructions, particularly in condensed matter physics and machine learning, we can view ZX-diagram as a graphical representations of a specific type of tensor network. Seen in this light a wire between two spiders denotes the familiar tensor contraction of tensor network theory. Tensorially the Z and X spiders for the non-zero wire cases are:

$$(\textcircled{a})_{i_1 \dots i_m}^{j_1 \dots j_n} = \begin{cases} 1 & \text{if } i_1 = \dots = i_m = j_1 = \dots = j_n = 0 \\ e^{i\alpha} & \text{if } i_1 = \dots = i_m = j_1 = \dots = j_n = 1 \\ 0 & \text{otherwise} \end{cases} \quad (2.9)$$

$$(\textcircled{a})_{i_1 \dots i_m}^{j_1 \dots j_n} = \left(\frac{1}{\sqrt{2}}\right)^{n+m} \cdot \begin{cases} 1 + e^{i\alpha} & \text{if } \bigoplus_{\alpha} i_{\alpha} \oplus \bigoplus_{\beta} j_{\beta} = 0 \\ 1 - e^{i\alpha} & \text{if } \bigoplus_{\alpha} i_{\alpha} \oplus \bigoplus_{\beta} j_{\beta} = 1 \end{cases} \quad (2.10)$$

where i_{α}, j_{β} range over $\{0, 1\}$ and \oplus is addition modulo 2. By wire contraction one can deduce that the zero leg green and red phase spider is $1 + e^{i\alpha}$.

The importance of the ZX calculus however isn’t related to its representation of operators, but its system of complete rewrite rules. Indeed any equality between operators in \mathbb{C}^2 can be derived solely from the rewrites of ZX diagrams. A complete axiom set of rewrites is given in the appendix D.

ZX-diagrams have a number of symmetries that make them easy to work with. In particular, we can treat a ZX-diagram as an undirected (multi-)graph¹, so that we can move the vertices around in the plane, bending, unbending, crossing, and uncrossing wires, as long as the connectivity and the order of the inputs and outputs is maintained. These deformations of the diagram do not affect the linear map it represents. Indeed, the reader might have noticed that in the CNOT diagram (2.8) we drew a horizontal wire without explaining whether this denotes an input or an output from the Z- and X-spider. We are warranted in drawing it this way because:



$$= \quad (2.11)$$

¹A multi-graph is a graph where there can be multiple edges between the same vertices.

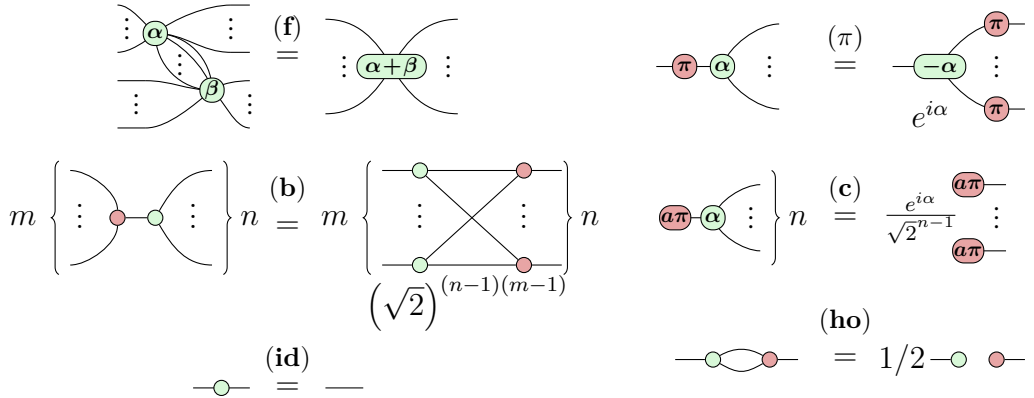


Figure 2.1: The rules of the ZX-calculus. These rules hold for all $\alpha, \beta \in [0, 2\pi)$, and $a \in \{0, 1\}$. They also hold with the colours red and green interchanged, and with inputs and outputs permuted freely. Note ‘..’ should be read as ‘0 or more’, hence the spiders on the left-hand side of (f) are connected by one or more wires. Furthermore, the addition in (f) is taken to be modulo 2π . The right-hand side of (b) is a fully-connected bipartite graph. The rulenames stand respectively for (f)use, (π)-copy, (b)ialgebra, (c)opy, (id)entity and (ho)pf. The shorthand names will later be used above equalities in doing diagrammatic derivations.

Besides these topological symmetries, ZX-diagrams have a set of rewrite rules associated to them, collectively referred to as the *ZX-calculus*. See Figure 2.1 for a set of these rules. As a small demonstration of these rewrite rules, let us prove diagrammatically that the CNOT diagram (2.8) indeed acts like the CNOT. The computational basis states are given by the following diagrams.

$$|00\rangle = \frac{1}{2} \begin{array}{c} \text{---} \\ \text{---} \end{array} \quad |01\rangle = \frac{1}{2} \begin{array}{c} \text{---} \\ \text{---} \end{array} \quad |10\rangle = \frac{1}{2} \begin{array}{c} \text{---} \\ \text{---} \end{array} \quad |11\rangle = \frac{1}{2} \begin{array}{c} \text{---} \\ \text{---} \end{array} \quad (2.12)$$

Then we can check that the diagram has the correct action on these basis states:

$$\begin{array}{c} \text{---} \\ \text{---} \end{array} \quad \propto \quad \begin{array}{c} \text{---} \\ \text{---} \end{array} = \begin{array}{c} \text{---} \\ \text{---} \end{array} \quad (2.13)$$

$$\begin{array}{c} \text{---} \\ \text{---} \end{array} \quad \propto \quad \begin{array}{c} \text{---} \\ \text{---} \end{array} = \begin{array}{c} \text{---} \\ \text{---} \end{array}$$

To summarise: ZX diagrams are generated from the composition rules discussed above applied to the core elements of green and red spiders² referred to as generators. These diagrams represent operators on \mathbb{C}^2 . The key result in the ZX calculus literature is that qubit quantum mechanics is complete with respect to the ZX calculus rewrite rules. This is to say that all equalities between

²It also usually includes the yellow 2 wire H box seen below in equation (2.16), though normalised, and the rewrites include equations involving it. Here we delay its introduction as doing so makes the articulation of the favoured variant of this thesis the ‘ZXH-calculus’ simpler.

operators, states, and measurements in qubit quantum mechanics are representable as rewrite rules of those diagrams.

It is practically desirable to have a concise description of multiply controlled gates, that is to say to have 'AND' logic, in the calculus. In general this is not possible cleanly in ZX. In 2018 a new graphical calculus was introduced to remedy this problem: the *ZH-calculus* [27]. This calculus adds another generator to the ZX-calculus that allows for a compact representation of an AND gate. This new generator is the *H-box*:

$$m \left\{ \begin{array}{c} \vdots \\ \text{[a]} \\ \vdots \end{array} \right\} n := \sum a^{i_1 \dots i_m j_1 \dots j_n} |j_1 \dots j_n\rangle \langle i_1 \dots i_m| \quad (2.14)$$

Here a can be any complex number, and the sum in this equation is over all $i_1, \dots, i_m, j_1, \dots, j_n \in \{0, 1\}$ so that an H-box represents a matrix where all entries are equal to 1, except for the bottom right element, which is a . As a tensor we can write it as:

$$(\text{[a]})_{i_1 \dots i_m}^{j_1 \dots j_n} = \begin{cases} a & \text{if } i_1 = \dots = i_m = j_1 = \dots = j_n = 1 \\ 1 & \text{otherwise} \end{cases} \quad (2.15)$$

Whereas for spiders we only draw the phase on the spider when it is nonzero, for H-boxes we only draw the label when it is not equal to -1 . This is because the 1-input, 1-output H-box with a phase of -1 corresponds to the familiar Hadamard gate (up to a global scalar):

$$\text{---} \text{[---]} = \begin{pmatrix} 1 & 1 \\ 1 & -1 \end{pmatrix} \quad (2.16)$$

Note that in this thesis we only need H-boxes labelled by -1 . We give the general definition for completeness' sake.

We have the following relations among the three generators, Z-spiders, X-spiders and H-boxes:

$$m \left\{ \begin{array}{c} \vdots \\ \text{[---]} \\ \vdots \end{array} \right\} n = \sqrt{2}^{n+m} m \left\{ \begin{array}{c} \vdots \\ \text{[---]} \\ \vdots \end{array} \right\} n \quad (2.17)$$

$$m \left\{ \begin{array}{c} \vdots \\ \text{[---]} \\ \vdots \end{array} \right\} n = \sqrt{2}^{n+m} m \left\{ \begin{array}{c} \vdots \\ \text{[---]} \\ \vdots \end{array} \right\} n \quad (2.18)$$

$$\text{[---]} = \text{[---]} \quad (2.19)$$

$$\text{[---]} = \frac{1}{\sqrt{2}} \text{---} \text{[---]} \text{[---]} \text{[---]} \quad (2.20)$$

Note that it is also possible to represent H-boxes of higher *arity*, i.e. boxes with a larger number of input and output wires, using just Z- and X-spiders, but this is quite involved and not necessary for our purposes [28].

In addition to the rules of the ZX-calculus of Figure 2.1 and the relations among the generators (2.17)–(2.20) we also have some rules specific to the ZH-calculus; see Figure 2.2. We present in Appendix D a condensed overview of all the rewrite rules and relations we have introduced so far.

An H-box with zero input and output wires that is labelled by a is equal to the scalar a . This means we can always translate the scalars in the hybrid notation of Figures 2.1 and 2.2 into a ZH-diagram. For instance, the self-inverseness of the Hadamard gate can be represented as follows:

$$\text{---} \square \text{---} = \boxed{2} \text{ ---} \quad (2.21)$$

ZH-diagrams are *universal*, meaning that any linear map between complex vector spaces of dimension 2^n can be represented as a ZH-diagram. Furthermore, the ZH-calculus is *complete*, meaning that if two diagrams represent the same linear map, then we can find a sequence of rewrites from Figures 2.1 and 2.2 and equations (2.17)–(2.20) that transforms one diagram into the other [27]. However, in general, such a sequence of rewrites will involve diagrams of size exponential in the number of inputs and outputs (as otherwise we could establish efficient classical simulation of quantum computation, among other unlikely consequences such as P=NP). The key to working with ZH-diagrams efficiently is then to find good heuristics for simplifying diagrams.

H-boxes allow us to straightforwardly represent controlled-phase gates. For instance, a CCZ(θ) gate, i.e. a gate that maps the computational basis state $|xyz\rangle$ to $e^{i\theta(xyz)}|xyz\rangle$ is given by:

$$\text{---} \circ \text{---} \square \text{---} = \begin{pmatrix} 1 & 0 & 0 & 0 & 0 & 0 & 0 & 0 \\ 0 & 1 & 0 & 0 & 0 & 0 & 0 & 0 \\ 0 & 0 & 1 & 0 & 0 & 0 & 0 & 0 \\ 0 & 0 & 0 & 1 & 0 & 0 & 0 & 0 \\ 0 & 0 & 0 & 0 & 1 & 0 & 0 & 0 \\ 0 & 0 & 0 & 0 & 0 & 1 & 0 & 0 \\ 0 & 0 & 0 & 0 & 0 & 0 & 1 & 0 \\ 0 & 0 & 0 & 0 & 0 & 0 & 0 & e^{i\theta} \end{pmatrix} \quad (2.22)$$

As a special case of (2.22) we also have the standard controlled-Z (CZ) gate:

$$\begin{array}{c} \text{---} \\ | \\ \text{---} \end{array} \quad = \quad \begin{pmatrix} 1 & 0 & 0 & 0 \\ 0 & 1 & 0 & 0 \\ 0 & 0 & 1 & 0 \\ 0 & 0 & 0 & -1 \end{pmatrix} \quad (2.23)$$

As another variation on these diagrams, we have the following diagram that we will use different iterations on throughout this paper:

$$\begin{array}{c} \text{---} \\ | \\ \text{---} \\ | \\ \text{---} \end{array} \quad = \quad \begin{pmatrix} 1 & 0 & 0 & 0 \\ 0 & 1 & 0 & 0 \\ 0 & 0 & 1 & 0 \\ 0 & 0 & 0 & 0 \end{pmatrix} \quad (2.24)$$

that is to say this linear map throws away a $|11\rangle$ input, but otherwise acts as the identity.

As another variation on (2.22) we can represent the CCNOT gate as follows:

$$\frac{1}{2} \quad \begin{array}{c} \text{---} \\ | \\ \text{---} \\ | \\ \text{---} \\ | \\ \text{---} \end{array} \quad = \quad \begin{pmatrix} 1 & 0 & 0 & 0 & 0 & 0 & 0 & 0 \\ 0 & 1 & 0 & 0 & 0 & 0 & 0 & 0 \\ 0 & 0 & 1 & 0 & 0 & 0 & 0 & 0 \\ 0 & 0 & 0 & 1 & 0 & 0 & 0 & 0 \\ 0 & 0 & 0 & 0 & 1 & 0 & 0 & 0 \\ 0 & 0 & 0 & 0 & 0 & 1 & 0 & 0 \\ 0 & 0 & 0 & 0 & 0 & 0 & 0 & 1 \\ 0 & 0 & 0 & 0 & 0 & 0 & 1 & 0 \end{pmatrix} \quad (2.25)$$

Those familiar with the ZX-calculus or the ZH-calculus might have noticed that they have conflicting definitions of the X-spider and the 2-ary H-box, resulting in different scalar factors of $\sqrt{2}$. Here we use the conventions also used in PyZX [29] in order to aid in our calculations. This means that our Z- and X-spider are defined as is usual in the ZX-calculus. However, most literature on the ZX-calculus also includes a yellow box to represent the Hadamard gate. In our case we use the convention of the ZH-calculus that such a box represents an *unnormalised* Hadamard gate (cf. (2.16)). Hence, certain scalar factors will be different than is usual in the literature on the ZX-calculus. Conversely, our H-box and Z-spider match the definition used in the ZH-calculus, but our X-spider does not match the corresponding definition in the ZH-calculus, and is off by certain factors of $\sqrt{2}$. It is unfortunately not possible to have a fully satisfactory convention when it comes to scalar factors in the ZX/ZH-calculus, and choices have to be made about where scalar corrections appear (see [30] for a longer discussion on this topic). In order to prevent confusion about these clashing scalar conventions, we will refer to our version of the ZX and ZH calculus as the *ZXH-calculus* throughout this thesis.

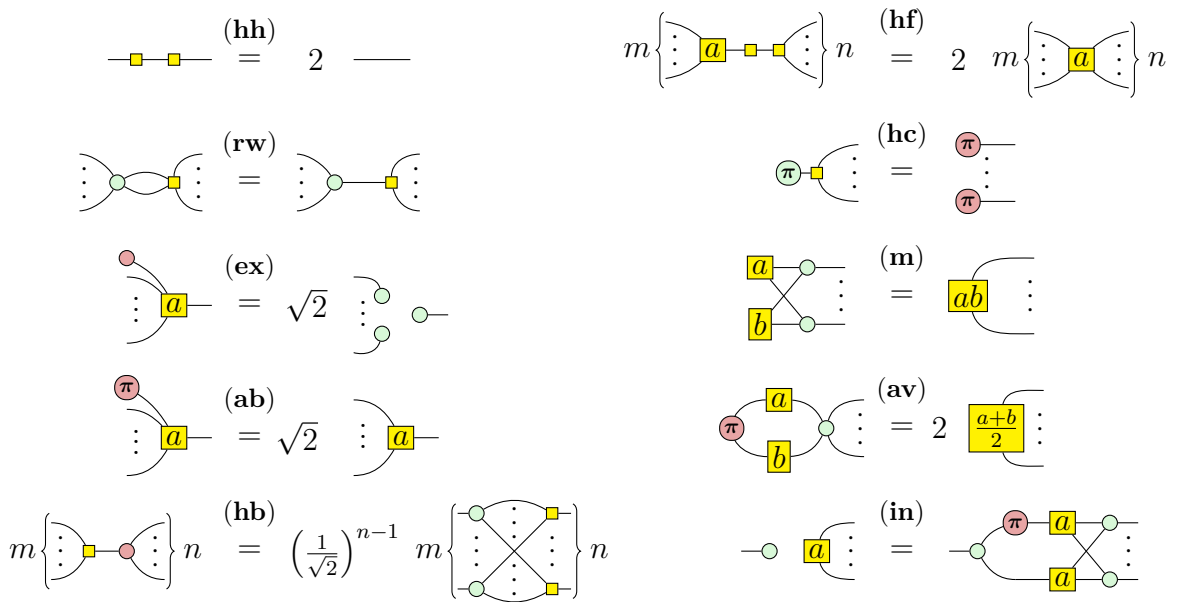


Figure 2.2: The rules of the ZH-calculus. These rules hold for all $a, b \in \mathbb{C}$. Note ‘..’ should be read as ‘0 or more’. The right-hand side of (in) and (hb) and the left-hand side of (m) contain fully connected bipartite graphs. In this thesis we will only need the rules in the left column. The rest are shown for completeness. The rule names stand for (hh)-cancellation, remove wire, (ex)plode, (ab)sorb, (hb)ialgebra, (hf)use, (hc)opy, (m)ultiplication, (av)erage and (in)roduction (as it introduces additional wires to the H-box on the left-hand side).

3

Diagrammatic representation theory of $SU(2)$

3.1 Constructing irreducible representations of $SU(2)$

There are two pertinent ideas to keep in mind to understand the motivation of this section. The first observation is that space of a single wire in ZXH diagrams is \mathbb{C}^2 . The second is that this is the space of the fundamental representation of $SU(2)$. If this terminology is novel a complete introduction over and above the aspects of $SU(2)$ representation theory required in this thesis is available in appendix I.

The fundamental representation of $SU(2)$ is the space of the complex 2×2 matrices:

$$\left\{ \begin{pmatrix} \alpha & -\bar{\beta} \\ \beta & \bar{\alpha} \end{pmatrix} : \alpha, \beta \in \mathbb{C}, |\alpha|^2 + |\beta|^2 = 1 \right\}$$

that make up the group $SU(2)$ itself.

Any such complex matrix can be alternatively parametrised as follows:

$$\begin{pmatrix} a + bi & c + di \\ -c + di & a - bi \end{pmatrix} \quad (a, b, c, d \in \mathbb{R})$$

We can use the fact that the determinant of this matrix can be written as the square norm of the corresponding quaternion¹ thus the unit quaternions are elements of $SU(2)$. Note that we can now write any element of $SU(2)$ as

$$a\hat{1} + b\hat{i} + c\hat{j} + d\hat{k}$$

¹A quaternion is an expression of the form $a + bi + cj + dk$ where a, b, c, d , are real numbers, and $\hat{i}, \hat{j}, \hat{k}$, are unit-vectors. The norm is defined as $\sqrt{a^2 + b^2 + c^2 + d^2}$.

In this way we see that the following matrices serve as a basis for $SU(2)$

$$\hat{1} = \begin{pmatrix} 1 & 0 \\ 0 & 1 \end{pmatrix} \quad \hat{i} = i\sigma_x = \begin{pmatrix} 0 & i \\ i & 0 \end{pmatrix} \quad \hat{j} = i\sigma_y = \begin{pmatrix} 0 & i \\ -i & 0 \end{pmatrix} \quad \hat{k} = i\sigma_z = \begin{pmatrix} i & 1 \\ 1 & -i \end{pmatrix}$$

Where the σ_i are the Pauli matrices. This shows then that the Pauli matrices, up to a complex scalar, can themselves serve as the basis of $SU(2)$. This is practical from a ZXH perspective as σ_z and σ_x (and therefore σ_y) are basic elements of ZXH diagrams. This in turns shows us that ZXH is not just capable of representing the fundamental representation of $SU(2)$ (which we know by virtue of the fact ZXH can represent all \mathbb{C}^{2n} to \mathbb{C}^{2m} maps) but we know we can describe a basis for it in very natural terms within the calculus. Consider now the

The structure of the ZXH calculus naturally gives us the fundamental representation of $SU(2)$. This humble observation is the route to the complete diagrammification of the representation theory of this group: recall all higher representations of $SU(2)$ can be constructed out of the fundamental ones [31].

Spin- j irrep. The fundamental irrep (spin-1/2) is simply the 2×2 matrix multiplication of $SU(2)$ over \mathbb{C}^2 . The higher-spins irreps (spin- j) are then defined over the Hilbert space \mathcal{H}_j ,

$$\mathcal{H}_j \stackrel{\text{def}}{=} \mathcal{S} \underbrace{\mathbb{C}^2 \otimes \dots \otimes \mathbb{C}^2}_{2j \text{ copies}}, \quad (3.1)$$

where \mathcal{S} is the *symmetrisation projector* defined as the linear map such that

$$\mathcal{S}(v_1 \otimes \dots \otimes v_{2j}) = \frac{1}{(2j)!} \sum_{\sigma \in \mathfrak{S}_{2j}} U_\sigma (v_1 \otimes \dots \otimes v_{2j}), \quad (3.2)$$

with \mathfrak{S}_{2j} the $2j$ -element permutation group and the permutation unitary

$$U_\sigma (v_1 \otimes \dots \otimes v_{2j}) \stackrel{\text{def}}{=} v_{\sigma(1)} \otimes \dots \otimes v_{\sigma(2j)}. \quad (3.3)$$

Let's denote the canonical basis of \mathbb{C}^2 as

$$|0\rangle \stackrel{\text{def}}{=} \begin{pmatrix} 1 \\ 0 \end{pmatrix} \quad |1\rangle \stackrel{\text{def}}{=} \begin{pmatrix} 0 \\ 1 \end{pmatrix}. \quad (3.4)$$

It will be practical for us to also make note of the canonical orthonormal basis of \mathcal{H}_j written as [32]

$$|jm\rangle \stackrel{\text{def}}{=} \sqrt{\frac{(2j)!}{(j+m)!(j-m)!}} \mathcal{S} \underbrace{|0\rangle \otimes \dots \otimes |1\rangle}_{j+m \text{ times } |0\rangle}, \quad (3.5)$$

with $m \in \{-j, \dots, j\}$.

So explicitly we can say that the n^{th} representation of $SU(2)$ can be obtained as the symmetric subspace of n copies of the space of the fundamental representation, which is to say, if $\mathcal{H} = \mathbb{C}^2$ then the space of the $(n + 1)$ -dimensional representation is $\text{Sym}(\mathcal{H}^{\otimes n})$. This is how we create the vector space of $spin - n/2$ from n copies of a $spin - 1/2$ space.

We can extend the group representations Π_1 and Π_2 to a combined representation $\Pi_1 \otimes \Pi_2$ acting on their independent spaces A and B as

$$(\Pi_1 \otimes \Pi_2)(A \otimes B) = \Pi_1(A) \otimes \Pi_2(B). \quad (3.6)$$

Where we understand this to mean that if we have a tensor product of maps belonging to two different representations we can create the maps of the combined representation by taking the tensor product of the separate maps. When these two representations are the same it is ambiguous as to whether one is applying $\Pi \otimes \Pi$ or merely the action of Π on the space, as such we may just say Π is acting on a space $A \otimes A$. One can then create the Lie group action for a higher $SU(2)$ representation from a lower one by simply applying the action on each element of the composite space to be symmetrised (see equation (I.5)). For the Lie algebra representation the composite action is slightly more complex as one needs the superposition of applying the algebra element to each part in turn $(\pi_1 \otimes \pi_2)(X \otimes Y) = \pi_1(X) \otimes Y + X \otimes \pi_2(Y)$. An explanation of this can be found in the appendix discussion of equation (I.6). With this introduction to hand we are now in a position to discuss these actions diagrammatically.

3.2 Diagrammatic construction of spin-spaces

Knowing that a single wire in ZXH provides the space of Spin-1/2 gives us the platform from which to build higher spin spaces via proposition I.1.5.1. To get spin- $n/2$ we require a method to project n qubits to their symmetric subspace [33].

As a basic example let us take spin-1. In this instance we are looking for an operator that adds the identity map on two qubits to their swap and in this way cancels the anti-symmetric

components (from the perspective of the underlying matrix). To get such an operator we first look to the CSWAP gate of quantum computing:

$$\begin{array}{c} \text{Diagram 1} \\ \text{Diagram 2} \\ \text{Diagram 3} \end{array} = \begin{array}{c} \text{Diagram 4} \\ \text{Diagram 5} \\ \text{Diagram 6} \end{array} = \frac{1}{\sqrt{2}} \begin{pmatrix} 1 & 0 & 0 & 0 & 1 & 0 & 0 & 0 \\ 0 & 1 & 0 & 0 & 0 & 0 & 1 & 0 \\ 0 & 0 & 1 & 0 & 0 & 1 & 0 & 0 \\ 0 & 0 & 0 & 1 & 0 & 0 & 0 & 1 \end{pmatrix} \quad (3.7)$$

Note how the top wire is the control, which is projected into the Z-basis from the unitary circuit perspective. By inputting a computational basis state we can verify that it indeed performs the maps required. First, when the input is $|0\rangle$:

$$\begin{array}{c}
 \text{Diagram (ex):} \\
 \text{Diagram (c):} \\
 \text{Diagram (2.17):} \\
 \text{Diagram (c):} \\
 \text{Diagram (f):} \\
 \text{Diagram (id):} \\
 \text{Diagram:} \\
 \text{Diagram:}
 \end{array}
 = \sqrt{2} \quad = \sqrt{2} \quad (3.8)$$

And second, when the input is $|1\rangle$:

Now as stated above, to write the symmetrising projector on $n = 2$ wires we need an equal superposition of the identity permutation and the SWAP. However these outcomes must be normalised which implies we need to rescale the final diagram. Hence the desired map is given by the diagram seen in equation (3.7) with $\sqrt{2}|+\rangle = |0\rangle + |1\rangle$ state as the control.

$$\begin{array}{c} \text{Circuit Diagram} \\ \text{with } \frac{1}{\sqrt{2}} \text{ and } \text{yellow squares} \end{array} = \begin{pmatrix} 1 & 0 & 0 & 0 \\ 0 & \frac{1}{\sqrt{2}} & \frac{1}{\sqrt{2}} & 0 \\ 0 & \frac{1}{\sqrt{2}} & \frac{1}{\sqrt{2}} & 0 \\ 0 & 0 & 0 & 1 \end{pmatrix} \quad (3.10)$$

In general we let $\sigma \in S_n$ be a permutation on n points. We write U_σ for the unitary on $\mathcal{H}^{\otimes n}$ that permutes each of the composite \mathcal{H} spaces via σ : $U_\sigma |x_1 \cdots x_n\rangle = |x_{\sigma 1} \cdots x_{\sigma n}\rangle$. We can symmetrise this space by taking the superposition over all the permutations as this amounts to

a sum over all the permutations which by definition will cancel all anti-symmetric components of the tensor. Hence, we can write the *symmetrising projector* $P_S^{(n)}$ on n wires as

$$P_S^{(n)} := \frac{1}{n!} \sum_{\sigma \in S_n} U_\sigma. \quad (3.11)$$

Each U_σ can straightforwardly be written as a ZXH-diagram by just permuting the wires using our CSWAP.

Given we have a coherent superposition of all the permutations on n wires $P_S^{(n)}$, then the way we get a coherent superposition of the permutations on $n + 1$ wires is to compose $P_S^{(n)}$ with a coherent superposition of the identity and the SWAP gates from the $(n + 1)$ th qubit to every other qubit: $\text{id} + \text{SWAP}_{1,n+1} + \text{SWAP}_{2,n+1} + \dots + \text{SWAP}_{n,n+1}$. We construct this superposition as a ZXH-diagram by writing CSWAP gates from the $(n + 1)$ th qubit to each other qubit and then connecting all the control wires in such a way that at most one CSWAP ‘fires’ at the same time.

By considering a few examples we can begin to understand a general procedure

For $n = 3$,

$$\frac{1}{3\sqrt{2}} \begin{array}{c} \text{Diagram: } \text{A 3-qubit system with wires labeled 1, 2, 3.} \\ \text{Control wires: } \text{Wires 1 and 2 are connected to a CSWAP gate (yellow square).} \\ \text{Control wires: } \text{Wires 1 and 3 are connected to a CSWAP gate (yellow square).} \\ \text{Control wires: } \text{Wires 2 and 3 are connected to a CSWAP gate (yellow square).} \\ \text{Control wires: } \text{Wires 1, 2, and 3 are connected to a SWAP gate (yellow square).} \\ \text{Control wires: } \text{Wires 1, 2, and 3 are connected to a SWAP gate (yellow square).} \end{array} \quad (3.12)$$

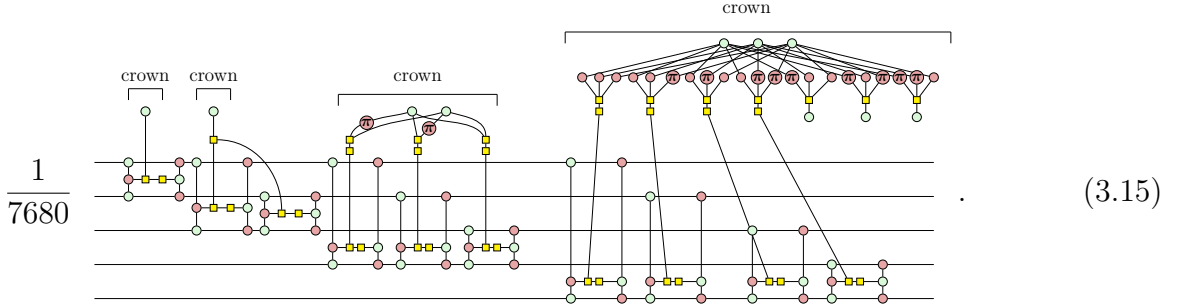
This works, because

$$\text{Diagram: } \text{A 3-qubit system with wires labeled 1, 2, 3.} = 2(|00\rangle + |10\rangle + |01\rangle), \quad (3.13)$$

For $n = 4$,

$$\frac{1}{48} \begin{array}{c} \text{Diagram: } \text{A 4-qubit system with wires labeled 1, 2, 3, 4.} \\ \text{Control wires: } \text{Wires 1 and 2 are connected to a CSWAP gate (yellow square).} \\ \text{Control wires: } \text{Wires 1 and 3 are connected to a CSWAP gate (yellow square).} \\ \text{Control wires: } \text{Wires 1 and 4 are connected to a CSWAP gate (yellow square).} \\ \text{Control wires: } \text{Wires 2 and 3 are connected to a CSWAP gate (yellow square).} \\ \text{Control wires: } \text{Wires 2 and 4 are connected to a CSWAP gate (yellow square).} \\ \text{Control wires: } \text{Wires 3 and 4 are connected to a CSWAP gate (yellow square).} \\ \text{Control wires: } \text{Wires 1, 2, and 3 are connected to a SWAP gate (yellow square).} \\ \text{Control wires: } \text{Wires 1, 2, and 4 are connected to a SWAP gate (yellow square).} \\ \text{Control wires: } \text{Wires 1, 3, and 4 are connected to a SWAP gate (yellow square).} \\ \text{Control wires: } \text{Wires 2, 3, and 4 are connected to a SWAP gate (yellow square).} \\ \text{Control wires: } \text{Wires 1, 2, 3, and 4 are connected to a SWAP gate (yellow square).} \end{array} \quad (3.14)$$

For $n = 5$,



In order to form a general method we should note how the smaller symmetrisers are contained within the larger. To generalise the construction to even higher spins, there are two non-trivial parts that require investigation: the global scalar of the diagram and the “crown”, which we label in the last diagram, which is the diagrammatic components that connect multiple CSWAPS and determine which occur in superposition.

The crown. ²

The function of the crown is to produce a superposition of states that triggers one or none of the CSWAP gates, i.e.

$$|0\dots0\rangle + |10\dots0\rangle + \dots |0\dots01\rangle. \quad (3.16)$$

We can consider these, in analogy with electrical engineering, one-hot encodings in super position where we take this to mean that there is at most one state bit that is 1 in each state.

This is the superposition of n states of the canonical basis. For instance, for $n = 3$,

(3.17)

By taking k adjacent single-wire Z-spiders we get the equal superposition of all 2^k elements of the canonical basis

$$|0\dots0\rangle + |0\dots01\rangle + |0\dots010\rangle + |0\dots011\rangle + \dots + |1\dots1\rangle. \quad (3.18)$$

From this state, we can obtain the state we need (3.16) by projecting the ‘unwanted’ states to 0. This requires $2^k \geq n$. We choose the minimal value of k that satisfies this inequality, i.e. $k = \lceil \log_2 n \rceil$. Then the crown is constructed as follows:

²It has been pointed out after the completion and submission of this thesis that the diagram given in equation 3.17 generalises and we can take the “crown” for any size superposition to be a totally connected graph of 0-boxes. Since my PhD is now defended and probably nobody will ever read this again I’m loath to change all the diagrams and scalars to accommodate this nice observation. The interested reader should note this however as it is a more elegant presentation.

1. Add k Z-spiders on top of the crown.
2. Add $2^k - 1$ groups of k X-spiders, each with phases 0 or π , such that each group of spiders has a different sequence of phases 0 and π . Connect each group with the row above.
3. Add $2^k - 1$ H-boxes. Connect each H-box to the k X-spiders of a single group.
4. To n of the H-boxes, connect a Hadamard, i.e. an arity-2 H-box, and connect each of these to the control-wire of one of the CSWAPs. This connectivity makes it so that *only* when every input to the H-box is an $X(\pi)$ state (i.e. $|1\rangle$) will the output be a $|1\rangle$ as well, which triggers the swap. In all other cases they become a plain single wire red spider which will not trigger the swap and leave it as an identity:

$$\begin{array}{c} \text{Diagram: } \text{Three red spiders with phases } \pi \text{ on top, connected to a yellow H-box.} \\ = \sqrt{2}^5 \text{ (red circle)} \end{array} \quad (3.19)$$

5. To the remaining $2^k - 1 - n$ H-boxes, connect a 0-phase Z-spider. Connect to the H-box above. This construction throws away the unnecessary states in the superposition: when all the inputs to the H-box are $|1\rangle$'s (i.e. X-spiders with π phase), the diagram evaluates to zero:

$$\begin{array}{c} \text{Diagram: } \text{Three red spiders with phases } \pi \text{ on top, connected to a yellow H-box.} \\ = \sqrt{2}^5 \text{ (red circle)} = 0 \end{array} \quad (3.20)$$

Let's demonstrate this procedure with an example. The simplest case for which this construction works is for $n = 3$. We then set $k = 2$. Unfusing a single-arity Z-spider, we get a state $(|0\rangle + |1\rangle) \otimes (|0\rangle + |1\rangle)$ on top. Expanding this we get a sum of four diagrams, where the Z-spiders are replaced by spiders representing respectively $|00\rangle, |10\rangle, |01\rangle, |11\rangle$:

$$\begin{array}{c} \text{Diagram: } \text{A complex circuit with a top row of red spiders with phases } \pi, \text{ followed by a row of yellow H-boxes, and then a row of green spiders with phases } \pi. \\ = \text{ (Diagram: A sum of four terms, each with a top row of red spiders with phases } \pi, \text{ followed by a row of yellow H-boxes, and then a row of green spiders with phases } \pi. \\ \text{(c)} = \frac{1}{2} \text{ (Diagram: A sum of four terms, each with a top row of red spiders with phases } \pi, \text{ followed by a row of yellow H-boxes, and then a row of green spiders with phases } \pi.} \\ \text{(ex)} \text{ (ab)} = \frac{1}{\sqrt{2}} \text{ (Diagram: A sum of four terms, each with a top row of red spiders with phases } \pi, \text{ followed by a row of yellow H-boxes, and then a row of green spiders with phases } \pi.} \\ \text{(c)} \text{ (2.17)} = \sqrt{2}^5 \text{ (red circle)} + \sqrt{2}^5 \text{ (red circle)} + \sqrt{2}^5 \text{ (red circle)} + \sqrt{2}^5 \text{ (red circle)} \end{array} \quad (3.21)$$

What this shows is that the crown decomposes into a superposition of qubit basis states with at most one $|1\rangle$ (red pi spider) in their respective tensor products. These are directly fed into the controlled swap gates and so we see we are indeed in a superposition of applying one or none of the swaps.

The scalar. In the given examples (3.12)–(3.15), we can see that each diagram requires a global scalar factor in order to get the correct normalisation. Let us describe how to calculate this scalar. We describe how to get the diagram for the *unnormalised* symmetrisation projector. We then get the actual scalar we need by dividing by $\frac{1}{n!}$, which gives us the correctly normalised symmetrisation projector. There are two contributions to the scalar:

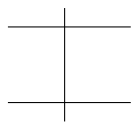
1. Each CSWAP diagram (3.7) is ‘too small’ by a factor of $\frac{1}{\sqrt{2}}$ so that we need to correct by a $\sqrt{2}$ for each CSWAP in the diagram. There are $\sum_{i=2}^n (i-1) = \frac{n(n-1)}{2}$ such gates in our diagram for the n -wire symmetriser.
2. When $n \geq 3$ we need to introduce corrections for the H-boxes in the crown. There is a special case for the $n = 3$ symmetriser, where the H-box is too large by 2, and requires a correction of $\frac{1}{2}$. Then for $n \geq 4$, every pair of H-box+Hadamard or H-box+Z-spider is too large by a factor of 2. In \mathcal{T}_n there are $2^k - 1$ such pairs, and thus $\sum_{i=4}^n (2^{\lceil \log_2 i \rceil} - 1)$ in all \mathcal{S}_n .

Combining this, we see that the scalar correction λ_n for the n -wire symmetriser is

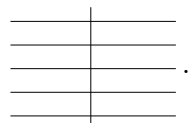
$$\lambda_n = \frac{2^{\frac{n(n-1)}{4}}}{n!} \cdot \left(\frac{1}{2}\right)^{\beta + \sum_{i=4}^n (2^{\lceil \log_2 i \rceil} - 1)} \quad (3.22)$$

where $\beta = 0$ if $n < 3$ else it is 1, which accounts for the absence of the 2 from the idiosyncratic $n = 3$ symmetriser for $n = 2$ case.

Symmetriser short hand It will be practical to adopt a diagrammatic short hand for our symmetrised wires. We will draw a line perpendicular through a series of wires to indicate the existence of a symmetriser over these wire rather than depict the ZXH-diagram for it explicitly. We do this when the structure of the symmetriser isn’t the component of interest. For instance we may write:



or



(3.23)

Note that this is just shorthand, and that we still consider it equal to the diagrammatic construction we introduced above.

3.3 Diagrammatic Lie algebra representation theory

As with everything in ZXH we are tethered to $\mathbb{C}^{2^n} \mapsto \mathbb{C}^{2^m}$ maps the underlying spaces of which are composed of \mathbb{C}^2 the fundamental representation of $SU(2)$. As such all representation theory depicted in ZXH must factor through this description. In order to explain how we describe $SU(2)$ representation theory diagrammatically in the language of ZXH, for pedagogical purposes, we will discuss the necessary components in terms of an intermediary ‘schematic description’. Before we describe the details of this let us consider at what it is we want to obtain.

As discussed above by taking the symmetric subspace on spin-1/2 spaces we obtain the space of a higher spin. We have the Pauli rotations σ_x and σ_x (and thereof σ_y) diagrammatically in the ZXH calculus as Lie algebra elements that act on the spin-1/2 space and who could be composed to form a representation of general spin-1/2 algebra elements by their composition. The question is, given this fact, how do we apply the same algebra elements on the higher representations? Algebraically we know we can write

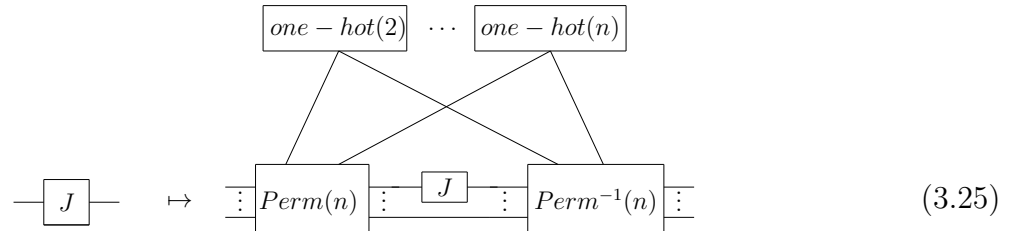
$$\pi(X \otimes X) = \pi(X) \otimes X + X \otimes \pi(X)$$

A concrete example of this is the $S_{\frac{1}{2}}^z$ operator, acting on, for example $\left| \frac{1}{2}; \frac{1}{2} \right\rangle$ we have that $S_{\frac{1}{2}}^z \left| \frac{1}{2}; \frac{1}{2} \right\rangle = \frac{\hbar}{2}$. If we then write $|1; 1\rangle = \left| \frac{1}{2}; \frac{1}{2} \right\rangle \otimes \left| \frac{1}{2}; \frac{1}{2} \right\rangle$ then we write $S_1^z = S_{\frac{1}{2}}^z \otimes Id + Id \otimes S_{\frac{1}{2}}^z$. From this we can see that indeed $S_1^z |1; 1\rangle = (S_{\frac{1}{2}}^z \otimes Id + Id \otimes S_{\frac{1}{2}}^z)(\left| \frac{1}{2}; \frac{1}{2} \right\rangle \otimes \left| \frac{1}{2}; \frac{1}{2} \right\rangle) = (\frac{\hbar}{2} + \frac{\hbar}{2})(\left| \frac{1}{2}; \frac{1}{2} \right\rangle \otimes \left| \frac{1}{2}; \frac{1}{2} \right\rangle)$ which gives \hbar the textbook answer.

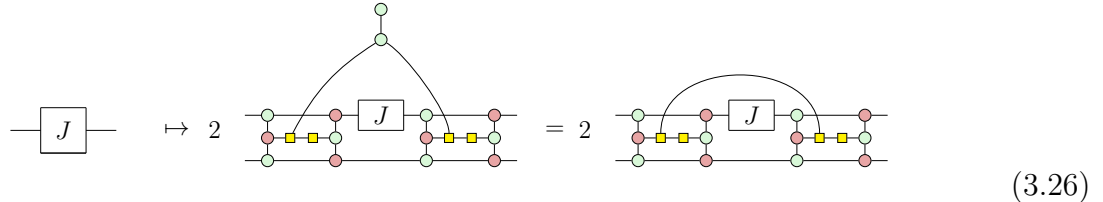
This extends by induction to arbitrary lengths so that

$$\pi(X \otimes X \cdots \otimes X) = \pi(X) \otimes X \cdots \otimes X + \cdots + X \otimes X \cdots \otimes \pi(X) \quad (3.24)$$

In this way then if we want to create operators acting on higher irreps of $SU(2)$ we can see that we must create an operator that is the superposition of the spin-1/2 operator acting on each different composite space.



What is being described here is how the action of the algebra element J on the fundamental representation can be ‘raised’ to one acting on a higher representation. The idea is that the ‘one-hot(n)’³ elements (we will shortly see these relate to crowns) are creating two copies of a superposition of n ‘trigger’ states (basis states can always be cloned). These are then simultaneously applied to the $Perm(n)$ and $Perm^{-1}(n)$ maps (this is why we require two copies) which apply a certain permutation that moves each wire, in superposition, such that it becomes the top most, this is then undone. This matches the operator required by equation (3.24). The form for raising the spin-1/2 algebra to spin-1 is the following



A reasonable choice for the ‘one-hot(n)’ functions are the ‘crowns’ with the addition of a green spider that copies the basis elements as discussed above. In the spin-1 case this means we are connecting a single green spider to the (computational) basis state splitting three legged green spider. This merely fuses together and the result is a bent identity wire between the two controlled swaps. This is as we would expect, as this is proportional to $|00\rangle + |11\rangle$ (which is the basis copied version of the crown $|0\rangle + |1\rangle$), which indicates the swaps are on and off at the same time.

To give some spin-1 examples for a particular algebra element, consider the S_1^x algebra element as our ' J ' for spin-1. We can construct this from the spin-1/2 element $S_{\frac{1}{2}}^x = \frac{\hbar}{2}\sigma_x$ via the method described above:

$$\frac{\hbar}{2} * 2 = \frac{\hbar}{2} \begin{pmatrix} 0 & 1 & 1 & 0 \\ 1 & 0 & 0 & 1 \\ 1 & 0 & 0 & 1 \\ 0 & 1 & 1 & 0 \end{pmatrix} \quad (3.27)$$

³This notation originates from electrical engineering where information is encoded in which single wire has current passing through it. Here we want states (in superposition) containing *one or zero* $|1\rangle$ elements.

Which if we project the domain and codomain to the spin-1 space from our qubit matrices we see that

$$\frac{\hbar}{2} \begin{pmatrix} 1 & 0 & 0 & 0 \\ 0 & \frac{1}{\sqrt{2}} & \frac{1}{\sqrt{2}} & 0 \\ 0 & 0 & 0 & 1 \end{pmatrix} \begin{pmatrix} 0 & 1 & 1 & 0 \\ 1 & 0 & 0 & 1 \\ 1 & 0 & 0 & 1 \\ 0 & 1 & 1 & 0 \end{pmatrix} \begin{pmatrix} 1 & 0 & 0 \\ 0 & \frac{1}{\sqrt{2}} & 0 \\ 0 & \frac{1}{\sqrt{2}} & 0 \\ 0 & 0 & 1 \end{pmatrix} = \frac{\hbar}{\sqrt{2}} \begin{pmatrix} 0 & 1 & 0 \\ 1 & 0 & 1 \\ 0 & 1 & 0 \end{pmatrix} \stackrel{\text{def}}{=} S_1^x \quad (3.28)$$

Where the matrices on the left and the right are the matrix projections from a qubit space, like that obtained in PYZX, and that of the spin-1 symmetric subspace.

To give a further example lets consider the lowering operator for the spin-1 space S_1^- algebra element which we will create from the spin-1/2 algebra element $\hbar \begin{pmatrix} 0 & 0 \\ 1 & 0 \end{pmatrix}$. We can construct this from the spin-1/2 elements $\frac{1}{2} - \bullet - \pi -$ the matrix correspondence for the entire diagram is as follows

$$2 * \frac{\hbar}{2} \begin{array}{c} \text{---} \\ \text{---} \\ \text{---} \\ \text{---} \end{array} = 2 * \frac{\hbar}{2} \begin{pmatrix} 0 & 0 & 0 & 0 \\ 1 & 0 & 0 & 0 \\ 1 & 0 & 0 & 0 \\ 0 & 1 & 1 & 0 \end{pmatrix} \quad (3.29)$$

Which if we project the domain and codomain to the spin-1 space from our qubit matrices we see that

$$\hbar \begin{pmatrix} 1 & 0 & 0 & 0 \\ 0 & \frac{1}{\sqrt{2}} & \frac{1}{\sqrt{2}} & 0 \\ 0 & 0 & 0 & 1 \end{pmatrix} \begin{pmatrix} 0 & 0 & 0 & 0 \\ 1 & 0 & 0 & 0 \\ 1 & 0 & 0 & 0 \\ 0 & 1 & 1 & 0 \end{pmatrix} \begin{pmatrix} 1 & 0 & 0 \\ 0 & \frac{1}{\sqrt{2}} & 0 \\ 0 & \frac{1}{\sqrt{2}} & 0 \\ 0 & 0 & 1 \end{pmatrix} = \sqrt{2}\hbar \begin{pmatrix} 0 & 0 & 0 \\ 1 & 0 & 0 \\ 0 & 1 & 0 \end{pmatrix} \stackrel{\text{def}}{=} S_1^- \quad (3.30)$$

Where the matrices on the left and the right are the matrix projections from a qubit basis, as one obtains from PYZX, and that of the spin-1 symmetric subspace.

We can see this on specific states purely diagrammatically, taking the input to be $2|00\rangle$ which is the product red input spiders:

$$\begin{aligned}
2 * \frac{1}{2} &= \frac{1}{2} \cdot \frac{1}{2} = \frac{1}{\sqrt{2}} \cdot \frac{1}{\sqrt{2}} = \frac{1}{2} \\
&= \frac{1}{2\sqrt{2}} \cdot \frac{1}{4\sqrt{2}} = \frac{1}{4} \cdot \frac{1}{2} = \frac{1}{2} = \frac{1}{2}
\end{aligned} \tag{3.31}$$

where the initial scalars are η_2 and the $\frac{1}{2}$ correction for the input states. Note how the final diagram where the matrix is translated to the spin-1 basis then gives:

$$\begin{pmatrix} 1 & 0 & 0 & 0 \\ 0 & \frac{1}{\sqrt{2}} & \frac{1}{\sqrt{2}} & 0 \\ 0 & 0 & 0 & 1 \end{pmatrix} \begin{pmatrix} 0 \\ 1 \\ 1 \\ 0 \end{pmatrix} = \begin{pmatrix} 0 \\ \sqrt{2} \\ 0 \end{pmatrix} = \sqrt{2}\hbar|1, 0\rangle \quad (3.32)$$

Which matches the textbook formula:

$$S^-|1, 1\rangle = \hbar\sqrt{j(j+1) - m(m-1)}|j, m-1\rangle|_{j=1, m=0} = \sqrt{2}\hbar|1, 0\rangle \quad (3.33)$$

and so we see this is as expected.

In general our structures requires a scalar correction. There is a distinction in that these operators are not seeking to produce normalised states. For spin operators for example they are specifically expected to produce measurement eigenvalue multiples of the normalised eigenstates. As such there is no scaling to account for the number permutations, the only consideration is ensuring diagrammatic linear maps we apply are exact and not proportional.

There are the same two contributions to the scalar as seen previously:

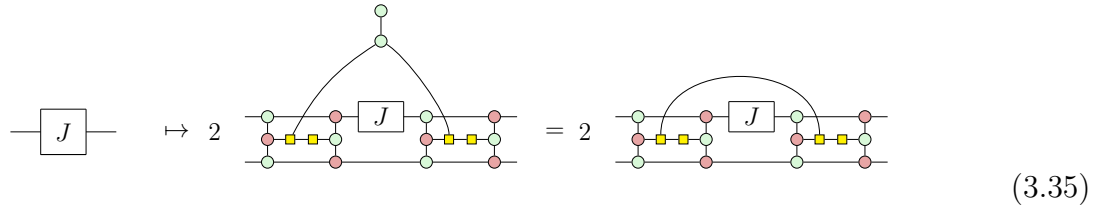
1. As before each CSWAP diagram (3.7) is ‘too small’ by a factor of $\frac{1}{\sqrt{2}}$ so that we need to correct by a $\sqrt{2}$ for each CSWAP in the diagram. There are $2 \sum_{i=2}^n (i-1) = n(n-1)$ such gates in our diagram for the n -wire algebra lifting operator.
2. When $n \geq 3$ we need to introduce corrections for the H-boxes in the crown. There is a special case for the $n = 3$ symmetriser, where the H-box is too large by 2, and requires a correction of $\frac{1}{2}$. Then for $n \geq 4$, every pair of H-box+Hadamard or H-box+Z-spider is too large by a factor of 2. For the n-wire raising operator there are $2^k - 1$ such pairs, and thus $(2^{\lceil \log_2 n \rceil} - 1)$.

We see that the scalar correction η_n for the n -wire algebra raising operator is

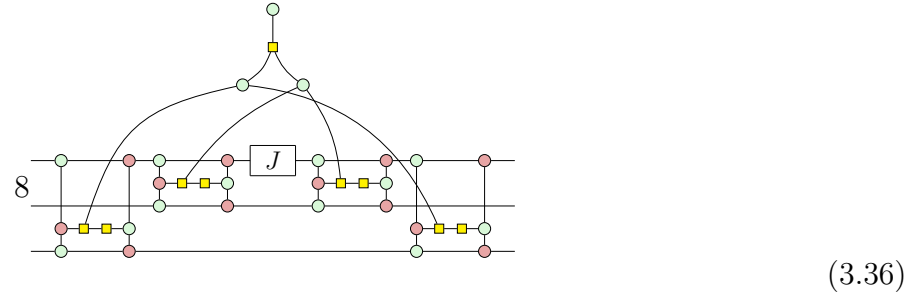
$$\eta_n = 2^{\frac{n(n-1)}{2}} \cdot \left(\frac{1}{2}\right)^{\beta(2^{\lceil \log_2 n \rceil} - 1)} \quad (3.34)$$

where $\beta = 0$ if $n < 3$ else it is 1, which accounts for the absence of the 2 from the distinctive $n = 3$ symmetriser for $n = 2$ case. Notice that unlike for the n-wire symmetriser there is no sum here as there is only the crown for the n-wires and not this crown and all smaller crowns.

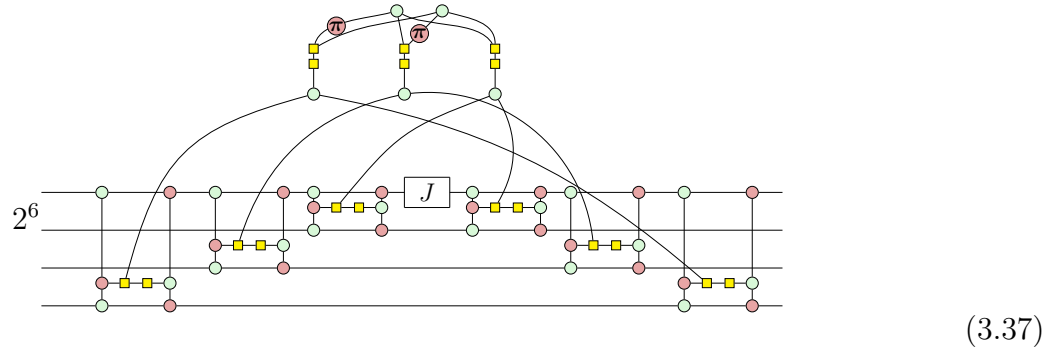
To give concrete examples, for $n = 2$ we will have



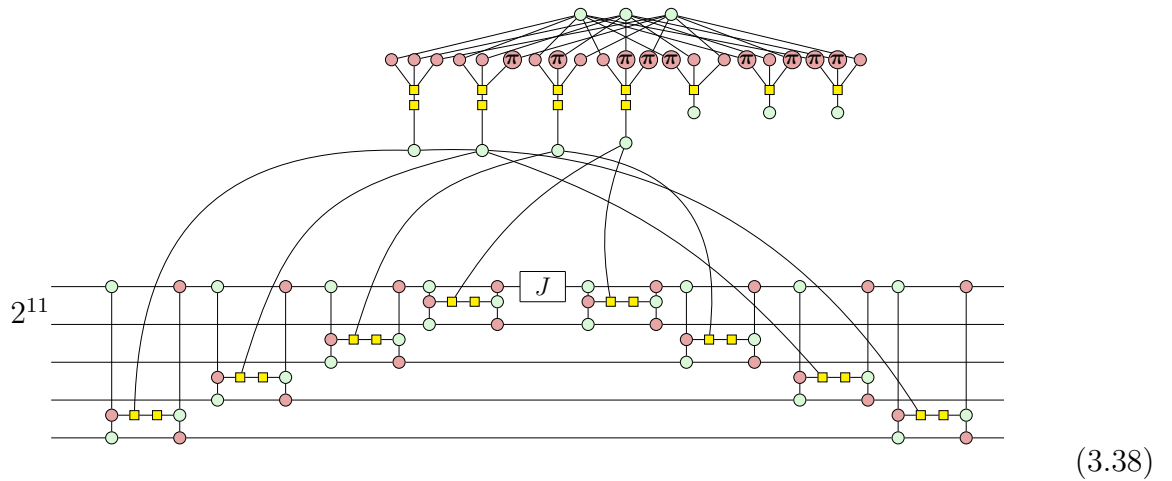
and for $n = 3$



and $n = 4$



and $n = 5$



this generalises in the obvious way.

4

Diagrammatic reasoning for condensed matter physics

4.1 Introduction to the relevant concepts in condensed matter physics

As a field that is primarily concerned with the macro and microscopic properties of matter the question for the reader from outside the field of condensed matter physics is: what is its subject of study? The answer is multi-particle physics.

In general matter, constructed as it is from multiple particles, appears in nature in multiple ‘phases’ where we define a phase as a collection of matter with uniform-macroscopic properties such as density, refractive index, or heat capacity. Implicit in this definition is that a collection of particles, the same ‘matter’, may, and indeed often does, have multiple phases. The prime example is water which we are all familiar with in its physically distinct states of solid, liquid, and gas. Condensed-matter physics is then the study of phases in general and the transitions between them normally in situations where the composite particles are strongly interacting.

Of particular interest to us are specific phases that distinguish matter with the same symmetry structure. It was an accomplishment of 20th century physics that a certain class of phases and their transitions were characterised by the symmetries of the underlying matter. Landau argued that the distinction between certain phases was tied to the symmetries of organisation (referred

4.1. Introduction to the relevant concepts in condensed matter physics

to as orders) of the composite particles[34]. Questions such as: are they in a lattice? Is it regular? Does it repeat? Can I tell if I rotated it? Came to be seen as the way to identity all possible phases. It was discovered however that these are insufficient. There are phases with the same symmetry that are distinguishable.

This observation ushered in the era of ‘topological phases’. This is a term that covers two slightly different concepts. The first alludes to topological order [35], where order is a general term for the arrangement of matter in strongly correlated systems, this topological order can be attributed to a phase possessing long range entanglement essentially because local states are correlated over large distances. The second concept, which is more of interest to this thesis, is that of symmetry protected topological (SPT) phases [36]. Here we are at zero temperature and the two phases being considered have the same bulk local symmetry but differing edge or surface states. It is known that no parametrised local perturbation of the Hamiltonian that preserves the symmetry of the underlying system can smoothly transition between the two phases without ‘closing the gap’ of the energy spectrum. This last phrase is of particular interest and relates to an important property of topological insulators. These phases can be seen as insulators in the bulk but have conductive surface states that are symmetry protected. In order to transition between two topologically distinct insulators it is necessary that the gap between the ground state and the excited states collapses.

So far what has been outlined is extremely broad. To provide a sensible precursor to the work in this thesis the next sections form an introduction targeted at the relevant parts of condensed matter for this thesis.

Order Parameters We have said that the same matter may exhibit different phases. Technically we require a way to distinguish these phases.

We often find that there exists some observable that is zero in one phase and non-zero in the other. An example of this is the magnetisation M of a magnet. Imagine 1D systems with local magnetisation $\vec{M}(x)$; on becoming a magnet the rotational symmetry is broken and a direction is chosen for the material overall. We can detect this by the considering the following operator $m^z = \frac{1}{N} \sum_i \sigma_i^z$. In the disordered non-magnetic phase the sum over randomly aligned spins will amount to zero, during the magnetic phase it will not. This is then a parameter that ‘detects’

4. Diagrammatic reasoning for condensed matter physics

when we have transitioned as from the non-magnetic to the magnetic phase. This parameter is referred to as the order parameter.

Introduction to the Berry Phase As was mentioned above order parameters are observables that indicate that the matter at hand is in a particular state of matter. One such observable of interest to us in this thesis is the Berry phase (in the sense of a complex exponent rather than a property of matter) that was introduced by Michael Berry [23]. He observed that the phase factor resulting from the adiabatic evolution of a Hamiltonian, that preserves the state of system in a specific eigenstate, has two distinct contributions if one has moved on a closed loop through the phase space. There is a component from the state's time evolution and another from the variation of the eigenstate as the Hamiltonian changes. The second component is in the Berry phase. In non-cyclical Hamiltonian variations this can be cancelled. If however the Hamiltonian is varied cyclically it is an irremovable invariant of the system.

We can write that given a Hamiltonian $H(x(t))$ where $x(t) \in \mathbb{R}^N$ is a vector of real parameters varying with time. The adiabatic theorem tells us that provided the n^{th} eigenvalue $\epsilon_n(x(t))$ is non-degenerate along its path and the variation is ‘sufficiently slow’¹ then a system in eigenstate $|\epsilon_n(x(0))\rangle$ will evolve to state in the same eigenstate up to a phase $e^{i\theta}\epsilon_n(x(t))$.

At any time t one can write

$$|\Psi_n(t)\rangle = e^{i\gamma_n(t)} e^{-\frac{i}{\hbar} \int_0^t dt' \epsilon_n(x)} |\epsilon_n(x)\rangle. \quad (4.1)$$

The first exponent is the Berry phase and the second is the dynamic phase. From this equation it can be shown that the Berry phase is the following [23]:

$$\gamma_n(t) = i \int_0^t dt' \left\langle \epsilon_n(x) \left| \frac{d}{dt'} \right| \epsilon_n(x) \right\rangle = i \int_{x'(0)}^{x(t)} dx \langle \epsilon_n(x) | \nabla_x | \epsilon_n(x) \rangle. \quad (4.2)$$

Then for cyclical path one writes that:

$$\gamma_n = i \oint_C dx \langle \epsilon_n(x) | \nabla_x | \epsilon_n(x) \rangle. \quad (4.3)$$

¹Read ‘asymptotically slow given the time scales of the system at hand’.

4.1. Introduction to the relevant concepts in condensed matter physics

As such there is a phase obtained by travelling a parametrised path in the phase space of the states. This phase can be used as an order parameter capable of detecting whether a state belongs to particular phase of matter [37]. Below it is shown how diagrammatic methods can facilitate this calculation. In particular showing the novel result that the AKLT spin-chain state possesses a Berry phase of π for all N , where N is the number of sites in the chain. Before we can expand on this we must first introduce the notion of a spin chain.

Spin chains In order to bring the discussion closer to chains of interacting spins which will be the focus of the bulk of the work in this chapter we will first discuss the Heisenberg model of ferromagnetism. It is composed of a lattice of spin ‘sites’ where each site represents a spin state being either up or down (we will often say $|0\rangle$ and $|1\rangle$ instead)². The neighbouring spins that point in the same direction have a lower energy than those that don’t. The model represents a system that will tend to alignment in the absence of the interference of heat. This is encapsulated by the Ising Hamiltonian

$$H(\sigma) = - \sum_{\langle ij \rangle} J_{ij} \sigma_i \sigma_j - \mu \sum_j h_j \sigma_j \quad (4.4)$$

where $\langle ij \rangle$ indicates we sum over adjacent sites, J_{ij} is the coupling constant between the spins, μ is the magnetic moment, h_j is an external magnetic field and the σ_i are the spin-1/2 Pauli Z matrices at that site.

The minus sign is ultimately a convention, but once fixed there are three classifications of the Ising model. When $J_{ij} > 0$ the interaction is ferromagnetic, $J_{ij} < 0$ the interaction is antiferromagnetic, and finally when $J_{ij} = 0$ the spins are non-interacting.

The model is called ferromagnetic or antiferromagnetic based on the spin-alignment of its ground state. In a ferromagnetic model the lowest energy state is achieved when spins align: as a result the configurations in which adjacent spins are of the same sign have higher probability at low energy. In an antiferromagnetic model the inverse is true and the lowest energy state is when the spins alternate from being up and down.

²The notion of a site itself is ubiquitous in discussions of spin chains and lattices. It simply indicates a position at which one can have a (quasi)particle.

4. Diagrammatic reasoning for condensed matter physics

Introduction to matrix product and tensor network states Within condensed matter matrix product states are a useful description for a broad collection of quantum systems such as 1 dimensional spin systems like the 1D-Ising model above. Their practicality stems from the fact that these states support a number of efficient algorithms for obtaining the ground state such as the DMRG or TEBD algorithms [38, 39, 40].

Definition 1. A Matrix product state (hereafter written MPS) is a multi-particle quantum state written in the following form:

$$|\Psi\rangle = \sum_{\{s\}} \text{Tr} \left[A_1^{(s_1)} A_2^{(s_2)} \cdots A_N^{(s_N)} \right] |s_1 s_2 \dots s_N\rangle$$

where $A_i^{(s_i)}$ are complex, square matrices of dimension χ . The indices s_i range over the states in the computational basis i.e $\{0, 1\}$ for qubits, or $\{0, 1, \dots, n - 1\}$ for n dimensional qudits.

From the perspective of this thesis MPS states form a touch point with the broader condensed matter literature. Below the MPS representation of the 1D AKLT state is explicitly linked to the diagrammatic formulation. Given that we will be seeking to present what can essentially be seen as a diagrammatic tensor network language for spin lattices I include this connection to the MPS formalism as a way to connect what is seen here with tensor representations often seen in the literature.

The tensor product state is the straightforward generalisation of the MPS state, where the MPS is a line of matrices that can be contracted to define state, the tensor product state is a product of tensors who contract in a similar manner. They are used to describe systems that cannot be reasonably described as a line of sites represented as matrices. In this way, just like the MPS state, the complex multi-partite state is decomposed into what we hope are manageable components. Indeed the MPS is a tensor network where the composing tensors are merely matrices. Unfortunately general tensor product states are known to be more difficult to compute with as in general there is no optimal method of contracting the relevant tensors required in concrete calculations. That said, heuristic algorithms do exist, such as those based on projected entangled pair states (PEPS) ansatz [41, 42, 43]. It is also difficult to represent certain states, notably states with chiral topological order such as those with time reversal and parity symmetries, but not the spin rotation symmetry [44, 45, 46, 47]. As was mentioned above, in this thesis we will be interested in a particular type of spin chain, which is often analysed via

4.1. Introduction to the relevant concepts in condensed matter physics

MPS methods, which is an example of an SPT phase. We must first articulate what exactly this means.

Symmetry protected phases Symmetry protected phases are referred to as topological states of matter because ultimately looking locally at the bulk one could never distinguish between these types of phases. Typically one topological properties not evident locally in the bulk for example to look to the edge states of the phase to identify the distinguishing features.

They are a type of zero temperature state of matter that have an underlying symmetry and a finite energy gap between the ground and first excited state. Crucially distinct SPT states with a particular symmetry cannot be smoothly transformed into each other by a local deformation that preserves the underlying symmetry. They can all be smoothly deformed to the product state by a deformation that breaks the symmetry. This is the reason for the terminology ‘symmetry protected’.

More concretely let us take some Hamiltonian H and suppose that at zero temperature we obtain a particular ground state with symmetry x . If we introduce some *local* perturbation δ_x where x indicates the perturbation preserves this symmetry then the ground state of $H' = H + \delta_x$ is in the same phase as the ground state of H . We will now look to a specific example: The AKLT state.

4.1.1 The 1D AKLT state

The one-dimensional AKLT Hamiltonian, named after Affleck, Lieb, Kennedy and Tasaki, is an extension of the Heisenberg spin model. Since its definition it has served, amongst other things, as prototypical example of symmetry protected topological states and matrix product state wave-functions. It is defined as [22]

$$H = \sum_i \vec{S}_i \vec{S}_{i+1} + \beta (\vec{S}_i \vec{S}_{i+1})^2, \quad (4.5)$$

where $\beta = 1/3$. This Hamiltonian acts on a chain of N spin-1 degrees of freedom. Hence, the local Hilbert space at each site is \mathbb{C}^3 , on which we act with the spin operator $\vec{S}_i = (S_i^x, S_i^y, S_i^z)$, where the S_i^a are the 3×3 spin-1 matrices (these matrices, along with other additional information

4. Diagrammatic reasoning for condensed matter physics

on the AKLT state is given in Appendix B). We know that representation theory shows us that the Hilbert space of a chain with N sites, $(\mathbb{C}^3)^{\otimes N}$, can be represented by N copies of the symmetric subspace of a pair of spin-1/2 particles. This decomposition is convenient to find the groundstate of the AKLT Hamiltonian Eq. (4.5) because this Hamiltonian can be written as a positive sum of projectors to $|2; 2\rangle$ on neighbouring sites. Hence, by finding a state where two neighbouring spins are not in this subspace, we can construct the ground state of the AKLT Hamiltonian (as it will be zero in this case). Specifically, the groundstate can be constructed by decomposing each spin-1 site into two spin-1/2 sites that form singlets between neighbouring sites (Fig. 4.1 (a)), and thus have a maximum spin eigenvalue of $s = 1$. These two spin-1/2 sites are then projected back to the physical $s = 1$ at each site by the appropriate symmetrising projectors (Fig. 4.1(b)). By construction, the resulting state, depicted in Fig. 4.1(c) is annihilated by the projectors to $|2; 2\rangle$, and is therefore an exact ground state of Eq. (4.5). We refer to this groundstate as the *AKLT state*³.

The AKLT state has three important physical properties that we will express using the ZXH-calculus [48, 49, 50, 51]. The first property stems from the fact that terminating the chain necessarily breaks two singlets, one at each edge, leaving two free spin-1/2 degrees of freedom at the edges. Since each spin-1/2 has a local Hilbert space of \mathbb{C}^2 (the dimensions corresponding to spin up or spin down), the AKLT state with open boundary conditions has a degeneracy of four (2^2).

The second property that we wish to express using the ZXH-calculus is that the AKLT state has a *string order* [48]. Namely, the AKLT state is a superposition of all spin configurations where, if we ignore the spins with $s_z = 0$, the remaining spins are ordered anti-ferromagnetically: a spin $s_z = \pm 1$ is followed by $s_z = \mp 1$ [52]. For example, $|j_1, j_2, \dots, j_N\rangle = |1, 0, 0, 0, -1, 0, 0, 0, 1\rangle$ is an allowed configuration, while $|1, 0, 0, 1, 0, 0, 0, 1\rangle$ is not. Analogous to how a spin-1/2 antiferromagnetic order can be captured by an alternating spin-spin correlation function, this string order can be captured by defining a *string order parameter* [48]. This diluted anti-ferromagnetism indicates a topological phase is present as no local operator could identity if after n lots of zeroes following a spin up there is then a spin down. Furthermore we can see

³With periodic boundary conditions the groundstate of the AKLT Hamiltonian is unique, but with open boundary conditions it is four-fold degenerate. When referring to ‘the AKLT state’ we don’t distinguish open or boundary conditions, but rather mean all these possible states, as is common practice in the literature.

it is a symmetry protected topological phase. If we were to add a perturbation that broke $SO(3)$ symmetry by imposing for example a direction via a strong magnetic field (such as a term $-\mu \sum_j \vec{S}_j$ as we increase μ) this encourages the spins to align. In the extreme it is clear that the AKLT phase is destroyed when all the spin align.

The final property of interest is that the Berry phase of the AKLT chain is non-trivial. From the literature it is known that in the thermodynamic limit it is π . This result is extended in this thesis where we show it is π for all chain lengths.

The AKLT state can be written as an exact MPS of bond dimension $\chi = 2$. The local Hilbert space of each site consists of three spin-1 states and, with periodic boundary conditions, each site is equivalent. The AKLT is defined by the three matrices

$$\begin{aligned} M^{[n]+1} &= \sqrt{\frac{2}{3}} \begin{pmatrix} 0 & 0 \\ 1 & 0 \end{pmatrix}, & M^{[n]0} &= \frac{1}{\sqrt{3}} \begin{pmatrix} 1 & 0 \\ 0 & -1 \end{pmatrix}, \\ M^{[n]-1} &= \sqrt{\frac{2}{3}} \begin{pmatrix} 0 & -1 \\ 0 & 0 \end{pmatrix}. \end{aligned} \quad (4.6)$$

which are the same for all sites $1 < n < N$ in the bulk (see Fig. 4.1(d)).

The ideas behind the AKLT state and its generalisations are widely used to understand more complicated condensed matter systems [53], and used as well as computational tools [54]. The one-dimensional AKLT state can also be generalized to two-dimensional lattices [55]. The particular case we will consider in Section 4.3 is the AKLT state on a hexagonal lattice with a spin-3/2 degree of freedom at each site. It can be constructed using entangled pairs of spin-1/2 states projected to the appropriate subspace. Hence the 2D AKLT state can be represented as a 2D PEPS with dimension $D = 2$ [43]. This state was shown to be a universal resource for measurement-based quantum computation [24].

4.2 The 1D AKLT state in the ZXH-calculus

We now have all we need to show how the AKLT state is represented in the ZXH-calculus and can progress in the manner first outlined in [33]. We start by representing the singlet operator $|01\rangle - |10\rangle$ of Fig. 4.1(a). Note that the Bell state $|00\rangle + |11\rangle$ is related to the singlet state by application of a Pauli Z and X on one of its qubits. Hence, the operator in ZXH is:

$$\begin{array}{c} \text{Diagram:} \\ \text{A green circle with } \pi \text{ and a red circle with } \pi \text{ connected by a horizontal line, with a curved line above it.} \end{array} = |01\rangle - |10\rangle. \quad (4.7)$$

4. Diagrammatic reasoning for condensed matter physics

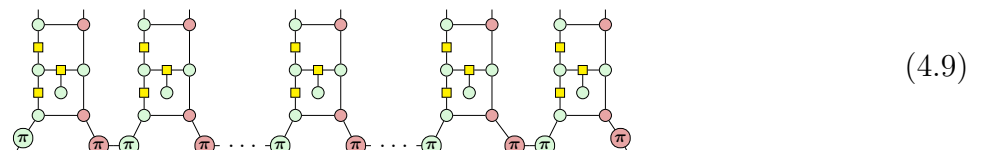
Indeed, an empty curved wire (commonly referred to as a ‘cup’ in the ZX-calculus literature) is the Bell state $|00\rangle + |11\rangle$. If we then apply a Z π -phase ($|0\rangle\langle 0| + e^{i\pi}|1\rangle\langle 1|$) to the first (upper) qubit we get $|00\rangle - |11\rangle$. Applying a NOT gate (an X π -phase) on the second (lower) qubit we then get $|01\rangle - |10\rangle$ as desired.

The next operator we need to represent is the symmetriser on two spin-1/2 spaces. We encode the spin-1 state $|+1\rangle$ as the paired spin-1/2 state $|00\rangle$, the spin-1 state $|0\rangle$ as $\frac{|01\rangle+|10\rangle}{\sqrt{2}}$ and $| -1\rangle$ as $|11\rangle$. This is a convenient basis for us, and indeed the projector operator in Fig. 4.1(b) acts as the identity on this basis. In fact, the only function of the operator Fig. 4.1(b) is to project away the $|01\rangle - |10\rangle$ state, which reduces the basis $\{|00\rangle, \frac{|01\rangle+|10\rangle}{\sqrt{2}}, \frac{|01\rangle-|10\rangle}{\sqrt{2}}, |11\rangle\}$ into a three-dimensional space with basis $\{|00\rangle, \frac{|01\rangle+|10\rangle}{\sqrt{2}}, |11\rangle\}$. We can represent the projection operator as a ZXH-diagram as follows:

$$\frac{1}{2} \quad \begin{array}{c} \text{---} \bullet \text{---} \text{---} \bullet \text{---} \text{---} \\ | \quad | \quad | \quad | \quad | \quad | \\ \text{---} \circ \text{---} \text{---} \text{---} \text{---} \text{---} \\ | \quad | \quad | \quad | \quad | \quad | \\ \text{---} \circ \text{---} \text{---} \text{---} \text{---} \text{---} \end{array} = \begin{pmatrix} 1 & 0 & 0 & 0 \\ 0 & \frac{1}{2} & \frac{1}{2} & 0 \\ 0 & \frac{1}{2} & \frac{1}{2} & 0 \\ 0 & 0 & 0 & 1 \end{pmatrix}. \quad (4.8)$$

Indeed, this can be shown by checking its action on each of the basis states in $\{|00\rangle, \frac{|01\rangle+|10\rangle}{\sqrt{2}}, \frac{|01\rangle-|10\rangle}{\sqrt{2}}, |11\rangle\}$ or composing the matrices presented in (2.8) and (2.24). We leave this as an exercise for the reader. Note how this diagram is symmetric under interchange of the inputs and outputs (i.e. under a horizontal flip), and hence we will generally not care about its orientation in our diagrams. Notice that this operator is in fact equivalent to the 2 wire symmetriser of the previous chapter (3.10).

In Figure 4.1 we summarise our construction of the one-dimensional AKLT state as a ZXH-diagram. We show the diagrammatic representation of its constituents, the singlet (Fig. 4.1(a)) and the projector (Fig. 4.1(b)). The ZXH-diagram of the 1D AKLT state is obtained by joining these in a (periodic) chain, as shown in Fig. 4.1(f). This diagram consists of repetitions of the same block which is built out the symmetriser projector (4.8) (Fig. 4.1(b)) and singlets (4.7) (Fig. 4.1(a)):



4.2. The 1D AKLT state in the ZXH-calculus

We can show explicitly how the ZXH-diagrammatic representation and the MPS representation of the AKLT state are connected. In Fig. 4.1(f) we have overlaid a gray box over the part of the ZXH-diagram that encodes the MPS matrices given in (4.6), as we now show.

Recall that we represent the spin-1 $|+1\rangle$ state as $|00\rangle$ on a pair of spin-1/2 wires. If we apply this state, given by the first diagram in Eq. (2.12), to one of the sites of (4.9), we get a diagram that can be drastically simplified and be shown to be equal as a matrix to $M^{[n]+1}$ up to a scalar factor of $\frac{1}{\sqrt{6}}$:

$$\begin{aligned}
 & \text{Diagram (2.18):} \\
 & \text{Diagram (2.18)} = \frac{1}{2\sqrt{2}} \text{Diagram (c)} = \frac{1}{2\sqrt{2}} \text{Diagram (f)} = \frac{1}{2\sqrt{2}} \text{Diagram (2.17)} \\
 & \text{Diagram (2.17)} = \frac{1}{2} \text{Diagram (ex)} = \frac{1}{2} \text{Diagram (f)} = \text{Diagram (f)} \\
 & = 2 \begin{pmatrix} 0 & 0 \\ 1 & 0 \end{pmatrix} = \frac{1}{\sqrt{6}} M^{[n]+1}
 \end{aligned} \tag{4.10}$$

As we are plugging $|00\rangle$ into the top wires, we start with a scalar $\frac{1}{2}$ as shown in (2.4). Note that in the last diagrammatic step we used that a Z-spider with no legs is equal to a scalar 2. The reason we keep track of scalars here is to recover the MPS representation it is important that the matrices are scaled correctly with respect to each other.

We now proceed analogously, showing that if we plug the two remaining spin-1 states, $|0\rangle$ and $| -1\rangle$, into one of the sites of (4.9) that we get the corresponding MPS matrices up to the same scalar factor of $\frac{1}{\sqrt{6}}$. First, we obtain $M^{[n]0}$ by plugging $\frac{1}{\sqrt{2}}(|01\rangle + |10\rangle)$, which corresponds to the $|0\rangle$ spin-1 state:

$$\begin{aligned}
 & \text{Diagram (2.17)} = \frac{1}{2\sqrt{2}} \text{Diagram (f)} = \frac{1}{2\sqrt{2}} \text{Diagram (c)} = \frac{1}{2\sqrt{2}} \text{Diagram (2.17)} \\
 & \text{Diagram (2.17)} = \frac{1}{\sqrt{2}} \text{Diagram (ab)} = \sqrt{2} \text{Diagram (id)} = \sqrt{2} \begin{pmatrix} 1 & 0 \\ 0 & -1 \end{pmatrix} = \frac{1}{\sqrt{6}} M^{[n]0}
 \end{aligned} \tag{4.11}$$

4. Diagrammatic reasoning for condensed matter physics

And similarly, we obtain $M^{[n]-1}$:

$$\begin{aligned}
 & \text{(ex)} \quad \text{(f)} \quad = \quad \frac{1}{2} \quad \text{(2.17)} \quad \text{(c)} \quad \text{(f)} \quad = \quad -\frac{1}{2} \quad \text{(2.18)} \quad \text{(c)} \quad \text{(f)} \quad = \quad -1 \\
 & \quad \quad \quad = \quad \frac{1}{2} \begin{pmatrix} 0 & -1 \\ 0 & 0 \end{pmatrix} \quad = \quad \frac{1}{\sqrt{6}} M^{[n]-1}
 \end{aligned}
 \quad (4.12)$$

Note here that the last instance of (c) introduced a $e^{i\pi} = -1$ scalar.

As summarized in Fig. 4.1(e), Eqs. (4.10), (4.11) and (4.12) show that the ZXH representation encodes the same information as the MPS representation Eq. (4.6), up to a global factor that can be fixed by normalising the state. We can conclude that our ZXH-diagram is indeed equal to the AKLT state. The advantage of the ZXH representation is that we can compute with it diagrammatically, as we will now show.

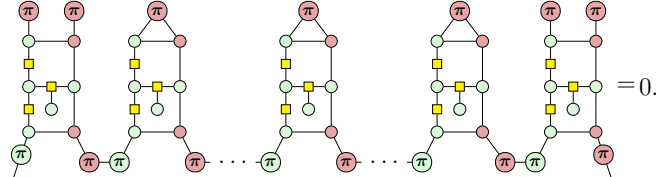
From the ZXH-diagram of the 1D AKLT state in Eq. (4.9) and Fig. 4.1(f) we can immediately infer one of its two main properties: the presence of spin-1/2 edge states under open boundary conditions. Observe that the finite chain Eq. (4.9) has two dangling wires at the bottom on the left and on the right. The precise way of ending the chain amounts to a choice in boundary conditions, as in a conventional MPS, which fixes the edge two-dimensional spin-1/2 degrees of freedom [56]. If the boundary condition is not fixed, the dangling edge wires can be understood as the projective (or fractionalized) symmetry representation of the bulk spin-1 rotation symmetry [57].

The second property of the AKLT state, the non-zero string order parameter, can be shown by direct computation on its ZXH-diagram as follows. We take L sites in a chain, and we post-select each of the physical indices on the sites $2, 3, \dots, L - 1$ to the state $|0\rangle$:

(4.13)

4.2. The 1D AKLT state in the ZXH-calculus

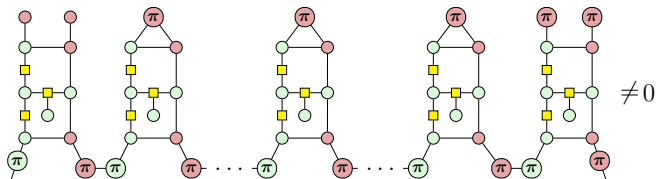
The non-vanishing of the string order parameter then tells us that the sites 1 and L cannot then both be in the spin $+1$ or spin -1 state. On the level of the diagram we can see this behaviour when we post-select both of the states j_1 and j_L to the same non-zero spin state:



$$(4.14)$$

That this diagram is zero tells us that the spin configuration where j_1 and j_L are equal is not part of the AKLT state.

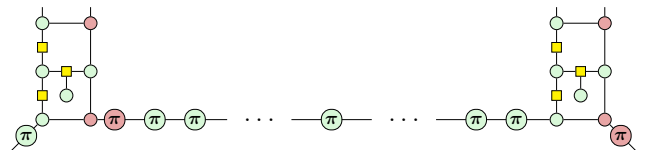
In contrast, when $j_1 \neq j_L$ we get



$$(4.15)$$

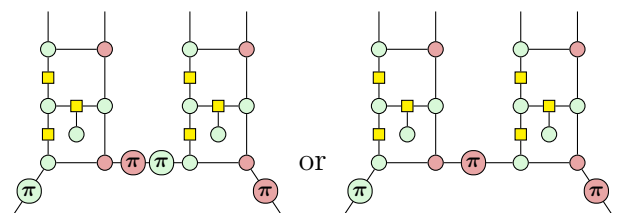
Hence, the configuration where $j_1 \neq j_L$ is part of the AKLT state. These results signify the dilute anti-ferromagnetic order characteristic of the 1D AKLT state.

While one could use software such as the PyZX PYTHON package [29] to simplify the diagrams above to show that these diagrams are indeed (non-)zero, it is illustrative to rewrite the diagram manually. Note that the central repeated building block, consisting of the projection to the spin-1 subspace followed by a post-selection for the $|0\rangle$ spin-1 state, is exactly the diagram we simplified in (4.11). Hence, (4.13) simplifies to:



$$(4.16)$$

Note that this diagram is only equal to (4.13) up to non-zero scalar, but as we only care about whether the coming diagrams are zero or not, this is enough for our purposes. Depending on the number of repetitions of the central block this diagram simplifies to one of the following:



$$(4.17)$$

4. Diagrammatic reasoning for condensed matter physics

Whether this middle Z phase appears depends on whether there are an even or odd number of intermediate $|0\rangle$ states applied - giving a $Z\pi$ -phase in the former case and none in the latter. Now suppose we take $j_1 = j_L = |+1\rangle$. Then we get the following diagram and simplification:

(4.10) \propto (4.18)

A spider with a phase π with no legs is equal to $1 + e^{i\pi} = 1 - 1 = 0$, and hence this is indeed zero as we expect. The case where we take $j_1 = j_L = |-1\rangle$ is shown similarly. Now when we set $j_1 \neq j_L$, for instance, $j_1 = |-1\rangle$ and $j_L = |+1\rangle$ we get a non-zero diagram:

(4.10) \propto (4.19)

Indeed, as the scalar red spider we get is equal to 2, this diagram is indeed non-zero.

To summarise: we started with the 1D AKLT chain (4.9). We then post-selected an arbitrary number of adjacent sites to the spin-1 $|0\rangle$ state, resulting in the diagram (4.13) which we simplified to one of the diagrams in (4.17) depending on the parity of the number of $|0\rangle$ sites. Then, in Eq. (4.18) we saw that post-selecting the j_1 and j_L sites to be equal but non-zero spins resulted in a zero diagram. However, in (4.19) we saw that post-selecting the j_1 and j_L sites to be different non-zero spins resulted in a non-zero diagram. These observations signal the non-vanishing of the anti-ferromagnetic string order, as expected for the AKLT state.

The calculations presented in this section are also available in the accompanying Jupyter notebook made for the paper this section originates from [33].⁴

4.2.1 Aside on the form of the diagrams for the 1D AKLT state

Notice that the symmetric subspace encoding for two wires of (3.10) seems to give an alternative form of the symmetrising projection given in (4.8). They can however be shown to be equal, up

⁴Click here to see the relevant Jupyter notebook.

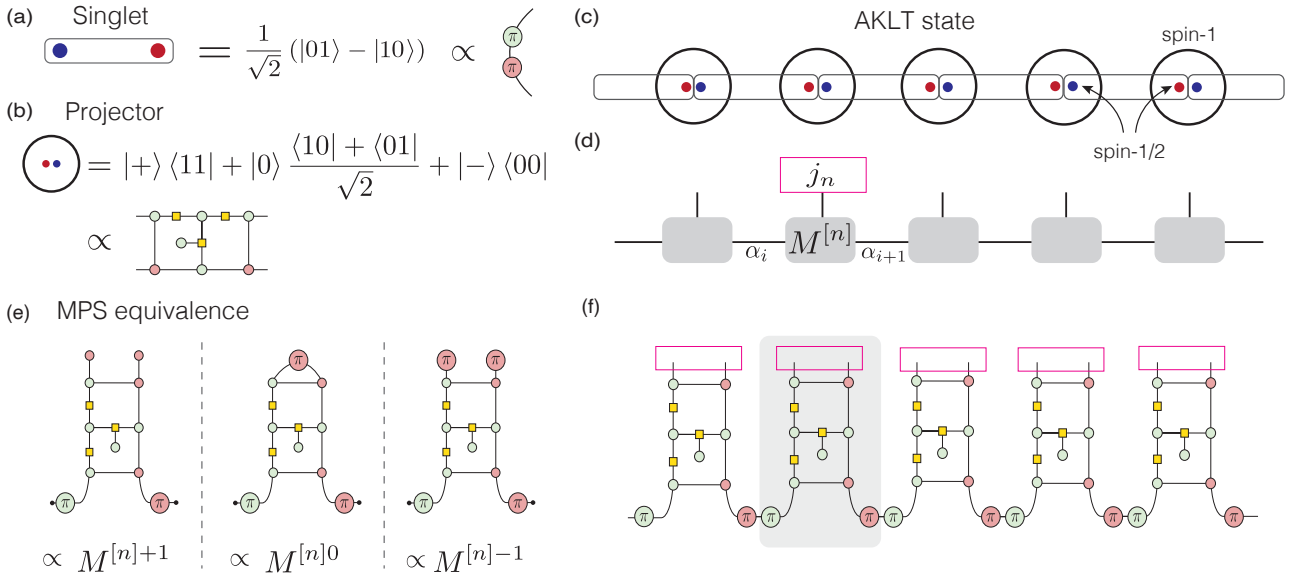


Figure 4.1: ZXH representation of the AKLT state. (a) and (b) show the singlet and symmetric projector and their ZXH representation. These are the basic building blocks of the 1D AKLT state, shown pictorially in (c). (d) gives the MPS representation of the 1D AKLT state, while (f) gives its ZXH representation, which consists of the components in (a) and (b). The shaded gray square in (f) highlights the part of the diagram from which one obtains the three MPS matrices $M^{[n]+1}$, $M^{[n]0}$, and $M^{[n]-1}$ needed for the AKLT state. The diagrams of these matrices are shown in (e), and are obtained by fixing the physical index (highlighted by the magenta rectangles in (f)).

to an irrelevant scalar:

$$\begin{array}{c}
 \text{(b)} \propto \text{Diagram} \\
 \text{(b)} \propto \text{Diagram} \quad (2.17) \propto \text{Diagram} \\
 \text{(b)} \propto \text{Diagram} = \text{Diagram} \quad \text{(ho)} \propto \text{Diagram}
 \end{array} \tag{4.20}$$

and as such our 1D AKLT chain (cf. Eq. (4.9)) can alternatively be written as:

$$\dots \text{Diagram} \dots \text{Diagram} \dots \text{Diagram} \dots \tag{4.21}$$

Where the projector now is of the form (3.10).

Note that there are modified versions of the ZX-calculus where a wire carries a three-dimensional Hilbert space [58, 59]. However, much less is known about rewriting those diagrams, and it is harder to reason about the types of diagrams we have in this thesis where we mix systems of different types of spins.

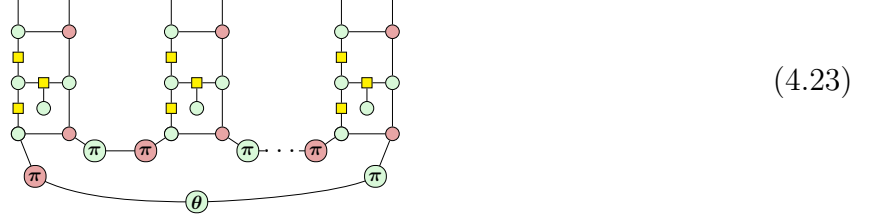
4.2.2 Quantized Berry phase

We now show how to calculate the Berry phase for the 1D AKLT state [51] diagrammatically, obtaining an exact result for any finite chain. To calculate the Berry phase one introduces a phase twist within a given bond (a phase in our case, but a unitary matrix in general). For the periodic 1D AKLT state, this amounts to picking one singlet of the AKLT state $|\psi\rangle$ and transforming it to $|10\rangle - e^{i\theta}|01\rangle$. This defines a twisted AKLT state $|\psi_\theta\rangle$ for each angle θ and we recover the standard 1D AKLT state when $\theta = 0$ [51]. The Berry phase is then defined as

$$\gamma = -i \int_0^{2\pi} \frac{\langle \psi_\theta | \partial_\theta | \psi_\theta \rangle}{\langle \psi_\theta | \psi_\theta \rangle} d\theta, \quad (4.22)$$

where we have used the expression for an unnormalised wavefunction (see e.g.[60]) in terms of the normalisation factor $\langle \psi_\theta | \psi_\theta \rangle$.

To calculate this value diagrammatically we start by writing the twisted AKLT state $|\psi_\theta\rangle$ as a ZXH diagram:



To obtain the Berry phase we need to take the derivative of this diagram. For this we could use the techniques for diagrammatic differentiation described in [61, 62]. For our purposes however it suffices to derive a couple of simple equations which can then be described as diagrams. In particular we will need the following diagram equality:

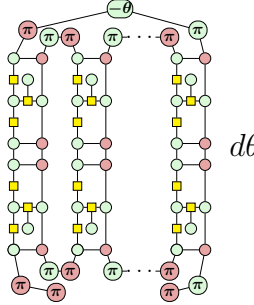
$$\partial_\theta -\theta- = \partial_\theta (|0\rangle \langle 0| + e^{i\theta} |1\rangle \langle 1|) = \frac{ie^{i\theta}}{2} -\pi- \pi- \quad (4.24)$$

Here the factor of $\frac{1}{2}$ is introduced because single-wire spiders are equal to states up to a constant $\sqrt{2}$. Using this identity we get:

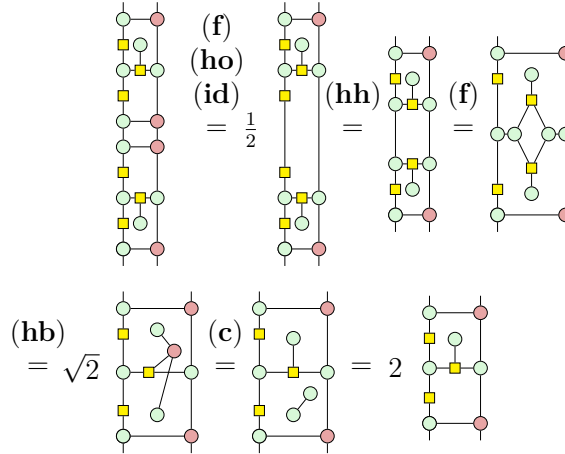
$$\partial_\theta |\psi_\theta\rangle = \frac{ie^{i\theta}}{2} -\pi- \pi- \quad (4.25)$$

4.2. The 1D AKLT state in the ZXH-calculus

We then have the integrand of the unnormalised Berry phase over which we must integrate:

$$\gamma = (-i) \int_0^{2\pi} \frac{ie^{i\theta}}{2 \langle \psi_\theta | \psi_\theta \rangle} d\theta \quad (4.26)$$


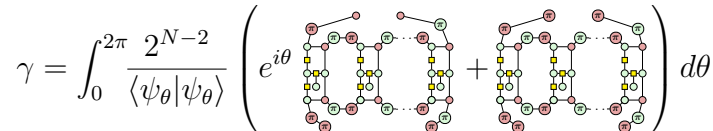
We can simplify this expression somewhat by combining the adjacent symmetrisers:

$$\begin{aligned} & \text{(f)} \quad \text{(ho)} \quad \text{(id)} = \frac{1}{2} \quad \text{(hh)} = \quad \text{(f)} = \\ & \text{(hb)} = \sqrt{2} \quad \text{(c)} = \quad 2 \end{aligned} \quad (4.27)$$


Now, in order to calculate the expression of (4.26) we split the diagram there up into two terms, using the following identity:

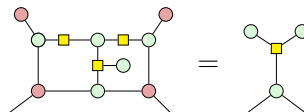
$$-\theta- = |0\rangle\langle 0| + e^{i\theta}|1\rangle\langle 1| \frac{1}{2} -\bullet\bullet- + \frac{e^{i\theta}}{2} -\pi\pi- \quad (4.28)$$

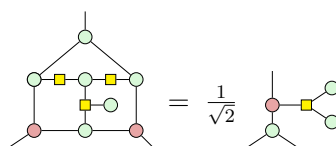
So, using (4.27) and (4.28) in (4.26) we arrive at:

$$\gamma = \int_0^{2\pi} \frac{2^{N-2}}{\langle \psi_\theta | \psi_\theta \rangle} \left(e^{i\theta} \text{Diagram A} + e^{i\theta} \text{Diagram B} \right) d\theta \quad (4.29)$$


Here N is the length of the chain and the 2^N term comes from repeated application of (4.27).

To arrive at an equation for all N we must decompose our diagrams in some systematic scalable fashion. To this end we use the following identities (see Appendix C.0.1 for the proofs):

$$\text{Diagram A} = \text{Diagram C} \quad (4.30)$$


$$\text{Diagram B} = \frac{1}{\sqrt{2}} \text{Diagram D} \quad (4.31)$$


4. Diagrammatic reasoning for condensed matter physics

$$\begin{array}{c} \text{Diagram 1} \\ \text{Diagram 2} \end{array} = \begin{array}{c} \text{Diagram 3} \\ \text{Diagram 4} \end{array} \quad (4.32)$$

We can similarly derive:

$$\begin{array}{c} \text{Diagram 5} \\ \text{Diagram 6} \end{array} = \begin{array}{c} \text{Diagram 7} \\ \text{Diagram 8} \end{array} \quad (4.33)$$

See (C.4) for the proof (and note that they are mirror images of each other). Now let's simplify the first term in the integrand of (4.29). We do this by repeatedly applying (4.33):

$$\begin{array}{c} \text{Diagram 9} \\ \text{Diagram 10} \end{array} = \begin{array}{c} \text{Diagram 11} \\ \text{Diagram 12} \end{array} \quad (4.33)$$

$$\begin{array}{c} \text{Diagram 11} \\ \text{Diagram 12} \end{array} = -1 \begin{array}{c} \text{Diagram 13} \\ \text{Diagram 14} \end{array} \quad (\pi c)$$

$$\begin{array}{c} \text{Diagram 13} \\ \text{Diagram 14} \end{array} = (-1)^{N-1} \begin{array}{c} \text{Diagram 15} \\ \text{Diagram 16} \end{array} \quad (\pi c)$$

$$\begin{array}{c} \text{Diagram 15} \\ \text{Diagram 16} \end{array} = (-1)^N \begin{array}{c} \text{Diagram 17} \\ \text{Diagram 18} \end{array} \quad (4.34)$$

Hence, this is equal to: $4(-1)^N$. We can similarly simplify the second term in the integrand by using Eqs. (4.30), (4.31) and (4.32):

$$\begin{array}{c} \text{Diagram 19} \\ \text{Diagram 20} \end{array} = \begin{array}{c} \text{Diagram 21} \\ \text{Diagram 22} \end{array} \quad (4.30)$$

$$\begin{array}{c} \text{Diagram 21} \\ \text{Diagram 22} \end{array} = \begin{array}{c} \text{Diagram 23} \\ \text{Diagram 24} \end{array} \quad (4.31)$$

$$\begin{array}{c} \text{Diagram 23} \\ \text{Diagram 24} \end{array} = \frac{1}{\sqrt{2}} \begin{array}{c} \text{Diagram 25} \\ \text{Diagram 26} \end{array} \quad (4.31)$$

$$\begin{array}{c} \text{Diagram 25} \\ \text{Diagram 26} \end{array} = \frac{1}{\sqrt{2^{N-2}}} \begin{array}{c} \text{Diagram 27} \\ \text{Diagram 28} \end{array} \quad (4.32)$$

$$\begin{array}{c} \text{Diagram 27} \\ \text{Diagram 28} \end{array} = \frac{1}{\sqrt{2^{N-2}}} \begin{array}{c} \text{Diagram 29} \\ \text{Diagram 30} \end{array} \quad (4.35)$$

So the value is:

$$\frac{1}{\sqrt{2^{N-2}}} \begin{array}{c} \text{Diagram 31} \\ \text{Diagram 32} \end{array} \quad (4.36)$$

We can fuse all the red spiders and then, using the equality $|0\rangle = \frac{1}{\sqrt{2}}(|+\rangle + |-\rangle)$, we can reduce it to a sum of two simpler diagrams:

$$\begin{aligned}
 & \text{Diagram (f) shows a tree structure with a root node labeled } \text{a}\pi \text{ (red circle). The left part of the equation shows the tree with a yellow square node at the root. The right part shows the tree with a yellow square node at the root, followed by a red circle node labeled } \text{b}\pi \text{ (red circle).} \\
 & \text{The equation is:} \\
 & (\pi\mathbf{c}) = \frac{1}{\sqrt{2}^N} \text{Diagram (f)} + \frac{1}{\sqrt{2}^N} (-1)^N c \text{Diagram (f)} \\
 & = \frac{1}{\sqrt{2}^N} c (6^N + (-2)^N) = 2(3^N + (-1)^N)
 \end{aligned} \tag{4.37}$$

Here $a \in \{0, 1\}$ depends on whether N is even ($a = 0$) or odd ($a = 1$), and we write $c = \left(\frac{1}{\sqrt{2}}\right)^{N-2} = \frac{2}{\sqrt{2}^N}$.

Now that we know the value of the two terms of the integrand of equation 4.29, it remains to calculate the normalisation factor $\langle \psi_\theta | \psi_\theta \rangle$. We first simplify the diagram by combining symmetrisers using (4.27) and then decompose the θ -labelled spiders using (4.28) twice to get the normalisation factor:

Each of the four diagrams we get we have already calculated the value of. The diagrams for $a = b = 0$ and $a = b = 1$ are equal to that in (4.35), while the other two are equal to those in (4.34). Hence:

$$\begin{aligned}
|\psi_\theta\rangle\langle\psi_\theta| &= \frac{1}{4}2^N((e^{i\theta} + e^{-i\theta}) \cdot 4(-1)^N + 2 \cdot 2(3^N + (-1)^N)) \\
&= 2^N(2(-1)^N \cos \theta + 3^N + (-1)^N)
\end{aligned} \tag{4.39}$$

It is simple to check that for $\theta = 0$ the norm can be rewritten as $6^N + 3(-2)^N = (\sqrt{6})^{2N}(1 + 3(-1/3)^N)$, which coincides with the usual AKLT normalisation (see e.g. below equation (90) in [63]) up to the prefactor $(\sqrt{6})^{2N}$. This different prefactor is the same $\sqrt{6}$ factor as seen in Eqs. (4.10), (4.11) and (4.12).

4. Diagrammatic reasoning for condensed matter physics

Combining Eqs. (4.39), (4.34) and (4.35) the Berry phase is given by

$$\gamma = \int_0^{2\pi} \frac{2^{N-2} (4(-1)^N e^{i\theta} + 3^N + (-1)^N)}{2^N (2(-1)^N \cos \theta + 3^N + (-1)^N)} d\theta \quad (4.40)$$

$$= \frac{1}{2} \int_0^{2\pi} \frac{2(-1)^N e^{i\theta} + 3^N + (-1)^N}{2(-1)^N \cos \theta + 3^N + (-1)^N} d\theta \quad (4.41)$$

Now, factor out the term $3^N + (-1)^N$ from the fraction and define the constant

$$g = \frac{2(-1)^N}{3^N + (-1)^N}. \quad (4.42)$$

We then see that

$$\begin{aligned} \gamma &= \frac{1}{2} \int_0^{2\pi} \frac{g e^{i\theta} + 1}{g \cos \theta + 1} d\theta = \frac{1}{2} \int_0^{2\pi} \frac{g \cos \theta + i g \sin \theta + 1}{g \cos \theta + 1} d\theta \\ &= \frac{1}{2} \left(\int_0^{2\pi} 1 d\theta + \int_0^{2\pi} \frac{i g \sin \theta}{(1 + g \cos \theta)} d\theta \right) \\ &= \frac{1}{2} (2\pi + 0) = \pi \end{aligned} \quad (4.43)$$

Here the second integral evaluates to zero because it is an odd function. We thus arrive to $\gamma = \pi$ as was already known in the thermodynamic limit, but which here is shown to hold for all finite lengths [51].

4.3 The 2D AKLT state as a universal resource for quantum computing

We will now study the generalization of the 1D AKLT state to the 2D hexagonal lattice [22], depicted in Fig. 4.2(a). First, we derive the representation of this state as a ZXH-diagram, and then we show how it can be used as a universal resource for quantum computing, by showing that it reduces to a graph state.

It is possible to construct an AKLT type state on a hexagonal lattice using spin-3/2 degrees of freedom at each site (Fig. 4.2(a)). Each spin-3/2 degree of freedom corresponds to a four-dimensional Hilbert space and, by the discussion in the previous section, can be represented on a set of three qubit wires with the projector presented in (3.12). So whereas in the 1D AKLT state we projected two spin-1/2 states down to the symmetric subspace to represent a spin-1 degree of freedom, here we project three spin-1/2 degrees of freedom to form a spin-3/2. This

4.3. The 2D AKLT state as a universal resource for quantum computing

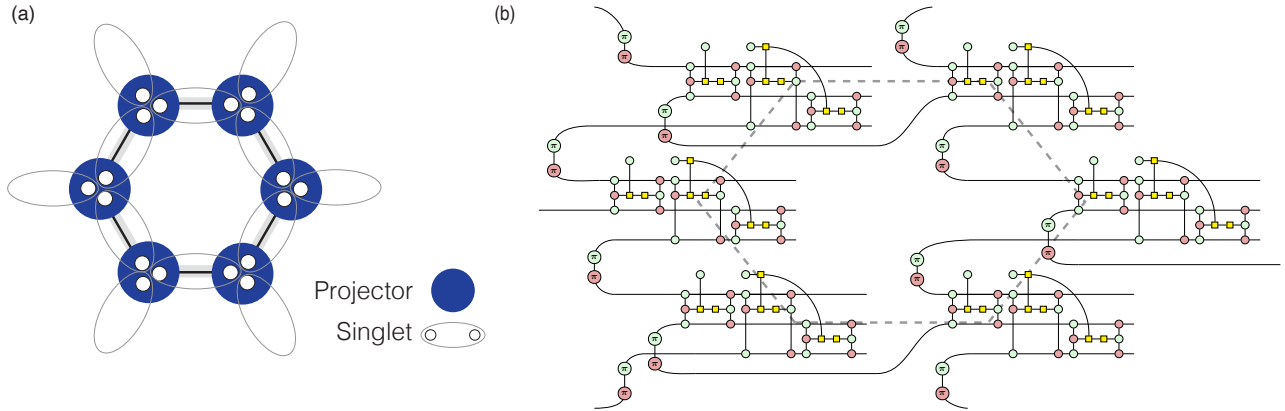
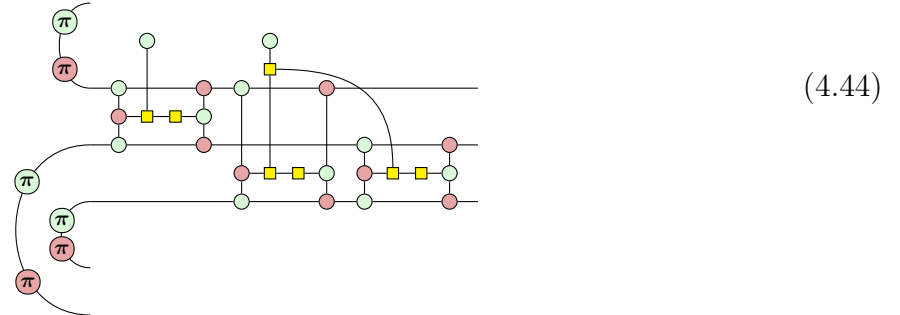


Figure 4.2: The 2D AKLT state on a hexagonal lattice and its representation as a ZXH-diagram. (a) Pictorial representation of the unit cell of the 2D AKLT state on a hexagonal lattice. At each site there is a spin-3/2 degree of freedom that can be decomposed into three spin-1/2 states that form singlets with their nearest neighbours (represented by oval shapes). The blue circles denote projectors to the appropriate symmetric subspace. The gray hexagon denotes a choice of unit cell. (b) The 2D AKLT state unit cell as a ZXH-diagram, with the same unit cell denoted by a gray dotted line.

projector, with each of the component spin-1/2 wires linked to another by singlet states, forms the basic unit (a site) of the 2D AKLT state. As a ZXH-diagram:



Here we have a single spin-3/2 degree of freedom of the 2D AKLT state with singlet states on each of its legs. These can then be combined to give a diagram of a lattice that is not just a convenient visual aid for the 2D AKLT state, but literally *is* the 2D AKLT state; see Figure 4.2(b).

Analogous to the 1D AKLT example in Fig. 4.1 where two wires corresponded to the physical spin-1 state, the triples of wires coming out to the right of (4.44) correspond to the physical spin-3/2 degrees of freedom that form the state. The remaining wires of the diagram should be considered to be connected to other parts in the hexagonal lattice periodically (see Fig. 4.2(b)).

We will now show how a hexagonal lattice AKLT state reduces to a graph state under a suitable measurement of the spin-3/2 degrees of freedom. A consequence of this result is that the 2D

4. Diagrammatic reasoning for condensed matter physics

AKLT state is a universal resource for measurement-based quantum computing [64]. This result was already shown in Ref. [24] and independently in Ref. [65]. The proof in Ref. [24] consists of two parts. First, they showed the hexagonal lattice reduces to a graph state. Second, they used a percolation argument to prove the resulting state is a universal resource for quantum computation. We will derive the first part entirely diagrammatically. In the process we will see that certain derivations concerning the simplification of the lattice presented in Ref. [24] are in our approach just the standard spider fusion rule (**f**) and the Hopf rule (**ho**) of the ZX-calculus.

To reduce the 2D AKLT state to a graph state, we need to reduce it to a simpler state. We do this by measuring each of the spin-3/2 states. Recall that each of these spin-3/2 states is presented as a symmetric three qubit state and hence a measurement on it can be presented as a simultaneous measurement on these three qubits. The measurement is a POVM (Positive operator-valued measurement, the most general type of measurement [66]) with three elements:

$$E_z := \frac{2}{3}(|000\rangle\langle 000| + |111\rangle\langle 111|), \quad (4.45)$$

$$E_x := \frac{2}{3}(|+++ \rangle\langle +++| + |--- \rangle\langle ---|), \quad (4.46)$$

$$E_y := \frac{2}{3}(|iii\rangle\langle iii| + |-i,-i,-i\rangle\langle -i,-i,-i|). \quad (4.47)$$

Here the sets $\{|0\rangle, |1\rangle\}$, $\{|+\rangle, |-\rangle\}$ and $\{|i\rangle, |-i\rangle\}$ denote respectively the eigenbases of the Z , X and Y Pauli matrices. Usually the elements of a POVM should sum up to the identity, but as we are working in the symmetric subspace, we instead have $E_z + E_x + E_y = P_S$, where P_S is the projection on the symmetric subspace, as desired. Notice here that though we are measuring with a POVM as its elements are themselves scaled down projectors the update to the new state from the action of the POVM is same as with a projector up to a scalar.

Conveniently, each of these POVM elements can be represented as a small ZX-diagram (up to global scalar):

$$E_z \propto \begin{array}{c} \text{---} \\ \text{---} \\ \text{---} \end{array} \quad (4.48)$$

$$E_x \propto \begin{array}{c} \text{---} \\ \text{---} \\ \text{---} \end{array} \quad (4.49)$$

$$E_y \propto \begin{array}{c} \text{---} \\ \text{---} \\ \text{---} \end{array} \quad (4.50)$$

4.3. The 2D AKLT state as a universal resource for quantum computing

The forms of E_z and E_x follow directly from the definition of the Z- and X-spider. To see the correctness of E_y note that a Z $\frac{\pi}{2}$ -rotation $R_z(\frac{\pi}{2})$ acts as $R_z(\frac{\pi}{2})|+\rangle = |i\rangle$ and $R_z(\frac{\pi}{2})|-\rangle = |-i\rangle$ where $|\pm i\rangle = |0\rangle \pm i|1\rangle$. Hence, we can see (4.50) as an X-projector surrounded by a basis transformation from the Y eigenbasis to the X eigenbasis. We could have equivalently chosen a Z-projector surrounded by X $\pm\frac{\pi}{2}$ rotations which corresponds to flipping the colours and the signs of the rotations; cf. [67, Section 9.4]. Note that E_y is not symmetric under interchange of inputs and outputs, and thus unlike the case for E_z or E_x , when considering E_y we must keep in mind what we consider an input and output.

Importantly, each of the POVM elements E_z , E_x , E_y projects to a 2D subspace, and hence encodes a spin-1/2 degree of freedom. While we could continue to work with the three output wires as a single qubit with the qubit operations encoded onto the three wires, we will instead represent the collapse to a single spin-1/2 degree of freedom by simply writing one wire:

$$E_z \rightsquigarrow \text{---} \quad (4.51)$$

$$E_x \rightsquigarrow \text{---} \quad (4.52)$$

$$E_y \rightsquigarrow \text{---} \quad (4.53)$$

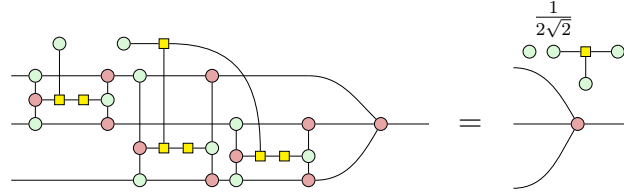
We will use this ‘squigly arrow’ \rightsquigarrow to denote when we make a step that corresponds to a redefinition of the output basis. Here this is a collapse of a two-dimensional degree of freedom spread out over three wires to a single wire, but later on we will also use redefinitions to absorb single qubit gates that appear on output wires. Physically, this corresponds to updating the correspondence between the ‘logical’ or ‘encoded’ $|0\rangle$ and $|1\rangle$, and the actual physical states.

As these POVM elements are symmetric on the three qubits, they are preserved by the projection to the symmetric subspace, a fact we can prove diagrammatically. For instance, considering E_x , we first show that it absorbs a CSWAP gate:

$$\begin{array}{ccccccc}
 \text{(f)} & = & \text{(ho)} & = & \frac{1}{2} & = & \frac{1}{\sqrt{2}} \\
 \text{(ex)} & = & \text{(c)} & = & \frac{1}{\sqrt{2}} & = & \frac{1}{\sqrt{2}}
 \end{array} \quad (4.54)$$

4. Diagrammatic reasoning for condensed matter physics

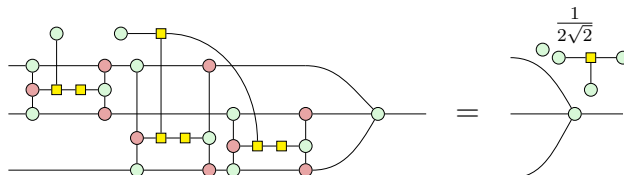
Iterating this three times we then get the following equality:



$$(4.55)$$

The floating scalar diagram on top multiplied by the scalar produced by the sequence of rewrites represents the eigenvalue of this operation under the projection. This scalar is not important for our purposes, and we will drop it implicitly in later diagrams.

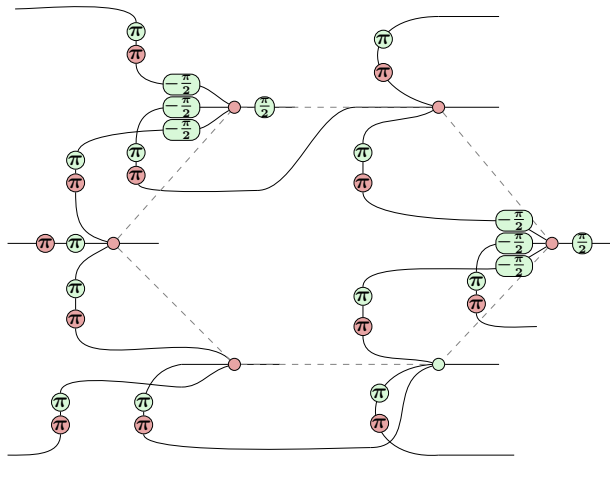
We can do a similar derivation for E_z (see Appendix C.0.2):



$$(4.56)$$

An analogous equation and derivation exists for E_y as well (see Appendix C.0.2).

We started with the 2D AKLT state on a hexagonal lattice (Figure 4.2), and then we measured each of the spin-3/2 states with this POVM $\{E_z, E_x, E_y\}$. Due to equations (4.55) and (4.56) and the analogous one for E_y , we see that regardless of the measurement outcome E_z , E_x or E_y that the symmetrising projector on each spin-3/2 output is ‘consumed’ and replaced by the spider associated to one of E_z , E_x and E_y . Hence, what remains of the 2D AKLT state is a set of singlet states, connected via a network of spiders of the form (4.51)–(4.53). The state resulting from applying this measurement to the 2D AKLT state will hence be a hexagonal lattice where at each site we randomly have a X, Y or Z spider (which depends on the measurement outcome), and these are connected via singlet states. For example, the hexagonal unit cell of Fig. 4.2(b) could be reduced to a diagram like the following:



$$(4.57)$$

4.3. The 2D AKLT state as a universal resource for quantum computing

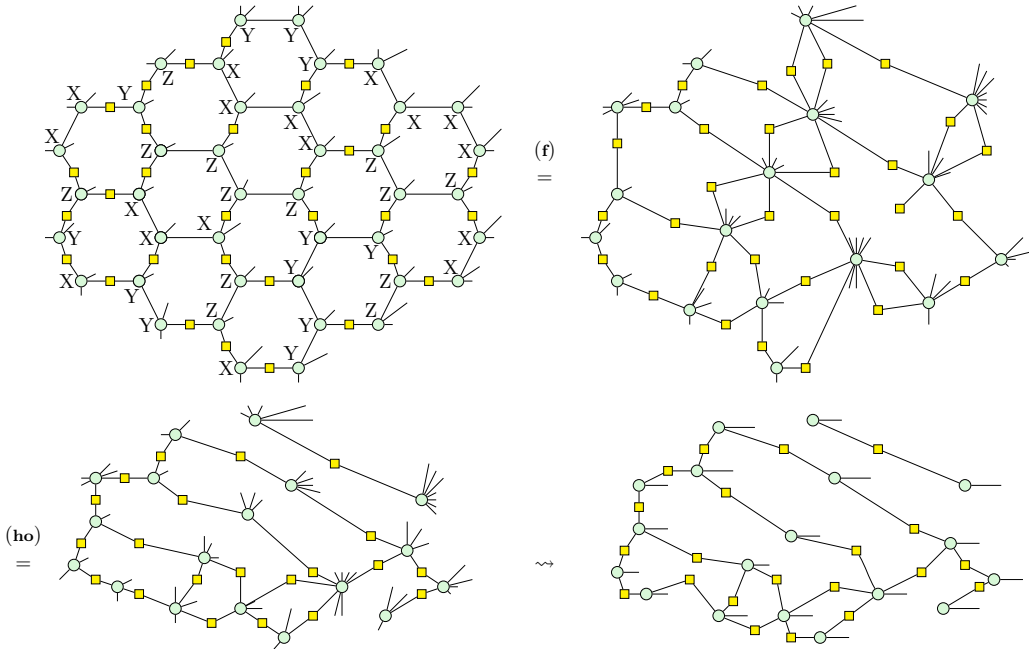


Figure 4.3: This figure shows the AKLT hexagonal lattice *after* the E_x , E_y , and E_z projectors have been applied and the π phases moved onto the external wires and absorbed into basis redefinitions. In the first diagram on the left note that we have added X,Y,Z labels to the Z-spiders. These aren't formally part of the diagram, but are just labels to indicate which projector was applied to reach this diagram. The first equality shows that spiders with the same measurement outcome are merged. Following this, the Hopf rule (ho) is applied to remove pairs of wires with a Hadamard box on them between the same spiders. The final step is to redefine the output basis to collapse multiple output wires coming from the same spider into a single wire. The resulting diagram can indeed be seen to be a graph state. This bears strong resemblance to the diagram seen in [24] (figure 4 diagram C) where now their ad-hoc reduction is describable entirely in quantum-informational terms via the ZXH-calculus.

Readers familiar with the ZX-calculus can easily see that the resulting diagram is a *Clifford diagram*. Indeed, it does not contain any higher-arity H-boxes, and the only phases that appear are multiples of $\frac{\pi}{2}$ making it a ZX-diagram in the Clifford fragment [68]. As it only has outputs, it is a state, and hence is a Clifford state⁵. Any Clifford state can be presented as a graph state with single-qubit Clifford unitaries on its outputs (see Ref. [69], or for a proof using the ZX-calculus, see for instance Refs. [68, 20]). Hence, we can already conclude that the state we get is a graph state.

However, to show that the state we obtain is a universal resource for quantum computing we need to know more about the specific construction of the graph state, so let us go through the derivation manually. This happens in a few steps.

⁵Recall that a Clifford state, also called a *stabiliser state*, is a state that is uniquely determined by being a eigenvalue 1 eigenvector of a set of Pauli operators. Any Clifford state can be represented by a ZX-diagram containing only spiders with phases that are multiples of $\frac{\pi}{2}$.

4. Diagrammatic reasoning for condensed matter physics

The first step is to get rid of the Z and X π -phases arising from the singlet states. We will do this by commuting these phases through the spiders onto the outputs of the state (the spin-3/2 outputs). For instance, for a E_z outcome, we can do the following:

$$\begin{array}{c} \text{---} \text{---} \text{---} \\ | \quad | \quad | \\ \text{---} \text{---} \text{---} \end{array} \xrightarrow{\substack{(\pi\mathbf{c}) \\ (\mathbf{f})}} \begin{array}{c} \text{---} \text{---} \text{---} \\ | \quad | \quad | \\ \text{---} \text{---} \text{---} \end{array} \quad (4.58)$$

Here the site is understood to be in the bulk of the lattice, with the top wire corresponding to its spin-3/2 degree of freedom⁶. Hence, we can remove the internal π phases by moving them onto the external edges. The analogous procedure for E_x and E_y measurement outcomes is demonstrated in Appendix C.0.3.

Since each Z and X π -phase is connected to two spiders we need to make a choice about which way to commute each π . As the hexagonal lattice is two-colourable this is indeed possible in a consistent way.

After this procedure, we will have a diagram where the only π phases are on the spin-3/2 outputs of the states. As discussed beneath (4.53), our choice of representation of the spin-3/2 degree of freedom can be chosen arbitrarily. Hence we can redefine our basis here to remove these π phases (this again corresponds to a redefinition of how we encode the $|0\rangle$ and $|1\rangle$ states on our physical system):

$$\begin{array}{c} \text{---} \text{---} \text{---} \\ | \quad | \quad | \\ \text{---} \text{---} \text{---} \end{array} \rightsquigarrow \begin{array}{c} \text{---} \text{---} \text{---} \\ | \quad | \quad | \\ \text{---} \text{---} \text{---} \end{array} \quad (4.59)$$

The second step is to bring the diagram closer to the form of a graph state as presented in (A.1) by changing the X-spiders coming from E_x and E_y measurement outcomes to Z-spiders. This can be done easily using (2.18), and a redefinition of the output basis to remove the resulting Hadamard:

$$\begin{array}{c} \text{---} \text{---} \text{---} \\ | \quad | \quad | \\ \text{---} \text{---} \text{---} \end{array} \xrightarrow{(2.18)} \begin{array}{c} \text{---} \text{---} \text{---} \\ | \quad | \quad | \\ \text{---} \text{---} \text{---} \end{array} \rightsquigarrow \begin{array}{c} \text{---} \text{---} \text{---} \\ | \quad | \quad | \\ \text{---} \text{---} \text{---} \end{array} \quad (4.60)$$

For the E_y outcomes, we additionally remove the $\frac{\pi}{2}$ phases. For instance:

$$\begin{array}{c} \text{---} \text{---} \text{---} \\ | \quad | \quad | \\ \text{---} \text{---} \text{---} \end{array} \xrightarrow{(\mathbf{f})} \begin{array}{c} \text{---} \text{---} \text{---} \\ | \quad | \quad | \\ \text{---} \text{---} \text{---} \end{array} \rightsquigarrow \begin{array}{c} \text{---} \text{---} \text{---} \\ | \quad | \quad | \\ \text{---} \text{---} \text{---} \end{array} \quad (4.61)$$

⁶For sites that aren't in the bulk of the lattice, the calculation would be slightly different in that phases would pass onto the other external disconnected edges. However, these π phases can be removed by redefining the basis of the external wires.

4.3. The 2D AKLT state as a universal resource for quantum computing

We leave the other cases to the reader. The diagram we have now consists solely of Z-spiders and Hadamards.

Now, the third step of our reduction to a graph state is to fuse all the spiders that can be fused. In practice this means that two adjacent sites that had the same measurement outcome will be fused together. This fusing results in sites that have multiple outputs, which we again collapse to a single output as we did in (4.51)–(4.53). See Figure 4.3 for a demonstration of this procedure.

The final step is to remove parallel Hadamard-edges that could have been introduced by sites that were fused together. To do this we use a variation on the Hopf rule (**ho**):

$$\begin{array}{c} (2.17) \\ (hh) \end{array} \propto \begin{array}{c} (ho) \end{array} \propto \begin{array}{c} (2.18) \end{array} \quad (4.62)$$

The resulting diagram consists of phaseless Z-spiders connected via single Hadamard-edges, and hence is a graph state, as was desired. Note that this entire procedure can also be done in an automated fashion using PyZX [29]; see the accompanying Jupyter notebook.⁷

Because neighbouring sites that have the same measurement outcome get fused, and parallel edges resulting from this fusing get disconnected, the highly regular hexagonal graph will generally collapse to a much less regular and more sparsely connected graph. For example, consider the hexagonal graph given in Figure 4.3 where the vertices are labelled by X, Y , or Z to denote the 2D AKLT state with the E_x, E_y or E_z measurement outcomes, and consider also its reduction with the rules outlined above.

Not any graph state can be used as a universal resource for measurement-based quantum computing. The most canonical example of a universal resource state is the *cluster state* that as a graph is just a regular square tiling. In Ref. [24] it is shown via a percolation argument that given a large enough initial hexagonal lattice the irregular graph state resulting from the measurement of a 2D AKLT state can, with high probability, be further reduced to a cluster state. In particular, they show that the expected connectivity of the graph is above the critical ‘percolation threshold’ [70] which means that it includes a large cluster state subgraph with high probability. Hence, for a large enough lattice we can use, with high probability, the 2D AKLT state to do universal measurement-based quantum computation.

⁷Click here to see the relevant Jupyter notebook.

4. Diagrammatic reasoning for condensed matter physics

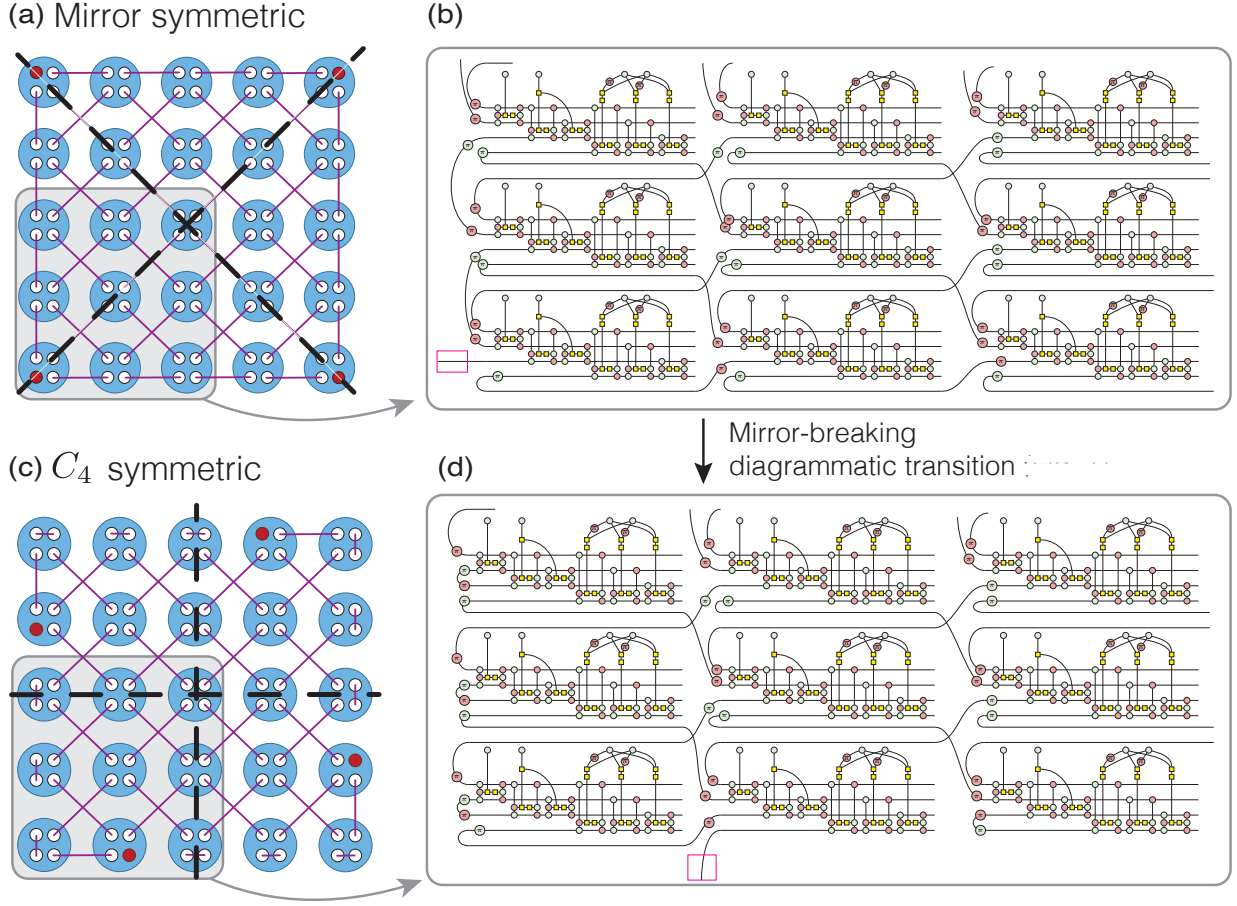


Figure 4.4: (a) A higher-order symmetry-protected topological phase with corner modes protected by mirror symmetries (diagonal dashed black lines). (b) The corresponding ZXH representation of the gray-shaded bottom-left quadrant. (c) When mirror symmetry is broken, C_4 symmetry protects the topological modes, which are then unpinned from the corners, as shown schematically. The transition between a higher-order topological state protected by mirror symmetry to one protected by C_4 symmetry can be modeled diagrammatically in ZXH, see Fig. 4.5, resulting in the ZXH diagram (d). In (b) and (d) the topological modes are dangling wires (marked by the magenta box), and correspond to the red dots in the gray shaded areas in (a) and (c), respectively.

4.4 Crystal symmetries and transitions in ZXH

Symmetries are at the core of our understanding of topological phases as they enrich their classification and simplify the calculation of topological invariants [71, 50, 72, 73, 74]. One remarkable consequence of crystal symmetries, like rotation or mirror symmetries, is that they can protect gapless topological states not only at the boundaries of insulators, but also at the boundary of a boundary. For example, a 2D (respectively 3D) insulator with insulator edges (resp. surfaces) can display protected (resp. hinge) corner modes. These phases, known as higher-order topological insulators [75, 76, 77, 78, 79], can only exist in the presence of crystal symmetries.

4.4. Crystal symmetries and transitions in ZXH

The goal of this section is to diagrammatically represent a transition between topological states with different crystal symmetries. Using mirror and rotational symmetries as a specific example, we will first discuss how to diagrammatically construct states that are symmetric crystal symmetries. This will require that the diagram representing the state is also symmetric, in a way that we will specify shortly. With these states in hand, we will construct a ZXH-diagram that transitions between two states with different crystal symmetries as a function of a control parameter. The possibility of diagrammatic transitions between topological states serves as an example of the potential of diagrammatic reasoning compared to other tensor networks, even for relatively simple states.

Concretely, we consider the higher-order symmetry protected topological state based on the AKLT state shown in Fig. 4.4(a) [77]. Each site represents a spin-2 degree of freedom, which can be decomposed into four spin-1/2 wires. Coupling these spin-1/2s with singlets in the configuration shown pictorially in Fig. 4.4(a) results in four unpaired spin-1/2 degrees of freedom that reside at the corners (red circles). The existence of each one of these unpaired spin-1/2 degrees of freedom is protected by mirror symmetry: they cannot be removed unless mirror symmetry is broken, for example by acting with different local unitary operators at sites related by mirror symmetry.

Constructing this state as a ZXH-diagram is straightforward using our previous discussions. For each site we construct the $n = 4$ symmetriser, as we did in Eq. (3.12) for $n = 3$. Then we connect the sites with singlets in the way specified in Fig. 4.4(a). This results in the diagram shown in Fig. 4.4(b), where we have only shown the lower-left quadrant for clarity. Note that we know that the symmetriser is symmetric under any permutation of its wires, by definition of it representing the symmetriser. Concretely this means it is irrelevant which intra-site wire connects to other sites as all wires within a site are equivalent. Hence, for the purposes of symmetry, any reordering of the connectivity at the individual site level is irrelevant and we need only to concern ourselves with the connectivity between different sites.

So long as we connect sites in a way that respects the desired symmetry (which will be either mirror or rotational symmetry in our example) the diagram will possess the same crystal symmetries as the state it represents. This follows from a general property of ZXH-diagrams. If one constructs a diagram which can be brought to a symmetric form with respect to some lattice

4. Diagrammatic reasoning for condensed matter physics

symmetry, the state that it represents must also have these symmetries. This is the case because the generating elements of the diagram, spiders and H-boxes, are themselves fully-symmetric tensors and thus any symmetry in the relation of the diagrammatic elements is *also* a symmetry of the tensors they represent. Note this does not imply that an asymmetric diagram represents an asymmetric tensor, as it is possible to apply rewrites to one side of a symmetric diagram to remove the diagrammatic symmetry. For instance, our symmetriser diagram is asymmetric, yet represents a symmetric tensor. Note however that because the calculus is complete, there will always be a series of rewrites that transforms a diagram representing a tensor with some symmetry to a diagram with the same symmetry.

Instead of constructing a state with a mirror symmetry, as in Fig. 4.4(a), we can similarly construct a state which has four-fold rotational symmetry; see Fig. 4.4(c). This state also has dangling spin-1/2 states on each side, at positions related by C_4 symmetry. Its corresponding ZXH representation is depicted in Fig. 4.4(d), where once more we only show the lower-left quadrant for clarity.

While a desirable property of ZXH-diagrams is that a symmetric diagram mathematically represents a symmetric state, one might feel that the schematic representations in Fig. 4.4(a) and Fig. 4.4(c) already imply that the states possess the symmetries we are interested in, even if they lack mathematical rigour. The ZXH-representations in and of themselves may then not seem like a sufficient advantage, at least for simple states. The advantage becomes clearer however when we consider what one can do once the states are rigorously defined. As we show next, the ZXH-diagrams allow us to go further than is possible with informal representations. We will show how to model a transition between these two states by diagrammatically breaking the symmetry. It is unclear how one would represent this schematically in a useful way. More importantly, it also goes beyond what one could achieve using other tensor network approaches, which would require explicit knowledge of the tensors that define these states.

Let us now describe how to interpolate between the mirror-symmetric state of Fig. 4.4(a,b) and the C_4 -symmetric state in Fig. 4.4(c,d) using a parametrised ZXH-diagram. Since we are dealing with (at least) C_4 -symmetric states it is sufficient to focus on a quadrant, e.g. the bottom-left quadrant. Our goal will be to break the symmetry by moving the corner mode one site down, from the corner to the edge, along with the relevant inter-site singlets. We can

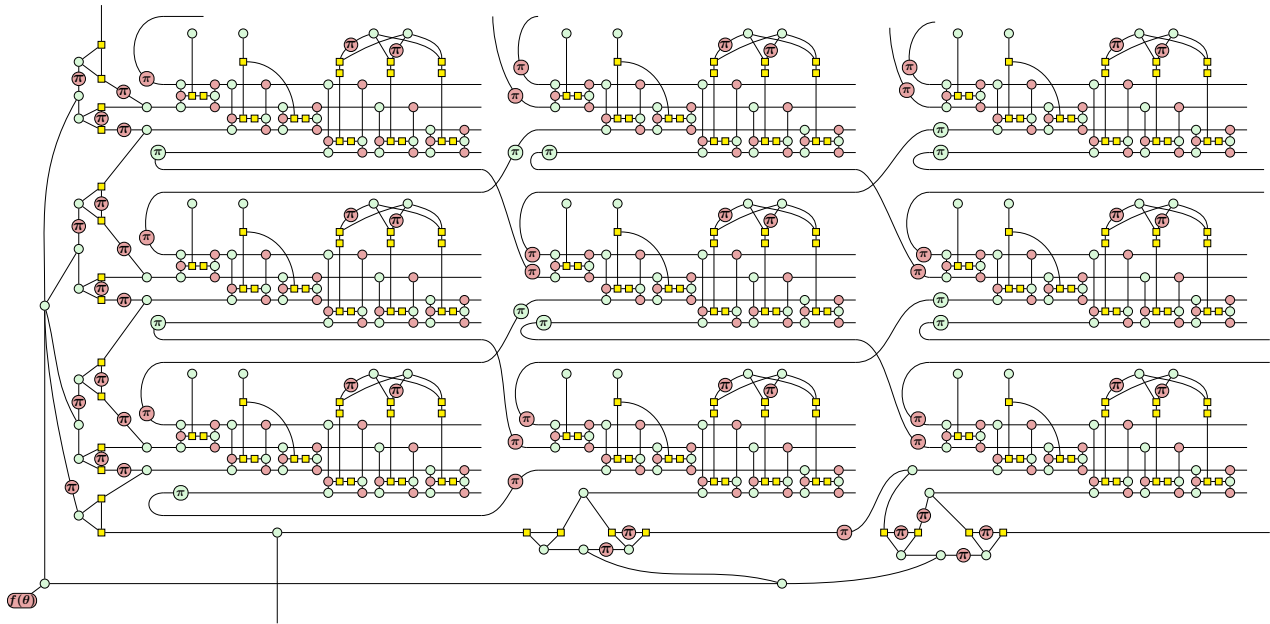


Figure 4.5: A demonstration of a diagrammatic symmetry transition. When $f(\theta) = 0$ (in the bottom-left corner) we recover the mirror-symmetric state of Fig. 4.4(a,b), while if $f(\theta) = \pi$ we recover the C_4 -symmetric state of Fig. 4.4(c,d).

represent the path between these two states by a parametrised ZXH diagram. To do this we will make repeated use of the following diagrammatic element that can represent both a singlet as well as a product state:

$$\begin{array}{c} \text{Diagram element} \\ \text{with } f(\theta) \text{ and } \pi \text{ nodes} \end{array} = \begin{cases} 2\sqrt{2} & \text{when } f(\theta) = 0 \\ 2\sqrt{2} & \text{when } f(\theta) = \pi \end{cases} \quad (4.63)$$

When $f(\theta) = 0$ it disconnects, while for $f(\theta) = \pi$ it generates a singlet between the spiders. These two cases are easily derived by application of **(ex)** and **(ab)**. By iterating this construction we can toggle the connectivity of many singlets at once in a diagram. It is precisely this mechanism that allows us to demonstrate a diagrammatic transition between the two symmetric higher-order symmetry-protected states of Fig 4.4; see Fig 4.5.

For $f(\theta) = 0$ or $f(\theta) = \pi$ we can start to apply **(c)** to push the corresponding X spider through the diagram, where it encounters some π phases to toggle its behaviour for that particular singlet.

4. Diagrammatic reasoning for condensed matter physics

To summarise, we have shown that if a diagram has crystal symmetries, or is built with elements that respect the symmetry, the state the diagram represents has the same symmetries. This allowed us to build a diagram that interpolates, as a function of a control phase, between two different symmetry-protected higher-order topological phases.

4.5 Summary of Condensed Matter Results

What has been shown is that the ZXH calculus can be productively applied to condensed matter physics. Firstly it was shown that one can take the AKLT chain and by representing it as a ZXH diagram demonstrate core properties via diagrammatic reasoning alone such as its dilute antiferromagnetism and edge states. It was also shown that the Berry phase for all chain lengths is π for the AKLT ground state which generalises what was previously known in the literature only in the thermodynamic limit.

It was then shown how one can take the 2D AKLT lattice and use this as a universal resource for quantum computing. While this result was shown previously [24] here the ZXH calculus has simplified the proof to the point it can be automated (see here), up to the stage of the statistical percolation argument at the end which links sufficient size lattices of the kind we derive to cluster states.

Finally it was shown how one can create parametrised diagrams that transition between two different lattice symmetries. In particular this technique was demonstrated for a transition between a lattice with mirror symmetry and a lattice with C_4 symmetry.

It is hoped this will serve as a stepping stone to the extension of the tools of formal diagrammatic languages (beyond mere representations) such as the ZXH calculus and the informational and compositional process based perspective they embody to condensed matter physics.

5

Diagrams for Spin-networks and Wigner symbols

In this section the diagrammatic techniques discussed above will be used to rewrite and unify Penrose's binor calculus, Wigner symbols written as Yutsis diagrams as sometimes seen in quantum chemistry, along with spin-networks of the kind used in loop quantum gravity, all as ZXH diagrams. The latter, while not the strictly the focus of this thesis is a quantum theory of space-time and motivates some of the technical decisions made in representing Spin-networks. As such a brief and wholly incomplete introduction LQG is presented in section 5.3 and while it makes no attempt at novelty, completeness, or rigour, it should serve to connect the dots in a non-trivial manner. This chapter is derived from the associated paper [80] though extends the work there somewhat.

5.1 From Yutsis diagrams to spin-networks

In mathematics the *theory of the representation of the $SU(2)$* is known in physics as the *quantum theory of angular momentum*. The latter has its origins in the early concerns of the first quantum theory about the orbits of electrons around nuclei. In 1960, Yutsis, Levinson and Vanagas¹ published Mathematical Apparatus of the Theory of Angular Momentum [1], which introduced a graphical calculus that we review in this section. This publication presents a form

¹Originally published in Russian although an English version was published in 1962. Their names have been translated from Russian in various ways, but they are Lithuanian, so they can be found as Jucys, Levinsonas and Vanagas[1].

of graphical representation to discuss spin recoupling, which can be described as the tensor product decomposition of higher spin representations into lower ones.

Penrose was soon to introduce another graphical calculation that works for general abstract tensors [21]. In fact, Yutsis diagrams can be integrated into a specific case of Penrose's calculus, called *binor calculus*. The binor calculus was applied by Penrose to propose a home-made model of quantum space-time called spin-networks [81].

5.1.1 Recoupling theory

The irreducible representations (irrep) of $SU(2)$ are labelled by half-integers $j \in \mathbb{N}/2$ dubbed *spins* (see appendix I). The spin- j irrep has dimension $2j + 1$ and is unique up to isomorphism. While there are several ways to actually realise these irreps the decomposition into symmetric subspaces will prove useful. For the specific needs of this part of the thesis practical condensed summary of the details in I is provided with an extension to include a discussion of intertwiners for which the interest is solely limited to this chapter. Recall the definition of the Spin- j irrep.

Spin- j irrep. The fundamental irrep (spin-1/2) is simply the 2×2 matrix multiplication of $SU(2)$ over \mathbb{C}^2 . The higher-spins irreps (spin- j) are then defined over the Hilbert space \mathcal{H}_j ,

$$\mathcal{H}_j \stackrel{\text{def}}{=} \mathcal{S} \underbrace{(\mathbb{C}^2 \otimes \dots \otimes \mathbb{C}^2)}_{2j \text{ copies}}, \quad (5.1)$$

where \mathcal{S} is the *symmetrisation projector* defined as the linear map such that

$$\mathcal{S}(v_1 \otimes \dots \otimes v_{2j}) = \frac{1}{(2j)!} \sum_{\sigma \in \mathfrak{S}_{2j}} U_\sigma (v_1 \otimes \dots \otimes v_{2j}), \quad (5.2)$$

with \mathfrak{S}_{2j} the $2j$ -element permutation group and the permutation unitary

$$U_\sigma (v_1 \otimes \dots \otimes v_{2j}) \stackrel{\text{def}}{=} v_{\sigma(1)} \otimes \dots \otimes v_{\sigma(2j)}. \quad (5.3)$$

The linear action of a group element $u \in SU(2)$ is given by

$$u \cdot (v_1 \otimes \dots \otimes v_{2j}) = (uv_1) \otimes \dots \otimes (uv_{2j}). \quad (5.4)$$

The action of a Lie algebra element, $a \in \mathfrak{su}(2)$, is given as

$$a \cdot (v_1 \otimes \dots \otimes v_{2j}) = \sum_{k=1}^{2j} v_1 \otimes \dots \otimes (av_k) \otimes \dots \otimes v_{2j}. \quad (5.5)$$

5. Diagrams for Spin-networks and Wigner symbols

Let's denote the canonical basis of \mathbb{C}^2 as

$$|0\rangle \stackrel{\text{def}}{=} \begin{pmatrix} 1 \\ 0 \end{pmatrix} \quad |1\rangle \stackrel{\text{def}}{=} \begin{pmatrix} 0 \\ 1 \end{pmatrix}. \quad (5.6)$$

It will be practical for us to also make note of the canonical orthonormal basis of \mathcal{H}_j written as [32]

$$|jm\rangle \stackrel{\text{def}}{=} \sqrt{\frac{(2j)!}{(j+m)!(j-m)!}} \mathcal{S} \underbrace{(|0\rangle \otimes \dots \otimes |1\rangle)}_{j+m \text{ times } |0\rangle}, \quad (5.7)$$

with $m \in \{-j, \dots, j\}$.

As mentioned before irreps are the fundamental elements from which other representations are constructed. Indeed any finite representation of $SU(2)$ is completely reducible, i.e. it can be written as a direct sum of irreps. In particular, a tensor product of irreps can be *decomposed* into a direct sum of irreps, i.e. there exists a bijective *intertwiner* (also known as an *equivariant* map) that maps the tensor product to a direct sum of irreps. It is the goal of *recoupling theory* to study the space of such intertwiners.

Definition 1. Given two representations V and W of a group G , a linear map $\iota : V \longrightarrow W$ is an *intertwiner* when it commutes with the group action, meaning that

$$\iota(g \cdot v) = g \cdot \iota(v) \quad (5.8)$$

for all $g \in G$ and $v \in V$.

In other words, an intertwiner is a natural transformation between two functors (representations) from the group G (seen as a one-element category) to $Hilb$, the category of Hilbert spaces. The set of intertwiners actually forms a vector space which we denote by $\text{Hom}_G(V, W)$.

This space $\text{Hom}_G(V, W)$ is isomorphic to $\text{Inv}_G(V \otimes W^*)$, where W^* is the dual vector space of W [25].

We define the *invariant subspace* for any representation on \mathcal{H} as

$$\text{Inv}_G(\mathcal{H}) \stackrel{\text{def}}{=} \{\psi \in \mathcal{H} \mid \forall g \in G, g \cdot \psi = \psi\}. \quad (5.9)$$

Equivalently, it can be characterised by

$$\text{Inv}_G(\mathcal{H}) = \{\psi \in \mathcal{H} \mid \forall a \in \mathfrak{g}, a \cdot \psi = 0\}. \quad (5.10)$$

5.1. From Yutsis diagrams to spin-networks

Clebsch-Gordan coefficients. The most common example of an intertwiner is the Clebsch-Gordan intertwiner. Given \mathcal{H}_{j_1} and \mathcal{H}_{j_2} , their tensor product $\mathcal{H}_{j_1} \otimes \mathcal{H}_{j_2}$ can be decomposed into a direct sum of irreps with the following equivalence of representations

$$\mathcal{H}_{j_1} \otimes \mathcal{H}_{j_2} \cong \bigoplus_{k=|j_1-j_2|}^{j_1+j_2} \mathcal{H}_k. \quad (5.11)$$

There is a historically preferred bijective intertwiner

$$C : \mathcal{H}_{j_1} \otimes \mathcal{H}_{j_2} \longrightarrow \bigoplus_{k=|j_1-j_2|}^{j_1+j_2} \mathcal{H}_k, \quad (5.12)$$

whose coefficients are called the *Clebsch-Gordan coefficients*

$$C_{j_1 m_1 j_2 m_2}^{jm} \stackrel{\text{def}}{=} \langle jm | C | j_1 m_1; j_2 m_2 \rangle. \quad (5.13)$$

The indices can be read as tensor indices, with $m \in \{-j, \dots, j\}$ labeling a canonical basis of \mathcal{H}_j (and similarly for m_1 and m_2). For all the coefficients we have $C_{j_1 m_1 j_2 m_2}^{jm} \in \mathbb{R}$. We have $C_{j_1 m_1 j_2 m_2}^{jm} = 0$ when the *Clebsch-Gordan conditions* are not satisfied:

$$\begin{aligned} j_1 + j_2 + j &\in \mathbb{N} \\ |j_1 - j_2| &\leq j \leq j_1 + j_2. \end{aligned} \quad (5.14)$$

Additionally, if $m \neq m_1 + m_2$, then also $C_{j_1 m_1 j_2 m_2}^{jm} = 0$. For all the non-zero coefficients we can find analytic expressions. For instance:

$$\begin{aligned} C_{j_1 m_1 j_2 m_2}^{jm} &= \delta_{m, m_1 + m_2} \sqrt{2j + 1} \\ &\times \sqrt{\frac{(j+m)!(j-m)!(-j+j_1+j_2)!(j-j_1+j_2)!(j+j_1-j_2)!}{(j+j_1+j_2+1)!(j_1+m_1)!(j_1-m_1)!(j_2+m_2)!(j_2-m_2)!}} \\ &\times \sum_k \frac{(-1)^{k+j_2+m_2} (j+j_2+m_1-k)!(j_1-m_1+k)!}{(j-j_1+j_2-k)!(j+m-k)!k!(k+j_1-j_2-m)!}. \end{aligned} \quad (5.15)$$

Wigner's $3jm$ -symbol. If the Clebsch-Gordan conditions (5.14) are satisfied, then

$$\dim \text{Inv}_{\text{SU}(2)}(\mathcal{Q}_{j_1} \otimes \mathcal{Q}_{j_2} \otimes \mathcal{Q}_{j_3}) = 1. \quad (5.16)$$

The unit vector in this subspace, unique up to a phase, is denoted

$$|j_1, j_2, j_3\rangle = \sum_{m_1, m_2, m_3} \begin{pmatrix} j_1 & j_2 & j_3 \\ m_1 & m_2 & m_3 \end{pmatrix} \bigotimes_i |j_i m_i\rangle = |00\rangle. \quad (5.17)$$

5. Diagrams for Spin-networks and Wigner symbols

with

$$\begin{pmatrix} j_1 & j_2 & j_3 \\ m_1 & m_2 & m_3 \end{pmatrix} = \frac{(-1)^{j_1+j_2-m_3}}{\sqrt{2j_3+1}} C_{j_1 m_1 j_2 m_2}^{j_3, -m_3}. \quad (5.18)$$

This collection of coefficients is called *Wigner's 3jm-symbol*. These symbols have more symmetries than the Clebsh-Gordan coefficients because they treat the three Hilbert spaces on the same level. This is useful for later graphical representation. We understand $|00\rangle$ as the $j = 0$ and $m = 0$ angular momenta state which is invariant under $SU(2)$ action.

Wigner's 4jm-symbol Moving to a tensor product of four Hilbert spaces, we can show that

$$\text{Inv}_{SU(2)} \left(\bigotimes_{i=1}^4 \mathcal{H}_{j_i} \right) \cong \mathbb{C}^{\max(|j_1-j_2|, |j_3-j_4|) - \min(j_1+j_2, j_3+j_4)}. \quad (5.19)$$

A possible orthogonal basis is labelled by $j \in \{\max(|j_1 - j_2|, |j_3 - j_4|), \dots, \min(j_1 + j_2, j_3 + j_4)\}$ and denoted

$$|j_1, j_2, j_3, j_4, j\rangle = \sum_{m_1, m_2, m_3, m_4} \begin{pmatrix} j_1 & j_2 & j_3 & j_4 \\ m_1 & m_2 & m_3 & m_4 \end{pmatrix}^{(j)} \bigotimes_i |j_i, m_i\rangle \quad (5.20)$$

with

$$\begin{pmatrix} j_1 & j_2 & j_3 & j_4 \\ m_1 & m_2 & m_3 & m_4 \end{pmatrix}^{(j)} \stackrel{\text{def}}{=} \sum_m (-1)^{j-m} \begin{pmatrix} j_1 & j_2 & j \\ m_1 & m_2 & m \end{pmatrix} \begin{pmatrix} j & j_3 & j_4 \\ -m & m_3 & m_4 \end{pmatrix}. \quad (5.21)$$

Wigner's 6j-symbol. Another basis of (5.19) could also be obtained by exchanging the labels 2 and 3 in (5.21). These two possible choices define two alternative bases which are related by a matrix whose coefficients are given by the *6j-symbol*:

$$\begin{aligned} \left\{ \begin{matrix} j_1 & j_2 & j_3 \\ j_4 & j_5 & j_6 \end{matrix} \right\} &\stackrel{\text{def}}{=} \sum_{m_1, \dots, m_6} (-1)^{\sum_{i=1}^6 (j_i - m_i)} \\ &\times \begin{pmatrix} j_1 & j_2 & j_3 \\ -m_1 & -m_2 & -m_3 \end{pmatrix} \begin{pmatrix} j_1 & j_5 & j_6 \\ m_1 & -m_5 & m_6 \end{pmatrix} \\ &\times \begin{pmatrix} j_4 & j_2 & j_6 \\ m_4 & m_2 & -m_6 \end{pmatrix} \begin{pmatrix} j_3 & j_4 & j_5 \\ m_3 & -m_4 & m_5 \end{pmatrix}. \end{aligned} \quad (5.22)$$

In terms of category theory, the 6j-symbol gives the component of an associator between $(\mathcal{H}_{j_1} \otimes \mathcal{H}_{j_2}) \otimes \mathcal{H}_{j_3}$ and $\mathcal{H}_{j_1} \otimes (\mathcal{H}_{j_2} \otimes \mathcal{H}_{j_3})$. It relates different ways to do the tensor product. It carries structural information about how various irreps relate to one another, without depending on the specific basis chosen within \mathcal{H}_j . We say it is an *invariant*. Surprisingly enough it has proved very useful in quantum gravity as we shall see in section ??!

5.1.2 Yutsis diagrams

The recoupling theory of $SU(2)$ can be graphically represented by Yutsis diagrams. There exist various conventions for Yutsis diagrams correspondence to recoupling in the literature. Here we use the original one, introduced by Yutsis in 1960 [1].

3-valent node. The basic object of for Yutsis diagrams is the 3-valent node, that represents Wigner's $3jm$ symbol:

$$\begin{pmatrix} j_1 & j_2 & j_3 \\ m_1 & m_2 & m_3 \end{pmatrix} = \begin{array}{c} j_1 m_1 \quad j_2 m_2 \quad j_3 m_3 \\ \diagup \quad \diagdown \quad \diagup \\ \diagdown \quad \diagup \quad \diagup \\ - \end{array} = \begin{array}{c} j_1 m_1 \quad j_3 m_3 \quad j_2 m_2 \\ \diagup \quad \diagdown \quad \diagup \\ \diagdown \quad \diagup \quad \diagup \\ + \end{array}. \quad (5.23)$$

The signs $+/-$ on the nodes indicate the sense of rotation (anticlockwise/clockwise) in which the spins must be read. To alleviate notations we choose the default orientation to be minus.

Only the topology of the diagram matters, which means that all topological deformations are allowed.

$$\begin{array}{c} j_1 m_1 \quad j_2 m_2 \quad j_3 m_3 \\ \diagup \quad \diagdown \quad \diagup \\ \diagdown \quad \diagup \quad \diagup \\ - \end{array} = \begin{array}{c} j_2 m_2 \\ \diagup \\ j_1 m_1 \end{array} = \begin{array}{c} j_1 m_1 \\ \diagup \\ j_3 m_3 \\ \diagup \\ j_2 m_2 \end{array} \quad (5.24)$$

For the arrows on the wires the *ingoing* orientation corresponds to *negating* the magnetic index.

For instance

$$\begin{array}{c} j_1 m_1 \quad j_2 m_2 \quad j_3 m_3 \\ \diagup \quad \diagdown \quad \diagup \\ \diagdown \quad \diagup \quad \diagup \\ - \end{array} = \begin{pmatrix} j_1 & j_2 & j_3 \\ -m_1 & m_2 & m_3 \end{pmatrix}. \quad (5.25)$$

An important case is when one of the strands has spin 0. The spin-0 strand is then represented with a dashed line (no arrow needed):

$$\begin{array}{c} j_1 m_1 \quad j_3 m_3 \\ \diagup \quad \diagup \\ \vdash \quad \diagup \\ \vdash \end{array} = \frac{(-1)^{j_1+m_1}}{\sqrt{2j_1+1}} \delta_{m_1, -m_3} \delta_{j_1, j_3}. \quad (5.26)$$

5. Diagrams for Spin-networks and Wigner symbols

We can then graphically define the two basic operations of multiplication and summation.

Multiplication is implemented simply by juxtaposition of diagrams:

$$\begin{array}{c} j_1 m_1 \quad j_2 m_2 \quad j_3 m_3 \quad j_4 m_4 \quad j_5 m_5 \quad j_6 m_6 \\ \diagup \quad \diagdown \quad \diagup \quad \diagdown \quad \diagup \quad \diagdown \\ \text{V} \quad \text{V} \quad \text{V} \quad \text{V} \quad \text{V} \quad \text{V} \end{array} = \begin{pmatrix} j_1 & j_2 & j_3 \\ m_1 & m_2 & m_3 \end{pmatrix} \begin{pmatrix} j_4 & j_5 & j_6 \\ m_4 & m_5 & m_6 \end{pmatrix} \quad (5.27)$$

Then, the gluing of two external wires with the same label jm , but opposite directions, defines the sum over m (from $-j$ to j), with the additional factor $(-1)^{j-m}$ in the summand, like:

$$\begin{array}{c} j_1 m_1 \quad j_2 m_2 \quad j_3 m_3 \quad j_4 m_4 \\ \diagup \quad \diagdown \quad \diagup \quad \diagdown \\ \text{V} \quad \text{V} \quad \text{V} \quad \text{V} \\ \text{---} \quad \text{---} \quad \text{---} \quad \text{---} \\ j \end{array} = \sum_{m=-j}^j (-1)^{j-m} \begin{array}{c} j_1 m_1 \quad j_2 m_2 \quad jm \quad jm \\ \diagup \quad \diagdown \quad \diagup \quad \diagdown \\ \text{V} \quad \text{V} \quad \text{V} \quad \text{V} \\ \text{---} \quad \text{---} \quad \text{---} \quad \text{---} \\ j_3 m_3 \quad j_4 m_4 \end{array} \quad (5.28)$$

On the RHS, we recognise the definition of the $4jm$ -symbol:

$$\begin{array}{c} j_1 m_1 \quad j_2 m_2 \quad j_3 m_3 \quad j_4 m_4 \\ \diagup \quad \diagdown \quad \diagup \quad \diagdown \\ \text{V} \quad \text{V} \quad \text{V} \quad \text{V} \\ \text{---} \quad \text{---} \quad \text{---} \quad \text{---} \\ j \end{array} = \begin{pmatrix} j_1 & j_2 & j_3 & j_4 \\ m_1 & m_2 & m_3 & m_4 \end{pmatrix}^{(j)} \quad (5.29)$$

The wire between the two nodes, whose magnetic index is summed over, is called an *internal* wire. Reversing the arrow of an internal wire gives an overall phase:

$$\begin{array}{c} j_1 m_1 \quad j_2 m_2 \quad j_3 m_3 \quad j_4 m_4 \\ \diagup \quad \diagdown \quad \diagup \quad \diagdown \\ \text{V} \quad \text{V} \quad \text{V} \quad \text{V} \\ \text{---} \quad \text{---} \quad \text{---} \quad \text{---} \\ j \end{array} = (-1)^{2j} \begin{array}{c} j_1 m_1 \quad j_2 m_2 \quad j_3 m_3 \quad j_4 m_4 \\ \diagup \quad \diagdown \quad \diagup \quad \diagdown \\ \text{V} \quad \text{V} \quad \text{V} \quad \text{V} \\ \text{---} \quad \text{---} \quad \text{---} \quad \text{---} \\ j \end{array} .$$

For convenience it is also helpful to consider a single wire with an arrow on it as an element of the graphical calculus:

$$\begin{array}{c} j_1 m_1 \\ \text{---} \\ j_2 m_2 \end{array} = (-1)^{j_2-m_2} \delta_{j_1 j_2} \delta_{m_1 m_2} \quad \text{or} \quad \begin{array}{c} m \\ \text{---} \\ j \\ \text{---} \\ n \end{array} = (-1)^{j-n} \delta_{mn} . \quad (5.30)$$

Invariant functions. We can apply the rule of summation to compute the trace of the single wire:

$$\begin{array}{ccc}
 \text{Diagram: } & & \text{Equation: } \\
 \text{A circle with a dot inside, labeled } j \text{ at the top left.} & = \sum_m (-1)^{j-m} & = \sum_m (-1)^{j-m} (-1)^{j-m} = 2j + 1. \\
 & & \text{A vertical line with a dot at the top, labeled } j \text{ at the top, } m \text{ at the bottom.} \\
 & & \text{A vertical line with a dot at the bottom, labeled } m \text{ at the top, } m \text{ at the bottom.}
 \end{array} \quad (5.31)$$

When a diagram has no external wires, it encodes a number (instead of a vector). In this case all magnetic indices are summed over, so that it is only a function of the internal spins j_i . We call such expressions *invariant functions*. On the other hand, a diagram with external wires encodes a tensor with one magnetic index for each external wire.

Let us give some examples. The Θ -graph evaluates to

$$\text{Diagram: } \begin{array}{c} j_1 \rightarrow \\ \text{A circle with three arrows pointing clockwise from the top, labeled } j_1, j_2, j_3 \text{ at the top, bottom, and right respectively.} \end{array} = (-1)^{j_1+j_2+j_3}. \quad (5.32)$$

Similarly, we can calculate

$$\text{Diagram: } \begin{array}{c} j_1 \\ j_2 \\ j_3 \\ j_4 \\ \text{A circle with four arrows pointing clockwise from the top, labeled } j_1, j_2, j_3, j_4 \text{ at the top, top-right, bottom-right, and bottom respectively.} \\ i \end{array} = \frac{\delta_{ik}}{2i+1}. \quad (5.33)$$

In this notation the Wigner 6j-symbol corresponds to quite a canonical diagram:

$$\left\{ \begin{array}{ccc} j_1 & j_2 & j_3 \\ j_4 & j_5 & j_6 \end{array} \right\} = \text{Diagram: } \begin{array}{c} j_1 \\ j_2 \\ j_3 \\ j_4 \\ j_5 \\ j_6 \\ \text{A large triangle with internal lines connecting vertices.} \end{array} \quad (5.34)$$

5. Diagrams for Spin-networks and Wigner symbols

We can define other invariant functions in the same spirit, like the 15j-symbol:

$$\begin{Bmatrix} j_1 & j_2 & j_{11} \\ j_4 & j_5 & j_{15} \\ j_7 & j_3 & j_{14} \\ j_9 & j_6 & j_{13} \\ j_8 & j_{10} & j_{12} \end{Bmatrix} = \begin{array}{c} \text{Diagram of a 3-valent graph with 15 links, labeled } j_1 \text{ to } j_{15} \end{array} \quad (5.35)$$

which is the definition used by [82]. In contrast to the 6j-symbol, there is no consensus on which convention should be used to define the 15j-symbol. In all cases it corresponds to an invariant function associated to a 3-valent graph with 15 links. There are 5 topologically distinct 15j-symbols [1]. Here we see the power of Yutsis diagrams: it makes huge expressions much more tractable and straightforward to reason about.

In terms of applications the $\{6j\}$ -symbol appears in quantum gravity due to the work of Ponzano and Regge who saw that the $\{6j\}$ -symbol approximates the action of general relativity in the semi-classical limit [83]. If you imagine the tetrahedron depicted in figure (5.34), with the labels j_i viewed as the lengths of its edges then its volume V in following asymptotic limit when $\lambda \rightarrow \infty$ is:

$$\begin{Bmatrix} \lambda j_1 & \lambda j_2 & \lambda j_3 \\ \lambda j_4 & \lambda j_5 & \lambda j_6 \end{Bmatrix} \sim \frac{1}{4\sqrt{3\pi\lambda^3 V}} (e^{iS} + e^{-iS}) \quad (5.36)$$

with the action

$$S \stackrel{\text{def}}{=} \sum_i \left(\lambda j_i + \frac{1}{2} \right) \xi_i + \frac{\pi}{4} \quad (5.37)$$

with ξ_i the exterior dihedral angle along the edge i [84]. If we ignore the constant $\frac{\pi}{4}$, S is the known as the *Regge action* of the tetrahedron, which is a discrete euclidean 3D version of the Einstein-Hilbert action which governs the equations of motion in general relativity.

Matrix representation. Generic Yutsis diagrams have external wires, i.e. they are tensors (and not scalars). They can thus be represented as matrices, but we must fix a convention to be able to read it appropriately.

1. The inbound arrows are treated as inputs, i.e. columns of the matrix. Dually, out-bound/output/rows.

2. Among all the inbound (resp. outbound) arrows, we must decide their ordering. We fix that the first one is the top left and the next ones follow with clockwise orientation.
3. Within each Hilbert space, we must decide the ordering of the canonical basis. We follow the natural ordering of the qubit basis. For $j = 1/2$, we have

$$\left| \frac{1}{2}, \frac{1}{2} \right\rangle = |0\rangle \quad \left| \frac{1}{2}, -\frac{1}{2} \right\rangle = |1\rangle \quad (5.38)$$

Thus in general, it goes from $|j, j\rangle$ to $|j, -j\rangle$, i.e. in decreasing order of magnetic index m .

For instance, consider the tensor

$$\begin{pmatrix} \frac{1}{2} & \frac{1}{2} & 1 \\ -m_1 & -m_2 & m_3 \end{pmatrix} \quad (5.39)$$

Its matrix representation is

$$\begin{array}{ccc} \frac{1}{2} & \frac{1}{2} & 1 \\ \swarrow & \downarrow & \nearrow \\ \bullet & & \end{array} = \begin{pmatrix} -\frac{1}{\sqrt{3}} & 0 & 0 & 0 \\ 0 & \frac{1}{\sqrt{6}} & \frac{1}{\sqrt{6}} & 0 \\ 0 & 0 & 0 & -\frac{1}{\sqrt{3}} \end{pmatrix} \quad (5.40)$$

The top left component corresponds to $m_1 = 1/2$, $m_2 = 1/2$ and $m_3 = 1$. If the arrow on j_3 is reverted, we get instead the tensor

$$\begin{pmatrix} \frac{1}{2} & \frac{1}{2} & 1 \\ -m_1 & -m_2 & -m_3 \end{pmatrix} \quad (5.41)$$

with the matrix representation

$$\begin{array}{ccc} \frac{1}{2} & \frac{1}{2} & 1 \\ \searrow & \downarrow & \nearrow \\ \bullet & & \end{array} = \begin{pmatrix} 0 & 0 & -\frac{1}{\sqrt{3}} & 0 & \frac{1}{\sqrt{6}} & 0 & 0 & \frac{1}{\sqrt{6}} & 0 & -\frac{1}{\sqrt{3}} & 0 & 0 \end{pmatrix} \quad (5.42)$$

The first $-\frac{1}{\sqrt{3}}$ still corresponds to $m_1 = 1/2$, $m_2 = 1/2$ and $m_3 = 1$.

5.1.3 Penrose diagrams

In Section 5.1.1, we saw that the spin- j irrep can be built from the symmetrisation of $2j$ copies of \mathbb{C}^2 . This suggests another graphical calculus that goes under the name of *Penrose binor calculus*. A clear introduction can be found in [85].

In this calculus, the identity over \mathbb{C}^2 is a single strand

$$\left| \right\rangle \cong |0\rangle\langle 0| + |1\rangle\langle 1| . \quad (5.43)$$

5. Diagrams for Spin-networks and Wigner symbols

The free legs carry implicit labels of copies of \mathbb{C}^2 . There is also a duality between up and down. The cap stands for i times the determinant (from $\mathbb{C}^2 \otimes \mathbb{C}^2$ to \mathbb{C}):

$$\cap \cong i \langle 01| - i \langle 10|. \quad (5.44)$$

The cup is

$$\cup \cong i |01\rangle - i |10\rangle. \quad (5.45)$$

The factor i is introduced for the diagram to be well-behaved under deformation:

$$\sim = | \quad (5.46)$$

Finally, the crossing is

$$\times = -|00\rangle\langle 00| - |10\rangle\langle 01| - |01\rangle\langle 10| - |11\rangle\langle 11|. \quad (5.47)$$

These rules guarantee the planar isotopy, i.e. diagrams can be treated as regular strings that bends and cross over.

Fundamental equations. Binor calculus has two core equations that can be deduced from the definitions above.

$$\circ = -2 \quad (5.48)$$

$$)(+ \times + \cup = 0 \quad (5.49)$$

The value of the loop in the first equation secretly gives the "dimension" of the tensor calculus. Here it is -2 , hence the name "binor". The second equation is known under the name of "skein relation" or "binor identity".

Connection to Yutsis diagram. To connect to Yutsis graphical calculus, we must build the spin- j irrep. This is done by anti-symmetrising the strands:

$$j \equiv \frac{1}{(2j)!} \sum_{\sigma \in \mathfrak{S}_{2j}} (-1)^{|\sigma|} \boxed{\sigma}, \quad (5.50)$$

with $|\sigma|$ the parity of σ and the σ -labelled box representing the corresponding permutation of the $2j$ strands from one side to the other. Although it looks like an anti-symmetrisation, the operator is actually a projector from $\mathbb{C}^2 \otimes \dots \otimes \mathbb{C}^2$ to $\mathcal{S}(\mathbb{C}^2 \otimes \dots \otimes \mathbb{C}^2)$, because of the minus sign in

5.1. From Yutsis diagrams to spin-networks

(5.47). So it is the identity over the spin- j irrep, and we have the following correspondence with Yutsis diagrams

$$\begin{array}{c}
 \text{Diagram:} \\
 \text{A vertical rectangle with a horizontal line segment in the middle. The top part is labeled '0 ... 1' with a brace above it, and the bottom part is labeled '0 ... 1' with a brace below it. The middle segment is labeled '2j' with a brace to its left. The total height is labeled 'j+m times 0' at the top and 'j+n times 0' at the bottom.} \\
 = \frac{(j+m)!(j-m)!}{(2j)!} \delta_{mn} = (-1)^{j-n} \frac{(j+m)!(j-m)!}{(2j)!} \\
 \text{Labels:} \\
 \text{On the right, there is a vertical arrow pointing up labeled 'm' at the top and 'n' at the bottom. The arrow is labeled 'j' with an arrow pointing up.}
 \end{array} \quad (5.51)$$

The series of 0's and 1's tells with which elements of the basis, e_0, e_1 of \mathbb{C}^2 , the strands are fed. The loop diagram takes the value

$$\text{Diagram:} \\
 \text{A circle with a horizontal line segment on the left labeled 'j'.} \\
 = (-1)^{2j} (2j + 1). \quad (5.52)$$

One would like to draw in binor calculus the analog of the 3-valent vertex, i.e. the 3jm-symbol. It can be shown to be proportional to

$$\text{Diagram:} \\
 \text{A complex network of strands labeled A and B. At the top, there are two strands labeled A₁ and B₁. Below them, there are two strands labeled A_{2j₁} and B_{2j₂}. These strands converge to a central horizontal line segment. Below this segment, there are strands labeled C_{2j₃}, ..., C₁.} \\
 \quad (5.53)$$

The norm of the projector can be computed as

$$\text{Diagram:} \\
 \text{A diagram showing three strands labeled j₁, j₂, and j₃ meeting at a central point. The strands are labeled with ellipses '...' on both sides of the central point.} \\
 = (-1)^{j_1+j_2+j_3} N^2(j₁, j₂, j₃), \quad (5.54)$$

5. Diagrams for Spin-networks and Wigner symbols

with

$$N(j_1, j_2, j_3) = \sqrt{\frac{(j_1 + j_2 + j_3 + 1)!(-j_1 + j_2 + j_3)!(j_1 - j_2 + j_3)!(j_1 + j_2 - j_3)!}{(2j_1)!(2j_2)!(2j_3)!}}. \quad (5.55)$$

Thus, we can finally write the correspondence² with Yutsis diagrams as

$$= N(j_1, j_2, j_3) \quad (5.56)$$

All the invariant functions that were introduced in the previous section can now be translated to binor diagrams. The strength of this calculus lies in the two core equations (5.48) and (5.49), which are sufficient to simplify the diagrams and compute their actual value.

In binor diagrams we can view the 3-valent node as a kind of “railroad switch”, where the fundamental wires within the three bundles redistribute between themselves. Because the bundles represent symmetrised spaces we only care about how many wires go from each bundle to the other bundle. It turns out that there is then actually only one way in which to connect the wires, when it is not impossible. The Clebsch-Gordan conditions (??) precisely state when such a recoupling is possible.

5.1.4 Spin-networks

Spin-networks were originally conceived by Penrose as a means of deriving continuous space-time from graphs colored by discrete spins [81]. They are initially formulated in terms of the binor calculus. They were later revived in the context of LQG, but with a different interpretation.

A *3-valent spin-network* is an open graph where each node has 3 associated links³ and where each link is associated with a spin $j_i \in \mathbb{N}/2$, such that the three spins of the links coming together in a node satisfy the Clebsch-Gordan conditions. An example of a 3-valent spin-network is shown in Figure 5.1. Such a diagram can be interpreted in binor calculus or as a Yutsis diagram.

²Strictly speaking, there may be a phase $(-1)^{f(j_1, j_2, j_3)}$ but I have been unable to fix this.

³Mathematicians usually say edge or arrow, but not "link", which has another meaning in knot theory. The terminology of LQG keeps "edge" for spin-foams, and uses "link" for spin-networks.

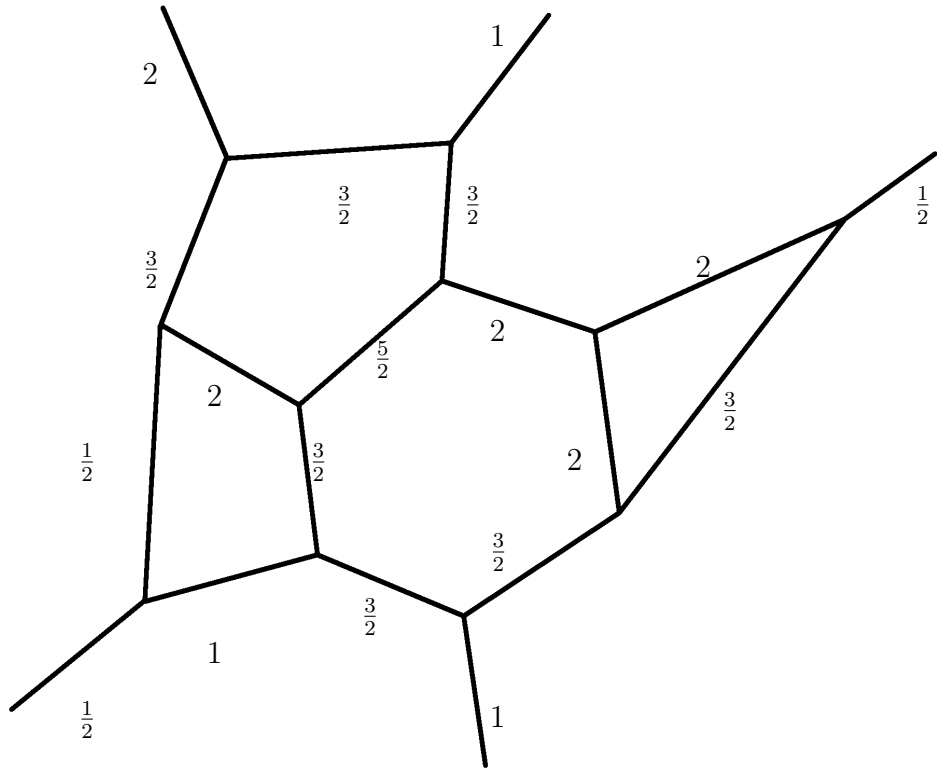


Figure 5.1: A 3-valent spin-network.

Similarly, a *4-valent* spin-network is an open graph where each node has 4 associated links and where each link l is labelled by a spin j_l such that for each set of four spins j_1, j_2, j_3 and j_4 coming together in a node we have:

$$\text{Inv}_{SU(2)}(\mathcal{H}_{j_1} \otimes \mathcal{H}_{j_2} \otimes \mathcal{H}_{j_3} \otimes \mathcal{H}_{j_4}) \neq 0. \quad (5.57)$$

This definition easily generalises to higher valencies, and in the case of 3-valent spin-networks we get back the definition above. In the 4-valent case, the invariant subspace can be more than one-dimensional. This dimension can be computed graphically by the number of ways to connect the four links at a node when viewed as a binor diagram.

Indeed for any graph we can see each intertwiner in an extremely direct manner as indexed by the number of connecting or internal links to the partitioned 4 valent node.

In the trivalent situation with the fundamental decomposition of a node there is a unique way to decompose it into fundamental wires. This is not true in the 4-valent case and higher.

5. Diagrams for Spin-networks and Wigner symbols

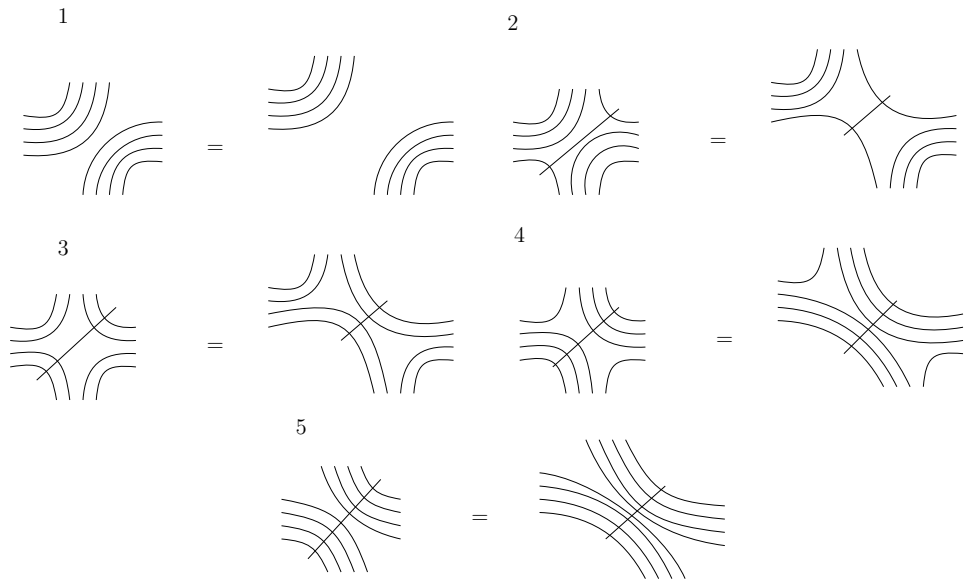


Figure 5.2: Here we can see the 5 different intertwiners that can be associated to the meeting of 4 spin 2 (4 representation) wires in the binor calculus. Notice how they are indexed by the double the number of internal vertices between the two resultant trivalent vertices.

In 1995, Rovelli and Smolin found that a variant of Penrose's original spin-networks could be used to label quantum states in space [86]. The spin-networks carry a physical interpretation as quantum states of space. We will go into detail about this in a later section.

5.2 The translation to ZXH

As the ZXH-calculus is a universal language for spin-1/2 systems, it does not come as a surprise that it can be used to express the quantum theory of angular momentum. However, the precise way to do this is not obvious, and takes quite some work. In this section we present this translation of the theory of angular momentum to the ZXH-calculus. First we introduce the building blocks, i.e. the links and the 3-valent nodes. Then we show how to connect them and compute invariant recoupling functions.

5.2.1 Links

Spin-1/2. The simplest Yutsis diagrams have only spin-1/2 links. From equation (5.30), we see that these links can be written as⁴

$$\left| \begin{array}{c} \text{ } \\ \text{ } \end{array} \right| = \begin{pmatrix} 1 & 0 \\ 0 & -1 \end{pmatrix} = |0\rangle\langle 0| - |1\rangle\langle 1| = \text{---} \frac{\pi}{\text{---}} \text{---} . \quad (5.58)$$

Spin-1 links [33] In Section 5.1.3, we have already seen that the spin-j Yutsis links can be expressed as the symmetrisation of $2j$ fundamental Penrose wires. So to represent higher spins in the ZXH-calculus, we just need to express the symmetriser of Eq. (5.2) as a ZXH-diagram.

Now, to write the symmetrisation projector on $n = 2$ wires we need an equal superposition of the identity permutation and the SWAP. As we recall from equation (3.10) We accomplish this by setting the control of (3.7) to $|+\rangle = |0\rangle + |1\rangle$:

$$1 \left| \begin{array}{c} \text{ } \\ \text{ } \end{array} \right| = |00\rangle\langle 00| + |11\rangle\langle 11| - \frac{1}{2} (|01\rangle + |10\rangle) (\langle 01| + \langle 10|) = \frac{1}{\sqrt{2}} \text{---} \frac{\pi}{\text{---}} \text{---} \frac{\pi}{\text{---}} \text{---} \frac{\pi}{\text{---}} \text{---} . \quad (5.59)$$

Here the $Z(\pi)$ rotation on each of the wires is necessary to add the -1 phase that is present in the Yutsis diagram. We will see such phases appear when representing higher-spin Yutsis wires as well.

Higher-spin links We construct the symmetriser for higher-spins just as we saw above in 5.1.3. The difference here is, as for spin-1 Yutsis wires, additional green π rotations on each wire, for example:

For $n = 3$ we have equation (3.12) with additional green π rotations,

$$\frac{3}{2} \left| \begin{array}{c} \text{ } \\ \text{ } \end{array} \right| = \frac{1}{3\sqrt{2}} \text{---} \frac{\pi}{\text{---}} \text{---} \frac{\pi}{\text{---}} \text{---} \frac{\pi}{\text{---}} \text{---} \frac{\pi}{\text{---}} \text{---} . \quad (5.60)$$

⁴It might be surprising that the Yutsis diagram on the LHS looks asymmetric while the ZXH diagram looks symmetric. The underlying matrix is indeed symmetric, but the arrow is here useful to abide by the convention and write the Yutsis diagram as a matrix (see *Matrix representation* on page 67). On the ZXH diagram, this information is implicit and globally carried by the polarisation left/right of the plane.

5. Diagrams for Spin-networks and Wigner symbols

For $n = 4$ this resembles (3.14) with additional green rotations,

$$2 \left| = \frac{1}{48} \right. \begin{array}{c} \text{Diagram for } n=4 \text{ with green rotations} \\ \text{A complex network of wires with red, green, and yellow nodes, and red arcs labeled } \pi. \end{array} \quad (5.61)$$

For $n = 5$ (3.12) this resembles (3.15),

$$\frac{5}{2} \left| = \frac{1}{7680} \right. \begin{array}{c} \text{Diagram for } n=5 \text{ with green rotations} \\ \text{A complex network of wires with red, green, and yellow nodes, and red arcs labeled } \pi. \end{array} \quad (5.62)$$

Note that each larger diagram contains the smaller diagrams.

Connecting wires. There are two ways to compose Yutsis diagrams: either by placing them adjacently, or by connecting wires. Adjacency simply corresponds to the tensor product, so that this corresponds to adjacency of ZXH-diagrams as well. Connecting two wires is more involved to describe in terms of ZXH-diagrams.

Recall that the connection of two wires in a Yutsis diagram corresponds to a summation over a magnetic index m together with a phase, see Eq. (5.28). To understand how this is described in ZXH, note that when we connect two spin- j wires we should again get a spin- j wire again:

$$\sum_k (-1)^{j-k} \left| \begin{array}{c} m \\ k \\ k \\ n \end{array} \right| = \left| \begin{array}{c} m \\ n \\ n \end{array} \right| \quad (5.63)$$

For the spin-1/2 this is achieved with an intermediate green π :

$$\left| \begin{array}{c} \pi \\ \pi \\ \pi \end{array} \right| = \left| \begin{array}{c} \pi \end{array} \right| \quad (5.64)$$

For general spin- j , the connection is performed by the intermediate diagram

$$\frac{1}{\lambda_n} \left| \begin{array}{c} \pi \\ \vdots \\ \pi \end{array} \right| \quad (5.65)$$

Thus, we have

$$\frac{\lambda_n^2}{\lambda_n} \quad \begin{array}{c} \text{---}(\pi)\text{---}(\pi)\text{---}(\pi)\text{---} \\ | \quad | \quad | \quad | \\ | \quad | \quad | \quad | \end{array} = \lambda_n \quad \begin{array}{c} \text{---}(\pi)\text{---} \\ | \\ | \end{array} \quad . \quad (5.66)$$

This rule can be explained as follows. We want to sum the magnetic index m_3 from $-j_3$ to j_3 . We can describe this as applying the operator $\sum_{m=-j_3}^{j_3} |j_3; m_3\rangle |j_3; m_3\rangle$ to our diagram of disconnected $3jm$ -symbols. This amounts to applying the operator $\sum_{m=-j_3}^{j_3} |j_3; m_3\rangle \langle j_3; m_3|$, which is the identity operator on the symmetric subspace, i.e. the symmetriser. However, the summation also requires a factor $(-1)^{j_3-m_3}$. This factor corresponds to a -1 phase being applied if there are an odd number of $|1\rangle$'s in the symmetric basis element. This phase is implemented by applying a $Z(\pi)$ rotation to each of the wires corresponding to the summed over spin j_3 (recalling that a $Z(\pi)$ rotation is $|0\rangle - |1\rangle$). The proportionality factor is determined straightforwardly.

From this rule, we can compute for instance the loop:

$$\text{---} \quad = 2 = \text{---} \quad . \quad (5.67)$$

5.2.2 Trivalent nodes

We have outlined how the links of Yutsis diagrams can be described as ZXH diagrams.

To start with, we look at the simplest possible 3-valent vertices:

$$\text{---} \quad = \frac{1}{\sqrt{2}} (|10\rangle - |01\rangle) = \frac{1}{\sqrt{2}} \text{---} \quad \begin{array}{c} \text{---}(\pi) \\ | \\ | \end{array} \quad (5.68)$$

$$\text{---} \quad = \frac{1}{\sqrt{2}} (\langle 01| - \langle 10|) = \frac{1}{\sqrt{2}} \begin{array}{c} \text{---} \\ | \\ | \end{array} \quad \begin{array}{c} \text{---}(\pi) \\ | \\ | \end{array} \quad (5.69)$$

$$\text{---} \quad = \frac{1}{\sqrt{2}} (|0\rangle\langle 0| - |1\rangle\langle 1|) = \frac{1}{\sqrt{2}} \text{---} \quad \begin{array}{c} \text{---} \\ | \\ | \end{array} \quad (5.70)$$

$$\text{---} \quad = \frac{1}{\sqrt{2}} (-|0\rangle\langle 0| + |1\rangle\langle 1|) = \frac{1}{\sqrt{2}} \text{---} \quad \begin{array}{c} \text{---} \\ | \\ | \end{array} \quad (5.71)$$

5. Diagrams for Spin-networks and Wigner symbols

To go further we look to equation (5.56) which shows how Penrose and Yutsis trivalent-nodes are related. The translation of the 3-valent vertex from Yutsis to ZXH is very similar, but we must careful about the normalisation and about the cups and caps that connects the wires. We have

$$\begin{array}{c} j_1 \quad j_2 \quad j_3 \\ \swarrow \quad \uparrow \quad \searrow \\ \bullet \end{array} = \frac{\alpha}{N(j_1, j_2, j_3)} \quad \text{ZXH diagram with } 2j_1, 2j_2, 2j_3 \text{ wires and } \pi \text{ gates.}$$
(5.72)

with N the binor calculus normalisation given by (5.55) and α the normalisation correction given by equation (3.22) (one per each link). The three links are connected with the cups of equation (5.68).

Reversing the arrows. As shown in Eq. (5.25), reversing the direction of a wire in a Yutsis diagram corresponds to mapping the $|j; m\rangle$ state to $|j; -m\rangle$. Recall that in our symmetrised representation of spins that the $|j; m\rangle$ state corresponds to the symmetrised computational basis state where there are $j - m$ $|1\rangle$'s. Hence, the mapping $|j; m\rangle \mapsto |j; -m\rangle$ is implemented by interchanging $|0\rangle$ and $|1\rangle$ on each of the component spin-1/2 wires, i.e. by doing a NOT gate on all the qubits. This means that in the ZXH-diagram, to reverse an edge, we need to apply a $X(\pi)$ rotation to the external wires of each wire involved in the spin and that these rotations must come before the $Z(\pi)$ rotations on this wire.

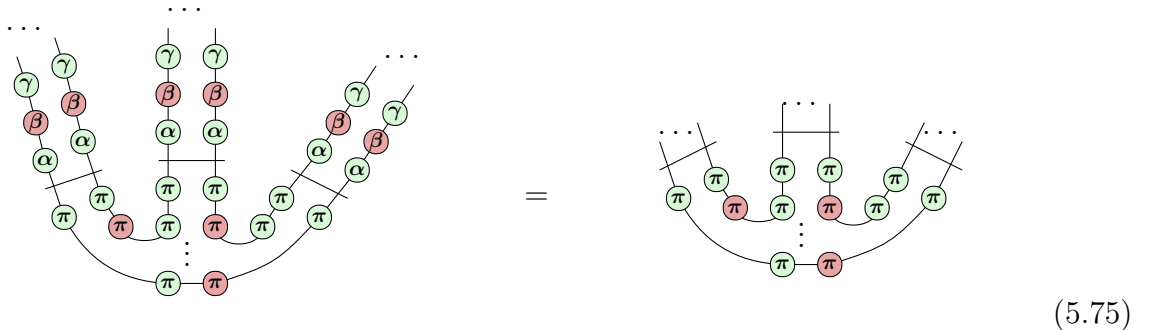
$$\begin{array}{c} j_1 \quad j_2 \quad j_3 \\ \swarrow \quad \uparrow \quad \searrow \\ \bullet \end{array} = \frac{\alpha}{N(j_1, j_2, j_3)} \quad \text{ZXH diagram with } 2j_1, 2j_2, 2j_3 \text{ wires and } \pi \text{ gates.}$$
(5.73)

Note that equations (5.68) and (5.71) are special cases of this. It may at first glance seem like these diagrams under-specify where the wires connect up but in fact given that the symmetrisers permute all wires in superposition the wire ordering attached to them is arbitrary. Only the fact that there are wires connecting two symmetrisers matter alongside their relative ordering which is indicated by the red-green ordering of the π rotations.

Diagrammatic invariance. The $3jm$ -symbol defines a tensor in the $SU(2)$ -invariant subspace of $\mathcal{H}_{j_1} \otimes \mathcal{H}_{j_2} \otimes \mathcal{H}_{j_3}$. This invariance can be checked concretely by applying an arbitrary $U \in SU(2)$ to each of the external wires and seeing that it can be removed. Using Euler decompositions, we can write any such U as⁵

$$H = e^{-\frac{i\alpha}{2}Z} e^{-\frac{i\beta}{2}X} e^{-\frac{i\gamma}{2}Z} = -\gamma\beta\alpha\text{---} , \quad (5.74)$$

for some α , β and γ . Recall, from Eq. (3.6) that the action of $SU(2)$ on higher spins is just applying the unitary to all the spin-1/2 space separately. The invariance condition hence becomes:



$$(5.75)$$

This can be shown to follow from the following equations:

$$\begin{array}{c} \text{---} \gamma \text{---} \beta \text{---} \alpha \text{---} | \\ \text{---} \gamma \text{---} \beta \text{---} \alpha \text{---} | \end{array} = \begin{array}{c} | \text{---} \gamma \text{---} \beta \text{---} \alpha \text{---} \\ | \text{---} \gamma \text{---} \beta \text{---} \alpha \text{---} \end{array} \quad (5.76)$$

$$\text{---} \gamma \text{---} \beta \text{---} \alpha \text{---} \pi \text{---} = -\pi \text{---} \gamma \text{---} -\beta \text{---} \alpha \text{---} \quad (5.77)$$

$$\text{---} \gamma \text{---} \beta \text{---} \alpha \text{---} \pi \text{---} = -\pi \text{---} -\gamma \text{---} \beta \text{---} -\alpha \text{---} \quad (5.78)$$

⁵The Euler decomposition is often defined with the Pauli Y instead of Z , but using Z is a more natural choice in ZX-calculus.

5. Diagrams for Spin-networks and Wigner symbols

The proof of (5.76) can be worked out easily for a spin-1 wire with some arbitrary single qubit operator g :

$$\begin{aligned}
 & \text{Diagram with } g \text{ boxes and a central node} \\
 & = \sqrt{\frac{1}{2}} \text{ (Diagram with } g \text{ boxes and a red circle, yellow square)} + \sqrt{\frac{1}{2}} \text{ (Diagram with } g \text{ boxes and a red circle, green circle)} \\
 & = \sqrt{\frac{1}{2}} \text{ (Diagram with crossing and } g \text{ box)} + \sqrt{\frac{1}{2}} \text{ (Diagram with crossing and green circle)}
 \end{aligned} \tag{5.79}$$

From this perspective the general principle with more permutations is directly analogous.

When we reverse the direction of a wire, we can similarly check that invariance is preserved. But instead of applying U , we need to apply XUX :

$$\text{Diagram with three nodes: } \text{---} \text{ (green circle, red circle)} \text{ ---} \text{ (green circle, red circle)} \text{ ---} \text{ (green circle, red circle)} \tag{5.80}$$

Note that this is not the adjoint of U , which might be seen as surprising as it is often the case in graphical calculi that reversing the diagram amounts to dualising the space, i.e. switching from U to U^\dagger . However, the inversion of an arrow as defined in the Yutsis calculus does not quite perform this transformation. Instead, it only does flips the basis states $|j, m\rangle$ (see Eq. (5.25)), which as we've seen corresponds to applying the NOT gate X to all the spin-1/2 wires in the symmetrised space.

With these considerations, the invariance condition for the $3jm$ -symbol with the direction of the leftmost input changed reads:

$$\text{Complex spin-network diagram} = \text{Simplified diagram with all nodes labeled } \pi \tag{5.81}$$

This can be checked to hold as before.

4jm symbol. By applying the rules for connecting wires, we find

$$\begin{aligned}
 & \begin{array}{c} j_1 \quad j_2 \quad j_4 \quad j_5 \\ \swarrow \quad \downarrow \quad \uparrow \quad \searrow \\ \bullet \quad j_3 \end{array} = \sum_{m_3=-j_3}^{j_3} (-1)^{j_3-m_3} \begin{array}{c} j_1 \quad j_2 \quad j_3 \quad j_4 \quad j_5 \\ \swarrow \quad \downarrow \quad \uparrow \quad \searrow \\ \bullet \quad m_3 \quad m_3 \end{array} \\
 & = \frac{\lambda_{2j_1}\lambda_{2j_2}\lambda_{2j_3}\lambda_{2j_4}\lambda_{2j_5}}{N(j_1,j_2,j_3)N(j_3,j_4,j_5)} \begin{array}{c} 2j_1 \quad 2j_2 \quad \dots \quad 2j_4 \quad 2j_5 \\ \dots \quad \dots \quad \dots \quad \dots \quad \dots \\ \text{SWAPs} \quad \text{SWAPs} \quad \dots \quad \text{SWAPs} \quad \text{SWAPs} \\ \text{SWAPs} \quad \text{SWAPs} \quad \dots \quad \text{SWAPs} \quad \text{SWAPs} \\ \text{SWAPs} \quad \text{SWAPs} \quad \dots \quad \text{SWAPs} \quad \text{SWAPs} \end{array} \quad (5.82)
 \end{aligned}$$

5.2.3 Examples

Now that we have the tools to describe arbitrary Yutsis diagrams as ZXH-diagrams, let us give some examples. We used **Sagemath** to check correctness of the values of the Yutsis diagrams, and **PyZX** to compute the values of the ZXH-diagrams, in order to verify that our constructions are correct.

The computations can be found in the appendix E.

3jm-symbol

Example 1. Let us consider the following 3-vertex:

$$\begin{array}{c} \frac{1}{2} \quad \frac{1}{2} \quad 1 \\ \swarrow \quad \downarrow \quad \searrow \\ \bullet \end{array} = \begin{pmatrix} -\frac{1}{\sqrt{3}} & 0 & 0 & 0 \\ 0 & \frac{1}{\sqrt{6}} & \frac{1}{\sqrt{6}} & 0 \\ 0 & 0 & 0 & -\frac{1}{\sqrt{3}} \end{pmatrix} \quad (5.83)$$

We get a 4×3 matrix as output because we input two spin-1/2's which means we have a $2 \cdot 2 = 4$ dimensional input, while we output a spin-1, which is 3-dimensional.

From our construction described above, this should correspond to the following ZXH diagram:

$$\sqrt{2}^{-1} * \sqrt{\frac{1}{3}} \begin{array}{c} \text{SWAP} \quad \text{SWAP} \quad \text{SWAP} \quad \text{SWAP} \\ \text{SWAP} \quad \text{SWAP} \quad \text{SWAP} \quad \text{SWAP} \end{array} = \begin{pmatrix} -\frac{1}{\sqrt{3}} & 0 & 0 & 0 \\ 0 & \frac{1}{2\sqrt{3}} & \frac{1}{2\sqrt{3}} & 0 \\ 0 & \frac{1}{2\sqrt{3}} & \frac{1}{2\sqrt{3}} & 0 \\ 0 & 0 & 0 & -\frac{1}{\sqrt{3}} \end{pmatrix} \quad (5.84)$$

The SWAPs on the inputs here are required to produce the correct matrix in **PyZX**, because of the peculiar convention on the input ordering.

5. Diagrams for Spin-networks and Wigner symbols

As we are working with a ZXH-diagram, its qubit matrix will always have the shape $2^n \times 2^m$, where n is the number of inputs, and m the number of outputs. In order to compare eq. (5.84) with the matrix of Eq. (5.83), we must project the codomain of this matrix to the symmetric subspace. This means multiplying the matrix of Eq. (5.84) on the left with

$$P_c = \begin{pmatrix} 1 & 0 & 0 & 0 \\ 0 & \frac{1}{\sqrt{2}} & \frac{1}{\sqrt{2}} & 0 \\ 0 & 0 & 0 & 1 \end{pmatrix}. \quad (5.85)$$

This matrix implements the relations

$$\begin{aligned} |1, 1\rangle &= |00\rangle \\ |1, 0\rangle &= \frac{1}{\sqrt{2}} (|01\rangle + |10\rangle) \\ |1, -1\rangle &= |11\rangle \end{aligned} \quad (5.86)$$

And then we see that the matrices indeed match. Without the matrix P_c , it would still be true that the LHS of (5.83) and (5.84) correspond to the same linear map as in both case one is in the symmetric subspace already, so what would usually be considered a projector is in fact merely a basis change here. The purpose of P_c is to match the representation bases and thus obtain rigorously the same matrix.

Example 2. Now, let's consider the 3-valent vertex

$$\begin{array}{c} 1 & 1 & 1 \\ \swarrow & \downarrow & \searrow \\ & \bullet & \end{array} \quad (5.87)$$

It can be computed with the following ZXH diagram:

$$M = \sqrt{2}^{-3} \sqrt{\frac{1}{3}} \quad \begin{array}{c} \text{ZXH diagram} \end{array} \quad (5.88)$$

PyZX outputs

$$M = \frac{1}{2\sqrt{3}} \begin{pmatrix} 0 & 1 & 1 & 0 & -1 & 0 & 0 & 0 & -1 & 0 & 0 & 0 & 0 & 0 & 0 & 0 \\ 0 & 0 & 0 & -1 & 0 & 0 & 0 & 0 & 0 & 0 & 0 & 0 & 1 & 0 & 0 & 0 \\ 0 & 0 & 0 & -1 & 0 & 0 & 0 & 0 & 0 & 0 & 0 & 0 & 0 & 1 & 0 & 0 \\ 0 & 0 & 0 & 0 & 0 & 0 & 0 & 1 & 0 & 0 & 0 & 0 & 1 & 0 & -1 & -1 \end{pmatrix} \quad (5.89)$$

To obtain the corresponding Yutsis, it is necessary to project the domains and codomains to the symmetric subspaces. The projector on the codomain is the same as (5.85). For the domain, the projector must send a tensor product of four qubits to two spin-1 spaces. This can be written explicitly as the following matrix:

$$P_d = \begin{pmatrix} 1 & 0 & 0 & 0 & 0 & 0 & 0 & 0 \\ 0 & \frac{1}{2}\sqrt{2} & 0 & 0 & 0 & 0 & 0 & 0 \\ 0 & \frac{1}{2}\sqrt{2} & 0 & 0 & 0 & 0 & 0 & 0 \\ 0 & 0 & 1 & 0 & 0 & 0 & 0 & 0 \\ 0 & 0 & 0 & \frac{1}{2}\sqrt{2} & 0 & 0 & 0 & 0 \\ 0 & 0 & 0 & 0 & \frac{1}{2} & 0 & 0 & 0 \\ 0 & 0 & 0 & 0 & \frac{1}{2} & 0 & 0 & 0 \\ 0 & 0 & 0 & 0 & 0 & \frac{1}{2}\sqrt{2} & 0 & 0 \\ 0 & 0 & 0 & \frac{1}{2}\sqrt{2} & 0 & 0 & 0 & 0 \\ 0 & 0 & 0 & 0 & \frac{1}{2} & 0 & 0 & 0 \\ 0 & 0 & 0 & 0 & \frac{1}{2} & 0 & 0 & 0 \\ 0 & 0 & 0 & 0 & 0 & \frac{1}{2}\sqrt{2} & 0 & 0 \\ 0 & 0 & 0 & 0 & 0 & 0 & 1 & 0 \\ 0 & 0 & 0 & 0 & 0 & 0 & 0 & \frac{1}{2}\sqrt{2} \\ 0 & 0 & 0 & 0 & 0 & 0 & 0 & \frac{1}{2}\sqrt{2} \\ 0 & 0 & 0 & 0 & 0 & 0 & 0 & 1 \end{pmatrix} \quad (5.90)$$

So we finally get

$$\begin{array}{c} 1 \quad 1 \quad 1 \\ \diagdown \quad \downarrow \quad \diagup \\ \bullet \end{array} = P_c M P_d = \begin{pmatrix} 0 & \sqrt{\frac{1}{6}} & 0 & -\sqrt{\frac{1}{6}} & 0 & 0 & 0 & 0 \\ 0 & 0 & -\sqrt{\frac{1}{6}} & 0 & 0 & 0 & \sqrt{\frac{1}{6}} & 0 \\ 0 & 0 & 0 & 0 & 0 & \sqrt{\frac{1}{6}} & 0 & -\sqrt{\frac{1}{6}} \end{pmatrix} \quad (5.91)$$

We can check this using standard **Sagemath** computation.

In general to write move from the spin basis to the qubit basis we make use of the canonical relationship given in equation (5.7) which we can use to construct the required basis transformation matrix.

Example 3. Instead of considering the entire matrix of coefficients, let us give another perspective by calculating a specific coefficient. In particular, let's consider the coefficient sending $|\frac{1}{2}, -\frac{1}{2}\rangle \otimes |\frac{1}{2}, -\frac{1}{2}\rangle \mapsto |1, -1\rangle$. First, let's note that some of our input wires are inbound on the node, so that the correspondence between the coefficient of the $3jm$ -symbol and the Yutsis diagram requires that we take the negative of the magnetic index of the symbol (cf. Eq. (5.25)). The explicit calculation is then:

5. Diagrams for Spin-networks and Wigner symbols

$$\begin{aligned}
 \left(\begin{array}{ccc} \frac{1}{2} & \frac{1}{2} & 1 \\ \frac{1}{2} & \frac{1}{2} & -1 \end{array} \right)_{3jm} &= \begin{array}{c} \frac{1}{2}, -\frac{1}{2} \quad \frac{1}{2}, -\frac{1}{2} \quad 1, -1 \\ \diagdown \quad \downarrow \quad \diagup \\ \bullet \end{array} \\
 &= \sqrt{2}^{-4} \sqrt{2}^{-1} \sqrt{\frac{1}{3}} \quad \text{Diagram} = -\sqrt{\frac{1}{3}} \quad (5.92)
 \end{aligned}$$

The LHS denotes a particular Wigner coefficient (not a matrix).

We've written the scalar of the diagram here as a product of terms in order to indicate their separate origins. First, we have a correction of $\sqrt{2}^{-4}$ because the plugged $X(\pi)$ states are equal to $\sqrt{2}|1\rangle$. The correction of $\sqrt{2}^{-1}$ is λ_2 . Finally, the $\sqrt{\frac{1}{3}}$ is binor calculus coefficient $N(\frac{1}{2}, \frac{1}{2}, 1)$. It is easy to verify that the diagram itself is equal to $-\sqrt{2}^5$,

$$\begin{aligned}
 &\text{Diagram} = -1 \quad \text{Diagram} = -\frac{1}{2} \quad \text{Diagram} = -\sqrt{2}^5 \\
 &\text{Diagram} = -\frac{1}{\sqrt{2}} \quad \text{Diagram} = -1 \quad \text{Diagram} = -\frac{1}{\sqrt{2}} \quad \text{Diagram} = -\frac{1}{\sqrt{2}} = -\sqrt{2}^5
 \end{aligned} \quad (5.93)$$

So that we arrive at the final correct answer of $-1/\sqrt{3}$.

4jm-symbol

Now let's consider a slightly more complex diagram: the Wigner $4jm$ -symbol (5.28).

Example 4. The simplest non-trivial $4jm$ -symbol diagram corresponds to four spin-1/2s joining together. There are then two possible ways to connect the wires (in other words, the space of intertwiners is 2-dimensional). First, where the internal wire is spin-1:

$$\begin{aligned}
 \begin{array}{c} \frac{1}{2} \quad \frac{1}{2} \quad \frac{1}{2} \quad \frac{1}{2} \\ \diagdown \quad \downarrow \quad \uparrow \quad \diagup \\ \bullet \quad \bullet \\ 1 \end{array} &= \begin{pmatrix} \frac{1}{3} & 0 & 0 & 0 \\ 0 & -\frac{1}{6} & -\frac{1}{6} & 0 \\ 0 & -\frac{1}{6} & -\frac{1}{6} & 0 \\ 0 & 0 & 0 & \frac{1}{3} \end{pmatrix} \\
 &= \sqrt{2}^{-1} \sqrt{\frac{1}{3}} \quad \text{Diagram} = \sqrt{\frac{1}{3}}
 \end{aligned} \quad (5.94)$$

5.2. The translation to ZXH

Note that unlike the previous $3jm$ -symbols we considered, here the matrices exactly correspond to each other, without requiring projectors, as we are mapping from spin- $\frac{1}{2}$ spaces to spin- $\frac{1}{2}$ spaces.

The other possible $4jm$ -symbol has the intertwiner be spin-0:

$$\begin{array}{c}
 \begin{array}{ccccc}
 \frac{1}{2} & & \frac{1}{2} & & \frac{1}{2} \\
 \diagdown & & \uparrow & & \diagup \\
 \bullet & & \bullet & & \bullet \\
 \rightarrow & & \rightarrow & & \rightarrow \\
 0 & & & &
 \end{array}
 & = & \begin{pmatrix} 0 & 0 & 0 & 0 \\ 0 & -\frac{1}{2} & \frac{1}{2} & 0 \\ 0 & \frac{1}{2} & -\frac{1}{2} & 0 \\ 0 & 0 & 0 & 0 \end{pmatrix} \\
 & & = & \sqrt{\frac{1}{2}}^2 \times \begin{array}{c} \text{X} \\ \text{---} \\ \text{---} \end{array} \quad \begin{array}{c} \text{---} \\ \text{---} \\ \text{---} \end{array} \quad (5.95)
 \end{array}$$

As the spin is zero there are no wires between the individual $3jm$ -symbols, and furthermore these $3jms$ reduce to the special cases of the cup and cap given in (5.68) and (5.69).

Example 5. Now let's consider a $4jm$ -symbol with some larger spins:

$$\begin{array}{c}
 \begin{array}{ccccc}
 1 & & 1 & & \frac{1}{2} & & \frac{1}{2} \\
 \diagdown & & \uparrow & & \uparrow & & \diagup \\
 \bullet & & \bullet & & \bullet & & \bullet \\
 \rightarrow & & \rightarrow & & \rightarrow & & \rightarrow \\
 & & & & 1 & &
 \end{array}
 & & & & & & (5.96)
 \end{array}$$

It can be computed with the following in ZXH diagram

$$M = \sqrt{\frac{1}{2}}^3 \sqrt{\frac{1}{3}} \sqrt{\frac{1}{3}} \times \begin{array}{c} \text{Complex ZXH diagram} \end{array} \quad (5.97)$$

PyZX outputs

$$M = \frac{1}{6} \begin{pmatrix} 0 & -1 & -1 & 0 & 1 & 0 & 0 & 0 & 1 & 0 & 0 & 0 & 0 & 0 & 0 & 0 \\ 0 & 0 & 0 & 1 & 0 & 0 & 0 & 0 & 0 & 0 & 0 & 0 & -1 & 0 & 0 & 0 \\ 0 & 0 & 0 & 1 & 0 & 0 & 0 & 0 & 0 & 0 & 0 & 0 & -1 & 0 & 0 & 0 \\ 0 & 0 & 0 & 0 & 0 & 0 & 0 & 1 & 0 & 0 & 0 & 1 & 0 & -1 & -1 & 0 \end{pmatrix} \quad (5.98)$$

5. Diagrams for Spin-networks and Wigner symbols

To obtain the final correct matrix, we only need to project on the domain to map between the spin-1 and spin-1/2 perspectives and so as we will have

$$\begin{aligned}
 & \begin{array}{c} 1 & 1 & \frac{1}{2} & \frac{1}{2} \\ \diagdown & \downarrow & \uparrow & \diagup \\ \bullet & \xrightarrow{1} & \bullet & \xleftarrow{1} \end{array} = MP_d \\
 & = \begin{pmatrix} 0 & -\frac{1}{3\sqrt{2}} & 0 & \frac{1}{3\sqrt{2}} & 0 & 0 & 0 & 0 & 0 & 0 & 0 \\ 0 & 0 & \frac{1}{6} & 0 & 0 & 0 & 0 & 0 & -\frac{1}{6} & 0 & 0 \\ 0 & 0 & \frac{1}{6} & 0 & 0 & 0 & 0 & 0 & -\frac{1}{6} & 0 & 0 \\ 0 & 0 & 0 & 0 & 0 & 0 & 0 & -\frac{1}{3\sqrt{2}} & 0 & \frac{1}{3\sqrt{2}} & 0 \end{pmatrix} \quad (5.99)
 \end{aligned}$$

Example 6. And again, let us demonstrate that we can also calculate directly specific coefficients of the $4jm$ -symbol:

$$\begin{aligned}
 & \left(\begin{array}{cccc} 1 & 1 & \frac{1}{2} & \frac{1}{2} \\ -1 & 0 & \frac{1}{2} & \frac{1}{2} \end{array} \right)^{(1)} = \begin{array}{c} 1, 1 \quad 1, 0 & \frac{1}{2}, \frac{1}{2} \quad \frac{1}{2}, \frac{1}{2} \\ \diagdown & \uparrow \\ \bullet & \xrightarrow{1} \end{array} \\
 & = \sqrt{\frac{1}{2}} \sqrt{\frac{1}{2}} \sqrt{\frac{1}{3}} \sqrt{\frac{1}{3}} \quad \text{Diagram:} \\
 & \quad \text{A complex spin network diagram with 12 nodes. Nodes are colored red (1), green (1/2), and white (0). Edges are labeled with } \pi. \quad \text{Diagram:} \\
 & = \sqrt{\frac{1}{3}} \sqrt{\frac{1}{6}} \quad (5.100)
 \end{aligned}$$

The scalar factor $\sqrt{2}^{-3}$ is λ_2^3 , the $\sqrt{2}^{-5}$ to rescale the inputs/outputs to basis elements (remembering that $|j=1; m=0\rangle = \frac{|01\rangle + |10\rangle}{\sqrt{2}}$ so that it only requires one $\sqrt{2}$ to be rescaled unlike the pairs of $|1\rangle$ input/output states) and the $\sqrt{\frac{1}{3}}$'s are the factors from the binor calculus $N(1, 1, 1)$ and $N(1/2, 1/2, 1)$. The diagram itself evaluates to $\sqrt{2}^7$:

6j-symbol

As a further example let us consider an invariant function, specifically the Wigner 6j symbol

$$\left\{ \begin{array}{ccc} j_1 & j_2 & j_3 \\ j_4 & j_5 & j_6 \end{array} \right\}$$

which as shown in equation 5.34 is composed of 4 interlinked 3jm symbols or equivalently as two 4jm-symbols. We will take the latter as a diagrammatic starting point and can therefore state explicitly that:

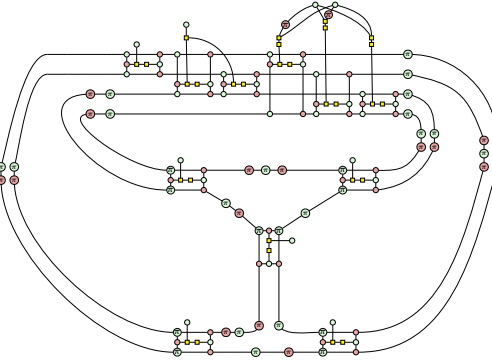
$$\begin{array}{c} \text{Diagram of a graph with 6 vertices labeled } j_1, j_2, j_3, j_4, j_5, j_6. \\ \text{Diagram of a complex circuit with nodes labeled } j_1, j_2, j_3, j_4, j_5, j_6, \text{ and } 2j_1, 2j_2, 2j_3, 2j_4, 2j_5, 2j_6. \\ = C \end{array} \quad (5.102)$$

5. Diagrams for Spin-networks and Wigner symbols

Where

$$C = \frac{\lambda_{2j_1}\lambda_{2j_2}\lambda_{2j_3}\lambda_{2j_4}\lambda_{2j_5}\lambda_{2j_6}}{N(j_1, j_2, j_3)N(j_1, j_6, j_5)N(j_2, j_6, j_4)N(j_3, j_4, j_5)} \quad (5.103)$$

Example 7. Let's work out a concrete example.

$$\left\{ \begin{array}{ccc} 2 & 1 & 1 \\ 1 & 1 & 1 \end{array} \right\} = \begin{array}{c} 2 \\ \diagup \quad \diagdown \\ 1 \quad 1 \\ \diagdown \quad \diagup \\ 1 \quad 1 \end{array} = C \quad \text{Diagram} \quad (5.104)$$


With

$$C = \frac{1}{48} * \left(\frac{1}{\sqrt{2}} \right)^5 * \left(\sqrt{\frac{2!2!2!}{4!1!1!1!}} \right)^2 * \left(\sqrt{\frac{4!2!2!}{5!2!2!0!}} \right)^2$$

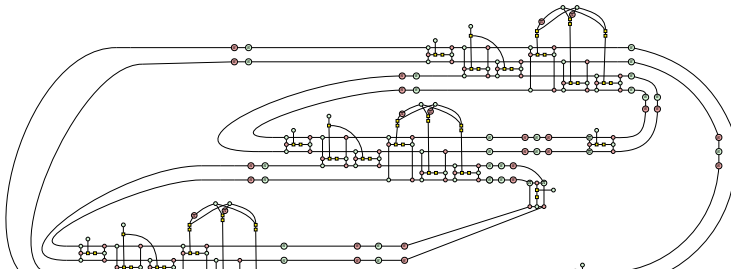
From which we can see

$$480\sqrt{2}C = \frac{1}{6}$$

Where we note that as a tensor (we calculated this in PyZX) this diagram evaluates to $480\sqrt{2}$.

To get the value of the actual Wigner symbol we then multiply this by the scalar corrections for the symmetrisers λ and by the four normalisations from the binor calculus N .

Example 8. As a further example consider the following $6j$ -symbol

$$\left\{ \begin{array}{ccc} 2 & 2 & 2 \\ 1 & 1 & 1 \end{array} \right\} = \begin{array}{c} 2 \\ \diagup \quad \diagdown \\ 2 \quad 1 \\ \diagdown \quad \diagup \\ 1 \quad 1 \end{array} = C \quad \text{Diagram} \quad (5.105)$$


with

$$C = \left(\frac{1}{48} \right)^3 \left(\frac{1}{\sqrt{2}} \right)^3 \left(\sqrt{\frac{4!4!4!}{7!2!2!2!}} \right)^2 \left(\sqrt{\frac{4!2!2!}{5!2!2!0!}} \right)^2 \quad (5.106)$$

From which we can see

$$645120\sqrt{2}C = \frac{\sqrt{21}}{30}$$

where $645120\sqrt{2}$ is the value of the diagram as calculated via tensor contraction in PyZX.

5.2.4 Higher Wigner invariants and the question of quantum computation

The extension to higher Wigner symbols is just an exercise in merging more and more $3jm$ symbols. That said, the representation is not a calculation. After representing these objects as ZXH tensor networks, two routes are available. As a ZXH diagram subject to ZXH rules, there is no obvious route for further simplification that would reduce to a small number of easily evaluated elements. As a tensor network, it is known that it is a classically hard (NP-hard) problem to contract a tensor network in general. Although there is likely to be a simplification in the case of contracting objects such as the symbol $6j$, due to the existence of relatively efficient numerical methods [87], the crude notion of simply representing such objects as tensors and then contracting them depends largely on the methods of optimising the contraction and is not guaranteed a priori to offer computational advantages over other approaches. The field of quantum computing may, however, offer a route to practical calculations for more complicated objects such as the amplitudes of the vertices of the spin-foams [88], a model of which can be seen as a 4-valence spin lattice, which are in general difficult to calculate classically. What we present here allows us to take $SU(2)$ spin networks and encode them directly into a framework that can be viewed as qubits and operators on them.

However, a qubit representation does not in itself guarantee that a problem is vulnerable to the computational advantages of a quantum computer. In the literature, the issue of obtaining a quantum algorithm is one of ‘circuit extraction’. The aim is to take a problem and describe it in terms of state inputs and output measures with units in the middle. Whether a problem is amenable to quantum algorithms is determined by the extent to which it does not adhere to this model, the complexity of the state preparation, and the error one can tolerate. If, as in the case of our CSWAPS, there are ‘post-selected measures’, i.e. measures that must have certain values when the algorithm is run, it is possible that when we run the algorithm we do not get the required values and we have to re-run the algorithm. This means that there is a question of scaling the number of post-selected measures, with the parameters of the problem, as each of

5. Diagrams for Spin-networks and Wigner symbols

these measures will reduce our chances of success. Secondly, the state inputs of the algorithm may themselves be complex to create, even if the unit operations on these inputs are very simple, which may hide the actual complexity of the algorithm, a problem not always addressed in the literature. For these reasons, the question of the appropriate way to use quantum computers for the computation of $SU(2)$ invariant symbols remains open. Given developments observed in the literature in the broader literature [89, 90] there are reasons to be optimistic. Indeed in [88] 4-valence intertwiners (fixed to dimension 2) are modelled and they attempt to determine spin lattice transition amplitudes based on the intertwiners by running a quantum algorithm on IBM superconducting devices.

5.2.5 The ZXH Spin-network

As seen above in section 5.1.4 the $3jm$ -symbols can be used to specify intertwiners of a spin-network. Having translated yutsis diagrams into ZXH it then possible to write spin-network diagrams as ZXH diagrams. The Clebsch-Gordon conditions are then subsumed by the fact that wires must match up for connections between the $3jm$ subdiagrams. The intertwiners themselves are literally specifications of how the strand intertwine within the $3jm$ symbols. As such we can easily construct an arbitrary spin-network by interconnecting compatible $3jm$ -symbols:

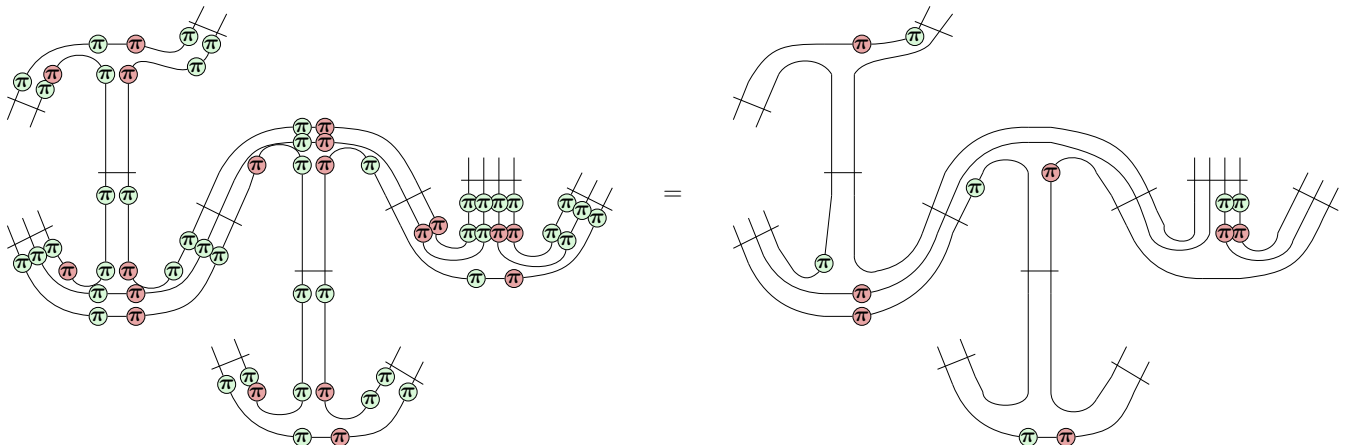


Figure 5.3: A spin-network composed of interconnected $3jm$ -symbols written as a ZXH-diagram fused so as to preserve $SU(2)$ invariance. On the left-hand side of the equality we have the spin-network simply as a raw composition of $3jm$ -symbols fused as per the rule outlined in equation 5.66. This results in a number of superfluous phases on either side of a symmetriser, which can be commuted through to be cancelled it is interesting to note the sheer scale of the redundancy that exists within the original $SU(2)$ invariant vertex description.

We can see from the construction that the arrangements of the π -phases, particularly the Z phases associated to the symmetrisers are removable given, some sign changes. We leave them

here as it overlaps with the construction as so far described and puts everything in terms of diagrammatic elements rather than having a parametrised scalar alongside our diagram. This is ultimately a matter of choice.

5.3 Motivating operators on spin-networks

We will soon move to discuss operators acting on the spaces defined by spin network states. To motivate this it is practical to know where such an ambition can arise from.

In general relativity the world is classical and space-time is defined as a manifold \mathcal{M} with a metric $g_{\mu\nu}$. At each point there is a metric $g_{\mu\nu}(x)$ giving at each point $x \in \mathcal{M}$ a pseudo-Riemannian scalar product (which takes in two vectors of the tangent space and returns a number linearly). This metric measures local distance. General relativity restricts the possible metrics of space-time to those that solve Einstein equations. These equations relate how matter moves in presence of gravity and how space-time curves in the presence of matter. It is curvature that leads to the gravitational ‘force’ as particles moving on the ‘straight paths’ of a curving manifold seem to come together when unaffected by other forces. It looks as if they are pulled together, but of course they feel no accelerating force acting on them (from a windowless pod they wouldn’t know if they were falling or floating), they are simply bodies in motion naturally following the curvature of the space they are in. It is likely however that general relativity is only an effective description of some more fundamental quantum theory of space-time. This problem has been met with modest success over the last century.

There is a method to build a quantum theory from a classical one via *canonical quantisation* though this route isn’t systematic in its approach. The first step is to determine a time parameter. For a 4D manifold \mathcal{M} this is achievable via (ADM see appendix H) splitting the space into 3D foliations Σ_t indexed by $t \in \mathbb{R}$, which turns out to be an arbitrary, choice of time. In this way space-time can be written as the direct product:

$$\mathcal{M} \cong \Sigma \times \mathbb{R}. \quad (5.107)$$

This set of possible metrics q_{ab} defined on the 3D foliation Σ defines the classical *configuration space* \mathcal{C} . The Einstein equations then provide the time evolution between one slice with metric q_{ab} on an initial slice Σ_0 with the additional requirement that one also specifies the a kind of “initial

5. Diagrams for Spin-networks and Wigner symbols

momentum" on Σ_0 which is the extrinsic curvature k_{ab} which can be seen as a complication of the usual notion of derivative of q_{ab}). With this defined it is possible to uniquely characterise a specific 4-dimensional metric $g_{\mu\nu}$ from the parameters (q_{ab}, k_{ab}) . In this way each (q_{ab}, k_{ab}) describes a possible *classical state* of space-time, and thus defines a point in the *phase space* \mathcal{P} of the theory.

There is a further restriction on the phase space we have now defined from the necessity of diffeomorphism invariance. A diffeomorphism is an isomorphism between manifolds and as such is essentially a relabelling of the same mathematical structure. The physical implication of this is that any parts of the phase space (q_{ab}^1, k_{ab}^1) and (q_{ab}^2, k_{ab}^2) that are equivalent under a diffeomorphism must physically correspond to the same state. This symmetry imposed by the diffeomorphism is said to *constraint* the phase space indicating that only a subspace of \mathcal{P} is required to characterise physical states.

To quantise we must move from a phase space \mathcal{P} to a Hilbert space \mathcal{H} and the coordinates of \mathcal{P} must become operators on \mathcal{H} . There are a number of significant technical hurdles to achieving this but they are somewhat ameliorated by moving to the *Ashtekar-Barbero variables* (A_i^a, E_a^i) , instead of (q_{ab}, k_{ab}) . The new coordinates are an equally valid choice of coordinates on the phase space \mathcal{P} , but working with these variables brings the formulation of general relativity closer to other gauge theories which have already been successfully quantised. In moving to these variables however the geometric intuition is suppressed. The connection A_i^a dictates how vectors are transported along curves on Σ and the triad E_a^i define a local basis at each point.

These coordinates on \mathcal{P} which we now refer to via their new (A_i^a, E_a^i) , which split \mathcal{P} into a subspace of "position" A_i^a and a subspace of "momentum" E_a^i . A major novelty of quantum mechanics is that systems can actually be in superposition of "positions". Mathematically, this means that the *quantum states* are functions of the "positions". These (wave) functions carry a probabilistic interpretation, which endows the space with a notion of scalar product, so that the space of quantum states is eventually a Hilbert space.

The promotion of the phase space variables (A_i^a, E_a^i) to operators implies that the Hilbert space would be made of (square-integrable) functions over the subspace of positions A_i^a . But each point A_i^a is itself a function over Σ , so that the resulting Hilbert space would be a space of "functions of functions", which is unfortunately too big to apply our cherished simple mathematical tools.

5.3. Motivating operators on spin-networks

So one has first to "truncate" the classical theory by selecting only a finite number of degrees of freedom: the Hilbert space should be made of functions over a finite dimensional space.

In general the phase space variable (A_i^a, E_a^i) remains too large to be practical and so "truncation" is performed by taking a finite graph Γ , with 'nodes' n and 'links' l embedded within Σ . The space is thus reduced from a 3D to a 1D manifold. Moreover instead of taking the value of $A_i^a(x)$ at every point x of Σ or Γ , we take the holonomy along the links l

$$h_l = Pe^{\int_l A} \quad (5.108)$$

where P means "path-ordered", and A is a short-cut for some linear function of A_i^a without indices. The holonomy technically determines 'curvature' of the region of a manifold it circumscribes. *The crucial thing here is that it can be shown that $h_l \in SU(2)$.* The new space of "positions" is now finite-dimensional: one holonomy h_l per link l of the graph Γ . It is homomorphic to $SU(2)^L$, where L is the total number of links of Γ . While this is still a classical description it can be readily quantised.

The resultant Hilbert space is given by the (square-integrable) functions of the holonomies

$$\mathcal{H}_\Gamma = L^2(SU(2)^L), \quad (5.109)$$

In order to impose the necessary physical constraints it is practical to rewrite this space somewhat. Firstly as the space of functions over a Cartesian product can be seen as a tensor product of functions of single variables, we can write

$$\mathcal{H}_\Gamma \cong \bigotimes_{l \in \Gamma} L^2(SU(2)), \quad (5.110)$$

with the tensor product made over all the links l of Γ . The Peter-Weyl theorem[31] tells us that functions over Lie group can be decomposed into a sum of irreducible representations. The Lie group is $SU(2)$ whose set of irreps is parametrised by the half-integers (spins) $j \in \mathbb{N}/2$. As such we can write

$$L^2(SU(2)) \cong \bigoplus_{j \in \mathbb{N}/2} (\mathcal{H}_j \otimes \mathcal{H}_j). \quad (5.111)$$

Putting together equations (5.110) and (5.111), and inverting the direct sum and the tensor product, we get

$$\mathcal{H}_\Gamma \cong \bigoplus_{j_L} \bigotimes_{l \in \Gamma} (\mathcal{H}_l \otimes \mathcal{H}_l). \quad (5.112)$$

5. Diagrams for Spin-networks and Wigner symbols

where the direct sum is made over all possible labelling that assign a spin j_l to each link l . Then the tensor product over the links of the space \mathcal{H}_l with itself can be regarded as a tensor product over the nodes of a single copy of \mathcal{H}_l , so that

$$\mathcal{H}_\Gamma \cong \bigoplus_{j_L} \bigotimes_{n \in \Gamma} \bigotimes_{l \in n} \mathcal{H}_l. \quad (5.113)$$

We are now in a position to impose the constraints. There are three that are required in LQG. The first constraint, termed the 'Gauss constraint', is a result of the previously discussed transition to the variables (A_i^a, E_a^i) instead of (q_{ab}, k^{ab}) . It restricts the Hilbert space to the invariant subspace:

$$\mathcal{H}_\Gamma \cong \bigoplus_{j_l} \bigotimes_n \text{Inv}_{SU(2)} \left(\bigotimes_{l \in n} \mathcal{H}_l \right). \quad (5.114)$$

The second constraint implements the restriction due to the diffeomorphism. The diffeomorphism alters the graph Γ by changing how it lies within Σ but leaves its topology and combinatorial properties unaffected. In short: isotopic graphs Γ label the same physical states. Thus graph doesn't need to be considered embedded in any space at all and the relevant space for us is characterised purely by the graph.

The final space then is the sum over all the possible graphs:

$$\mathcal{H}_{LQG} = \bigoplus_{\Gamma} \mathcal{H}_{\Gamma}. \quad (5.115)$$

As we now have a physically motivated quantisation of space-time we can now look at how properties of this Hilbert space can be obtained.

5.4 Operators on spin networks

With spin-networks defined and alluded to as characterising spin-network states a natural question is how to apply operators of interest on these networks. This question is still under active research by myself and others and as such the section is less complete in its content than previous sections however it serves as example of one of the directions the work in this thesis can go in the future.

As has been discussed above the total Hilbert space of spin-network states is given by summing over all possible graphs:

$$\mathcal{H} = \bigoplus_{\Gamma} \mathcal{H}_{\Gamma} \quad (5.116)$$

where the sum is made over all 4-valent spin-networks, and

$$\mathcal{H}_\Gamma = \bigotimes_{n \in \Gamma} \text{Inv}(n). \quad (5.117)$$

So given a spin-network, a state is a choice of a state in each invariant subspace of the nodes, or a superposition of such choices.

The question is then what interesting operators could be applied to it and how would we define such things? In this chapter we will discuss what are often referred to as the geometric operators. If one takes a spin network and considers the dual structure where each edge is passing through the centre of a face of a tetrahedron, then one can imagine three different measurements one might be interested in. The area of a face, which is determined by the spin-network edge that passes through it, the angle between two adjacent faces determined by two adjacent edges entering a vertex, and finally a volume which acts on the vertex itself [25].

Area. There is one area operator for each link of the graph. The area operator on the link l is

$$\hat{A}_l = 8\pi\gamma \frac{\hbar G}{c^3} \sqrt{\vec{J}_l^2} \quad (5.118)$$

The spin-network states are eigenstates of the area operators:

$$\hat{A}_l |\Gamma\rangle = 8\pi\gamma \frac{\hbar G}{c^3} \sqrt{j_l(j_l + 1)} |\Gamma\rangle \quad (5.119)$$

Angle. There is one angle observable for each pair of links meeting at a node.

$$\Theta_{12} = \vec{J}_1 \cdot \vec{J}_2 \quad (5.120)$$

Strictly speaking, we should have $\theta_{12} = \arccos(J_1 \cdot J_2) / j_1 j_2$. This operator can be diagonalised within the invariant subspace with the $4jm$ -Wigner symbol.

Volume. The volume is defined as

$$V = \frac{\sqrt{2}}{V} (8\pi G \hbar \gamma)^{3/2} \sqrt{\vec{J}_1 \cdot (\vec{J}_2 \times \vec{J}_3)} \quad (5.121)$$

Unfortunately the volume isn't diagonal in the same basis as the angles.

One should note however that these operators do not all commute. This means we can, for example, fix either the volume or the angle between two faces, but never both of them. The

5. Diagrams for Spin-networks and Wigner symbols

quantum geometry is always indeterminate in the manner of the Heisenberg uncertainty principle. In this way we have a discretised tetrahedral space-time made up of quantised lumps tetrahedra glued to neighbouring ones.

5.5 Diagrammatic Spin network operators

We are now looking at the 3D states of space as spin-networks. We will be discussing examples of quantised area and volume operators on the 4-valent spin-network states.

5.5.1 Quantised Area

The simplest operator to be applied to a spin network is the Area operator that acts on a single wire and gives the total angular momentum of the associated spin which corresponds to the area of one of the faces of the tetrahedron each vertex represents.

Recall that in the context of ZXH diagrams we are discussing each spin or otherwise put each representation of $SU(2)$ in terms of the fundamental representation or spin $\frac{1}{2}$.

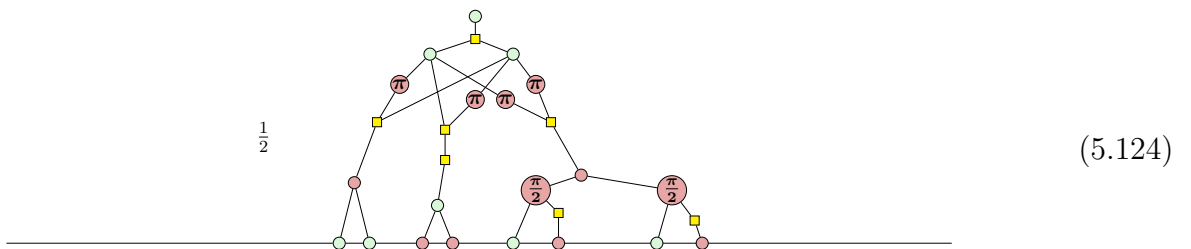
Recalling that the total angular momentum J is calculated via the square operator:

$$J^2 = J_x^2 + J_y^2 + J_z^2 \quad (5.122)$$

We know that for a spin $\frac{1}{2}$ the $J_i = \frac{\sigma_i}{2}$ in natural units. We are therefore looking for a diagram that represents

$$J_{\frac{1}{2}}^2 = \frac{\sigma_x^2}{4} + \frac{\sigma_y^2}{4} + \frac{\sigma_z^2}{4} \quad (5.123)$$

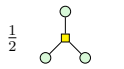
To this end consider the following diagram



Even a passing familiarity with the rules of ZXH tells us that this has immediate simplifications but we present it in this form to highlight its component-wise structure. The crown of the diagram serves to offer the sum via being a coherently control resulting in three states (there

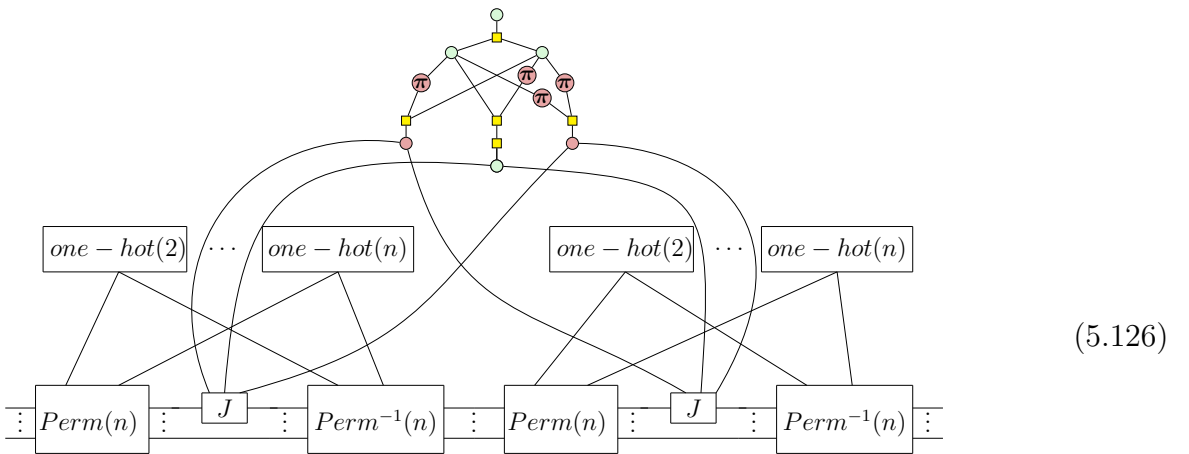
5.5. Diagrammatic Spin network operators

are two controls but the fourth state is projected to zero). For the states $|00\rangle, |01\rangle$, and $|10\rangle$ we have two sequentially controlled Z gates, X gates, and Y gates which are respectively activated i.e we apply σ_z^2 , σ_x^2 or σ_y^2 respectively. This diagram is provably equal to the following using applying the fusion and bialgebra rules in a blunt fashion repeatedly:


(5.125)

Where one can validate by hand the scalar diagram is equal to 6 and as such the overall scalar is indeed $\frac{3}{4}$.

There is a slight complication to the extension of operator to higher spins (representations). If we consider our schematic once again we are going to have something, by virtue of the description of a lie algebra element in terms the fundamental representation and the fact in $J^2 = J_x^2 + J_y^2 + J_z^2$ each J_i is applied twice, that looks like this:



The crown at the top should be understood to be allowing us to apply each of the J_i together in superposition. In summary this diagram is a superposition of applying $J_i \circ J_i$ for each i , where each J_i is itself the raised version of the spin-1/2 operator.

For the spin 1 edge for example this gives us the following diagram:

5. Diagrams for Spin-networks and Wigner symbols

$$\frac{1}{2} * 4 * \frac{1}{4} = 2 \begin{pmatrix} 1 & 0 & 0 & 0 \\ 0 & 2^{-1} & 2^{-1} & 0 \\ 0 & 2^{-1} & 2^{-1} & 0 \\ 0 & 0 & 0 & 1 \end{pmatrix} \quad (5.127)$$

Note the $\frac{1}{2}$ is due to the multi-legged H bow followed by an normal H-box, the 4 and $\frac{1}{4}$ are the symmetriser correction and the two $\frac{1}{2}$ contributions from the spin operators respectively. Here we have used that the operator $|00\rangle + |11\rangle$ coherently controlling the two swaps is merely the bending of the identity wire.

Now if we change to the spin-1 basis as follows by mapping the domain and codomain appropriately:

$$2 \begin{pmatrix} 1 & 0 & 0 & 0 \\ 0 & \frac{1}{\sqrt{2}} & \frac{1}{\sqrt{2}} & 0 \\ 0 & 0 & 0 & 1 \end{pmatrix} \begin{pmatrix} 1 & 0 & 0 & 0 \\ 0 & 2^{-1} & 2^{-1} & 0 \\ 0 & 2^{-1} & 2^{-1} & 0 \\ 0 & 0 & 0 & 1 \end{pmatrix} \begin{pmatrix} 1 & 0 & 0 \\ 0 & \frac{1}{\sqrt{2}} & 0 \\ 0 & \frac{1}{\sqrt{2}} & 0 \\ 0 & 0 & 1 \end{pmatrix} = 2 \begin{pmatrix} 1 & 0 & 0 \\ 0 & 1 & 0 \\ 0 & 0 & 1 \end{pmatrix} \quad (5.128)$$

Thus we see we have the correct total angular momentum value eigen value $j(j+1)$ which is 2 for spin 1.

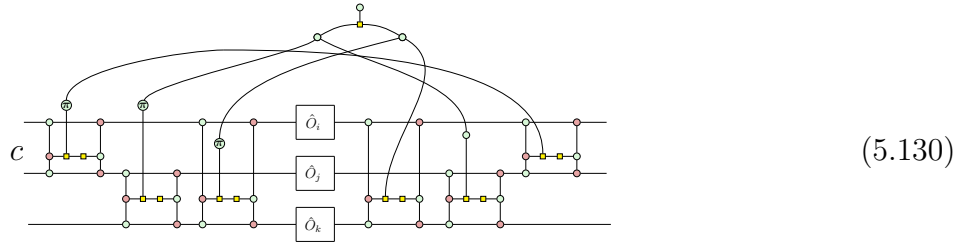
5.5.2 Quantised Volume

Spin half volume operator

We begin with the simplest example of a quadrivalent spin half vertex. Here the volume operator, taking the spin half simplification of equation (5.121) and using the Levi-Civita description of the cross product, is proportional to the following

$$V^2 \propto \tilde{V}^2 = \epsilon_{ijk} J_x^i J_y^j J_z^k = \frac{1}{8} \epsilon_{ijk} \sigma_x^i \sigma_y^j \sigma_z^k \quad (5.129)$$

This needs to act on the Hilbert spaces of three spin-1/2 wires. Before we can discuss the rotations we need to diagrammatically form the ZXH diagram $\epsilon_{ijk} \hat{O}_i \hat{O}_j \hat{O}_k$, this can be seen to be as follows:



Where \hat{O}_i , \hat{O}_j and \hat{O}_k are the single space operators represented by the square boxes with these labels. At first glance we can see this has the contains similar structure to the symmetriser. This shouldn't surprise us as they both talk in terms of permutations. The difference here is that the permutations that involve an odd number of swaps should induce a negative sign. This is achieved by the subtle addition of a green π which we recall is $|0\rangle\langle 0| - |1\rangle\langle 1|$ thus when the swap is to occur (i.e the state is $|1\rangle$) we will get a minus sign as required. The scalar c represents the correction required for the anti-permutation structure and operators \hat{O}_x .

The idea here is to achieve the different permutations of operators not by crudely implementing different combinations of rotations but by, as before, implementing coherent swaps of the of the underlying Hilbert spaces. We apply the operators then undo the coherent permutation. The result is a sum of all the combinations of wire swaps with the operators applied (giving all the combinations of operators on each space) ordered as required. The volume operator of the spin- $\frac{1}{2}$ operator then implements $\epsilon_{ijk}\sigma_x^i\sigma_y^j\sigma_z^k$ on three incident edges and acts as the identity of the fourth - in this way it acts on the whole vertex. As a result we have defined an operator that up to a scalar functions as the volume operator on node with 4 incoming spin half wires (it is the identity on last wire, which is viewed as 'last' is physically irrelevant [26]). We can calculate directly that

$$\epsilon_{ijk}\sigma_x^i\sigma_y^j\sigma_z^k = 2i \begin{pmatrix} 0 & 0 & 0 & 0 & 0 & 0 & 0 & 0 \\ 0 & 0 & 1 & 0 & -1 & 0 & 0 & 0 \\ 0 & -1 & 0 & 0 & 1 & 0 & 0 & 0 \\ 0 & 0 & 0 & 0 & 0 & -1 & 1 & 0 \\ 0 & 1 & -1 & 0 & 0 & 0 & 0 & 0 \\ 0 & 0 & 0 & 1 & 0 & 0 & -1 & 0 \\ 0 & 0 & 0 & -1 & 0 & 1 & 0 & 0 \\ 0 & 0 & 0 & 0 & 0 & 0 & 0 & 0 \end{pmatrix} \quad (5.131)$$

From this we can show that:

5. Diagrams for Spin-networks and Wigner symbols

$$\epsilon_{ijk} J_x^i J_y^j J_z^k = \frac{1}{2} \begin{array}{c} \text{Diagram} \\ \text{with} \\ \text{curly} \\ \text{wires} \end{array} = \frac{i}{4} \begin{pmatrix} 0 & 0 & 0 & 0 & 0 & 0 & 0 & 0 \\ 0 & 0 & 1 & 0 & -1 & 0 & 0 & 0 \\ 0 & -1 & 0 & 0 & 1 & 0 & 0 & 0 \\ 0 & 0 & 0 & 0 & 0 & 0 & -1 & 1 \\ 0 & 1 & -1 & 0 & 0 & 0 & 0 & 0 \\ 0 & 0 & 0 & 1 & 0 & 0 & -1 & 0 \\ 0 & 0 & 0 & -1 & 0 & 1 & 0 & 0 \\ 0 & 0 & 0 & 0 & 0 & 0 & 0 & 0 \end{pmatrix} \quad (5.132)$$

Now for the area operator the spin basis diagonalised the operators and as such the basis elements could be taken as eigenvectors. This is explicitly not the case for the volume operator.

The eigenvector of this operation is known to live in the space spanned by the two possible intertwiners of the 4-valent spin-1/2 vertex ι_0 and ι_1 and is $\iota_0 + i\sqrt{3}\iota_1$ [26]. Where ι_0 given by

$$\iota_0 = \frac{1}{2} \begin{array}{c} \text{Diagram} \\ \text{with} \\ \text{two} \\ \text{curly} \\ \text{wires} \end{array} = \frac{1}{2} \begin{pmatrix} 0 & 0 & 0 & 0 \\ 0 & 1 & -1 & 0 \\ 0 & -1 & 1 & 0 \\ 0 & 0 & 0 & 0 \end{pmatrix} \quad (5.133)$$

ι_1 is simply a small deviation to the symmetriser:

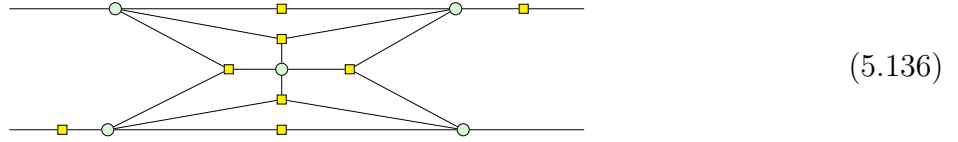
$$\iota_1 = \frac{1}{3\sqrt{2}} \begin{array}{c} \text{Diagram} \\ \text{with} \\ \text{one} \\ \text{curly} \\ \text{wire} \end{array} = \begin{pmatrix} 0 & 0 & 0 & \frac{1}{3} \\ 0 & -\frac{1}{6} & -\frac{1}{6} & 0 \\ 0 & -\frac{1}{6} & -\frac{1}{6} & 0 \\ \frac{1}{3} & 0 & 0 & 0 \end{pmatrix} \quad (5.134)$$

which resembles and inverted yutsis wire if we viewed this as attached to a vertex on the left.

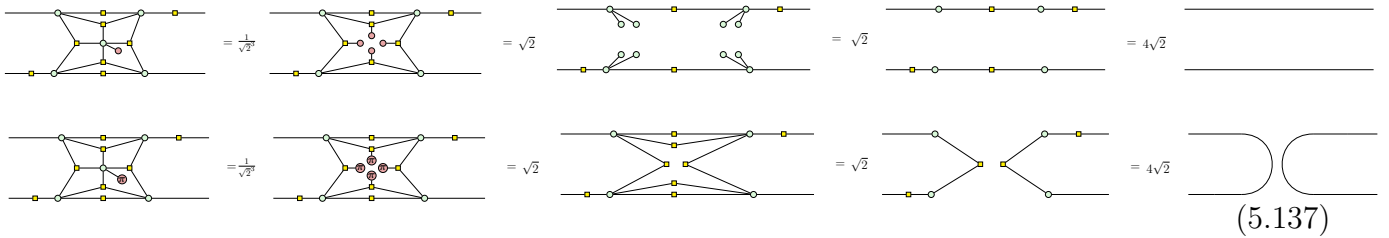
In matricial form the desired operator is the following:

$$\iota_0 + i\sqrt{3}\iota_1 = \frac{1}{\sqrt{3}} \begin{pmatrix} 0 & 0 & 0 & i \\ 0 & e^{-i\frac{\pi}{6}} & e^{-i\frac{5\pi}{6}} & 0 \\ 0 & e^{-i\frac{5\pi}{6}} & e^{-i\frac{\pi}{6}} & 0 \\ i & 0 & 0 & 0 \end{pmatrix} \quad (5.135)$$

The complication of building the operator $\iota_0 + i\sqrt{3}\iota_1$ is firstly that the two operators have a different topology so we must first build an operator capable of representing this. Such a diagram can be written as follows:

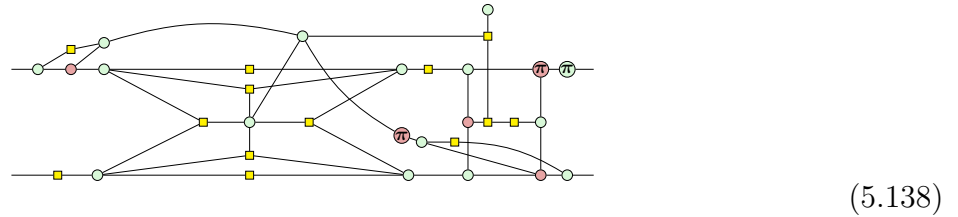


We can see this is correct via the following explicit demonstrations of the equivalence of each element of the superposition and the desired map :



Note how when the control is green, that is to say we are in the superposition $|0\rangle + |1\rangle$, this can merge with the central vertex which is exactly what we see in the original diagram.

Given this structure minor alteration to give ι_0 and ι_1 exactly leads us to the following diagram:



This is still not quite right however. The eigenvector for the volume operator is $\iota_0 + i\sqrt{3}\iota_1$ not $\iota_0 + \iota_1$ so we must account for this scalar. The final diagram can be found (via PyZX) to be the following:

$$\frac{-i}{\sqrt{2^5}\sqrt{3}} \times \sqrt{3}i = \frac{1}{\sqrt{3}} \begin{pmatrix} 0 & 0 & 0 & i \\ 0 & e^{-i\frac{\pi}{6}} & e^{-i\frac{5\pi}{6}} & 0 \\ 0 & e^{-i\frac{5\pi}{6}} & e^{-i\frac{\pi}{6}} & 0 \\ i & 0 & 0 & 0 \end{pmatrix} \quad (5.139)$$

$$= \frac{-i}{\sqrt{3}} \begin{pmatrix} 0 & 0 & 0 & 1 \\ 0 & -e^{i\frac{\pi}{3}} & e^{i\frac{2\pi}{3}} & 0 \\ 0 & e^{i\frac{2\pi}{3}} & -e^{i\frac{\pi}{3}} & 0 \\ 1 & 0 & 0 & 0 \end{pmatrix} \quad (5.140)$$

5. Diagrams for Spin-networks and Wigner symbols

Or to write it in terms usable in PyZX (generic H boxes aren't possible in PyZX)

$$\iota_0 + i\sqrt{3}\iota_1 = \frac{-i}{\sqrt{2^9}\sqrt{3}} \quad \text{Diagram} \quad (5.141)$$

where the sole function of the extra elements are to address the scalar issue described and to account for the extra scalar this induces. Note the use of two forms of the operator (one with 'i' factorised out) which is to allow the interested reader to more easily replicate these results in PyZX which presents the factorised version. It is one thing to describe an operator and quite another to be able to diagrammatically apply it.

This thesis shows the validity of the diagrams outlined numerically as tensors but the question of diagrammatic rewrite strategies for the application of this left open and remains unresolved here. We can use PyZX to perform this numerical validation via the following eigen-equation. Let us convert this volume element to a state column vector

$$\left| \iota_0 + i\sqrt{3}\iota_1 \right\rangle = \frac{-i}{\sqrt{2^9}\sqrt{3}} \quad \text{Diagram} \quad = \frac{-i}{\sqrt{3}} \quad \begin{pmatrix} 0 \\ 0 \\ 0 \\ 1 \\ 0 \\ -e^{i\frac{1}{3}\pi} \\ e^{i\frac{2}{3}\pi} \\ 0 \\ 0 \\ e^{i\frac{2}{3}\pi} \\ -e^{i\frac{1}{3}\pi} \\ 0 \\ 1 \\ 0 \\ 0 \\ 0 \end{pmatrix} \quad (5.142)$$

where the ket merely indicates the operator has been converted to a state (the matrix is now a

column vector). As we can show (via PyZX) that:

$$\tilde{V}^2 \sqrt{2}^9 \begin{pmatrix} 0 \\ 0 \\ 0 \\ 1 \\ 0 \\ -e^{i\frac{1}{3}\pi} \\ e^{i\frac{2}{3}\pi} \\ 0 \\ 0 \\ e^{i\frac{2}{3}\pi} \\ -e^{i\frac{1}{3}\pi} \\ 0 \\ 1 \\ 0 \\ 0 \\ 0 \end{pmatrix} = \text{Diagram} = 8\sqrt{6} \begin{pmatrix} 0 \\ 0 \\ 0 \\ 1 \\ 0 \\ -e^{i\frac{1}{3}\pi} \\ e^{i\frac{2}{3}\pi} \\ 0 \\ 0 \\ e^{i\frac{2}{3}\pi} \\ -e^{i\frac{1}{3}\pi} \\ 0 \\ 1 \\ 0 \\ 0 \\ 0 \end{pmatrix} \quad (5.143)$$

Which indicates the eigenvalue in this diagram equation $\frac{8\sqrt{6}}{\sqrt{2}^9} = \frac{\sqrt{3}}{2}$. If we consider the eigenvalue equation

$$\tilde{V}^2 |\iota_0 + i\sqrt{3}\iota_1\rangle = a\tilde{V}^2 |\psi\rangle = ae |\psi\rangle = e |\iota_0 + i\sqrt{3}\iota_1\rangle \quad (5.144)$$

where we write $|\iota_0 + i\sqrt{3}\iota_1\rangle = a |\psi\rangle$ and e is the eigenvalue and $|\psi\rangle$ is some proportional state. Then this shows that the scalar correction to the eigenstate state cancels in the eigenvalue equation and so the only correction that needs to be considered is that for the diagram representing \tilde{V}^2 which by inspection of the matrix in equation (5.132) is 4 times too small.

This implies the eigenvalue must be $\frac{\sqrt{3}}{2}$ multiplied by $\frac{1}{2}$. This gives the final eigenvalue for \tilde{V}^2 as $\frac{\sqrt{3}}{4}$.

Now by using the true volume operator (5.121) we can see that the quantised eigenvalues must be

$$V(\iota_0 + i\sqrt{3}\iota_1) = \pm \frac{\sqrt{2}}{3} (8\pi G\hbar\gamma)^{3/2} \sqrt{\frac{\sqrt{3}}{4}} \quad (5.145)$$

These are the correct non-trivial eigenvalues for the minimal quantised volume [26].

5.6 Orderless information conception of space-time

At this point we have described spin-networks in the ZXH calculus which is at heart a framework for analysing quantum information. As has been discussed these spin-networks form the state space of LQG. There is a historical route to demonstrate why this is the case [91] but the convoluted technical arguments that lead to this result are somewhat unsatisfactory from a philosophical perspective. A theory should stand freely and to as large a degree as possible self-justify, it is more than a few lines of mathematics, it is a statement about how reality can be understood from some limited perspective and granularity of observation. The fusion of the state-space of LQG gives us the opportunity to think about what we are saying reality is in the model that is LQG. Though this is perhaps misleading to say, the formulation of a theory in informational terms renders LQG, less about what ‘is’ and ‘is not’ but more about how whatever ‘is’ can be specified or spoken of and how this grows to inform the nature of geometry, and the fundamentality of $SU(2)$. I argue that the concept of *orderless quantum information* induces much of the anticipated geometry and symmetries of our reality from the ground up, rather than relying on its imposition from the top down.

What is required to specify a place? Functionally we express ourselves as being in some bounded region: In a some city, or street, or room. Taking a quantum informational perspective. What would the quantum mechanical expression of location mean⁶? Of course we are working in terms of modern physics so space and time are somewhat mixed-up concepts and it is not so much a case of being somewhere at some time, but being ‘some-when’, if you will, a region in space-time.

To be located in any sense of the term must require certain divisions, some region must be ‘different’ from another, or from an informational perspective we require information that specifies such a division. For this reason let us define a plane and assume it has an orientation. For the specification of being on one side or the other of this plane a qubit suffices. A problem emerges for qubit quantum information as more planes are added, now we require multiple labels to specify location. The issue is subtle. In specifying more than one qubit to represent something what does this qubit ordering correspond to? It is no physical thing, since there is no notion of an order here, we are using an ordered concept of information (bits/qubits) to label a

⁶Note I write ‘location’, not ‘a location’

5.6. Orderless information conception of space-time

universe prior to the existence of order. We are saying a thing that cannot actually be spoken from the pre-geometry perspective of constructing space-time. The ordering of the qubits should have no meaning. Can we induce this state of affairs? Yes, we can take the symmetric subspace of the informational space which by definition has nor preferred ordering. So considerations regarding the impossibility of specifying ordered information prior to the establishment of a space-time has led us to the the symmetric⁷ sub-space of n qubits. Recall however that the symmetric subspace of a qubit system are the representations of $SU(2)$. Orderless quantum information *is* spin!

Now a couple of planes will fail to define a region of space-time. We should enclosing a 4D volume and so in principle will need enough sides to delimit a 4-simplex (4D tetrahedra), and these sides will need to be 3D (1D lines delimit the triangle, 2D planes a tetrahedra, so it's 3D delimiters in 4D). We will restrict ourselves somewhat and consider the quantisation solely of space. In this way a lump of space is merely 3D so we are looking at tetrahedra, bounded by 4 planes.

Now given a tetrahedra in some embedding space 4 pieces of information will sufficient to be able to tell whether we were inside the space they bound or outside it. In our heads however we have probably already made the necessary leap to creating planes that intersect in the proper way. In the embedded space they are at different angles to each other, 4 parallel planes would hardly suffice. We want to be careful though, while we reference an embedding space, this is something we want to throw away in the end, to retain a minimal description of quantised space-time. This means we need to somehow define these angles without formally referencing the idea of there being a space in which to be at an angle with each other! Penrose also saw this issue and we'll use a similar strategy to him here[81].

We have no notion of angles but we do have magnitudes of spin imagine we have two spins spin- $\frac{N}{2}$ and spin- $\frac{M}{2}$. On re-coupling them in the sense of two angular momenta coming together we know that there fixed set of outcomes with a resultant spin s between them becoming $-\frac{|N+M|}{2} < s < \frac{N}{2} + \frac{M}{2}$. These can be interpreted as referring to an angle, that is to say though we don't specify angles, spin-re-coupling theory creates a situation where things that are often

⁷Having seen the argument that one should take the symmetric subspace, one may ask, why not go in a more fermionic direction and take the antisymmetric space. The fermionic choice however makes exactly the distinction we want to avoid, a swap induces a negative sign, but if we can't define an order in the first place how can we talk about inversions of it inducing negatives?

5. Diagrams for Spin-networks and Wigner symbols

interpreted as angles emerge. Specifically the angle between the spins for the different final values of s are

$$\theta = \arccos(J_M \cdot J_N) / j_N j_M \quad (5.146)$$

where J_N and J_M are the total spins and j_i are the magnetic indices for the different options⁸.

To justify the use of spin-recoupling to arrive at angles we naturally open ourselves up to larger spins than spin-1/2 what are we to make of this? Again we find an intimate geometric interpretation emerging from the what for us interacting orderless quantum information in terms of spin-recoupling. Consider the Clebsch-Gordon conditions for spin recoupling, though they have an arbitrary appearance what they in fact outline is when spins defining a volume are valid. It is often noted that the second Clebsch-Gordon coefficient is merely the triangle inequality, it literally determines when you could define a triangle with these sides. What we are seeing is that the conditions of recoupling quantum information in a non-trivial fashion directly impose conditions that seem geometric. Indeed for a 3D volume of space the same conditions emerge but can be shown to coincide with when 4 areas can form a valid tetrahedra [26]. These different spin magnitudes now define the area of volumes shared intersection.

We now have planes, in the sense of having labels that can be interpreted as being on one side or another and the means to describe them being at angles in a manner that doesn't reference our intuitively useful embedding space. So we can now speak of areas enclosing a space in purely informational terms via orderless information i.e spin. There is a caveat however, as is often the case with quantum mechanics, few variables are commuting, which is to say as a theory tethered to the notion probability waves the specification of some variables sharply necessarily means other variables, related to the Fourier transform, become less well defined. The angles and areas are exactly this. They are not commuting so one can never specify both - immediately we can see that this implies the boundaries we can define are fuzzy. This isn't shocking from the perspective of quantum mechanics but is interesting for those used to the idea of smooth determinate space-time.

What I have sought to argue is the necessity that the description of 'place' in terms of orderless quantum information naturally leads via spin recoupling of correlated orderless qubits to fuzzy

⁸In the literature often the angle operator is abbreviated to $\theta = J_M \cdot J_N$ as was seen with equation (5.120).

5.7. Summary of Yutsis Diagram and Spin-Network Results

tetrahedra. These can then be used to build quantised space via their combination via yet more spin-recoupling and so a spin-network determines a quantised region of space.

This cannot be the full story however, we actively restricted ourselves just to looking at space, there remains the question of the role of time and also there is the issue of the origins of special-relativity. An interesting strategy from the literature is to take $SU(2)$ $3jm$ symbols coming together to form space-time vertices and then ‘boosting’ them such that the resultant objects are $SL(2;C)$ intertwiners ($SL(2;C)$ being the lie group of interest in special relativity) that are anticipated to make up the space-time geometry [92]. This leads to the generalised spin-foam model[26] which resemble $SL(2;C)$ spin-networks rather than $SU(2)$ spin networks (the edges have different group labels). The informational content of this approach is not clear to me however.

In truth, at present I can offer no concrete suggestions. There are however two curious technical properties of $SL(2;C)$ intertwiners that may lead the way. Firstly an $SL(2;C)$ representation can be decomposed into a direct product (could we read this as superposition?) of $SU(2)$ elements [25]. Secondly the intertwiners themselves are mysteriously known to have, despite the countably infinite nature of their components, a mapping to $SU(2)$ $3jm$ symbols via a finite sum [93]. This secret finite decomposition of intertwiners and the direct product construction of the group from $SU(2)$ perhaps offers a way forward in linking orderless quantum information to models of full quantised space-time.

5.7 Summary of Yutsis Diagram and Spin-Network Results

In this section it has been shown that one can how Penrose’s binor calculus, wigner symbols and spin-networks can be interpreted and understood as ZXH diagrams. To this authors knowledge, leaving aside the ZXH elements of this, the clear outline of the relation between Yutsis diagrams and binor calculus is itself partially novel. In addition to this the construction of operators on spin-networks as ZXH diagrams is presented and two basic ‘geometric’ operators of LQG, the area and volume operators (for spin-1/2 vertices), are presented in diagrammatic form and validated via their application as eigen-operators to certain intertwiner bases.

5. Diagrams for Spin-networks and Wigner symbols

Specifically with Yutsis diagrams and binor calculus delineated the latter is used as a stepping stone to the diagrammatification of the former. With this to hand it is shown how $SU(2)$ invariance of the $3jm$ Wigner symbol is trivial with the group rotations on each external wire clearly cancelling.

With the general principles outlined a large number of examples are provided showing how specific $3jm$ symbols and elements derived from them like the $4jm$ and $6j$ symbols can be written in specific cases which are then validated in `PyZX`. With the Wigner symbols defined it is then possible to use them to construct spin-networks which can be seen as the $SU(2)$ invariant fusion of $3jm$ symbols. In addition to this some comment is made about the computability of these things.

Finally the notion of operators on spin-networks is discussed in relation to their application as defining the state space of loop quantum gravity. The diagrammatic construction of these operators is discussed and in limited cases and examples are given in particular for the area and volume operator which are validated numerically and shown to be in agreement with the literature.

It is considered desirable in the LQG community that the formalism is brought closer to quantum information and indeed is the subject of active research[94]. Here it is shown how the state-space of certain models of LQG, and kinematical operators on this space, can be written in terms of a diagrammatic language originally designed for qubit quantum computing. It is my belief that what is written here marks a serious technical step in precisely this direction.

6

Conclusion

In this thesis I introduced a version of ZX calculus I referred to as the ZXH calculus from which I used the multi-legged Hadamard box as a means to describe quantum AND gates. This was not new and can essentially be seen as the ZH calculus with different colours and a different focus. What is new is that I have taken the ability to describe quantum AND logic to formally describe operators that allow one to project to the symmetric sub-space of qubits which is the space of $SU(2)$ representations. I then provided a general method for the diagrammatic construction of raising algebraic operators from the single qubit spin-1/2 to arbitrary spin spaces spin-n/2. I then took these general principles and applied them to theoretical and mathematical physics proper demonstrating their utility as a technique in two different areas of physics.

Firstly I applied it to condensed matter physics where I showed how one can construct the 1D AKLT state and how its conventional properties can be identified diagrammatically, via diagrammatic calculations, while connecting to outlining the relation to more traditional tensor network descriptions of the state. I then show a novel result via diagrammatic differentiation that the 1D AKLT state posses a Berry phase of π at all orders which was previously only shown to be true in the thermodynamic limit. I then showed how one can also describe the 2D AKLT state and offered a new, arguably much simpler given it can be automated, proof that the 2D AKLT is a resource for measurement based quantum computing. I then outline how diagrammatic techniques provide a new way to formally represent phase transitions and

6. Conclusion

advocate for it's use for states that have traditionally been considered difficult to represent via tensor networks such as those with chiral symmetry.

The second field of physics to which I applied my approach to diagrammatic spin physics was to the spin-network formulation of LQG, and along the way to this the spin recoupling theory of quantum chemistry (via Yutsis diagrams). Specifically: A translation is provided between Penrose binor calculus spin-networks, which is viewed as the state space of LQG; Yutsis diagrams, which originate from quantum chemistry and provide a description of the $SU(2)$ invariant Wigner symbols that form the vertices of spin-networks; and ZXH an extension of the formal qubit language the ZX calculus. I then show how, by using the diagrammatic lie-algebra theory described in earlier sections, one can diagrammatically apply geometric quantum measurement operators. While this approach doesn't immediately lend itself to easy calculation it does open the door to a tensor-network approach to viewing these calculations as well as, perhaps, offering a path to the use of quantum computers for LQG calculations.

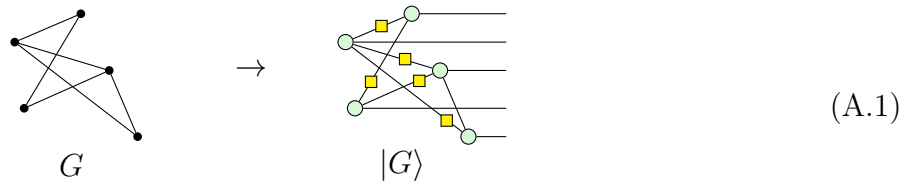
Appendices

A

Graph states

This appendix section is from [33]. Given a simple undirected graph $G = (V, E)$, there is a corresponding graph state $|G\rangle$. The state $|G\rangle$ is constructed by preparing for each vertex $v \in V$ a qubit in the $|+\rangle$ state, and for each edge $(v_1, v_2) \in E$ applying a CZ gate between the qubits corresponding to v_1 and v_2 [95]. Recall that graph states are important as all stabiliser states can be reduced to a graph state (up to local Cliffords) [69], and because most measurement-based quantum computation protocols use a graph state as their resource state [96].

The representation of a graph state in the ZX-calculus is most easily explained by an example:



In words: for each vertex of the graph we add a Z-spider with a single output, and for each edge we add a corresponding wire between spiders with a Hadamard gate on it.

B

Spin matrices and representation theory

This appendix section is from [33]. The Hilbert space of a spin-chain with N spins is a tensor product of the Hilbert space for each individual spin s : $(\mathbb{C}^{2s+1})^{\otimes N}$. For the spin $s = 1$ chain this is simply $(\mathbb{C}^3)^{\otimes N}$. At each site, the spin-1 matrices that can be used to construct the AKLT Hamiltonian Eq. (4.5) in the main text can be taken to be

$$S^x = \frac{1}{\sqrt{2}} \begin{pmatrix} 0 & 1 & 0 \\ 1 & 0 & 1 \\ 0 & 1 & 0 \end{pmatrix}, \quad S^y = \frac{i}{\sqrt{2}} \begin{pmatrix} 0 & -1 & 0 \\ 1 & 0 & -1 \\ 0 & 1 & 0 \end{pmatrix}, \quad (B.1)$$

$$S^z = \frac{1}{\sqrt{2}} \begin{pmatrix} 1 & 0 & 0 \\ 0 & 0 & 0 \\ 0 & 0 & -1 \end{pmatrix}, \quad (B.2)$$

which can be used to define a spin vector at each site $\vec{S}_i = (S_i^x, S_i^y, S_i^z)$. The spin operator S_i^a at site i acts on the local Hilbert space of the i -th spin, and thus acts trivially on the full Hilbert space:

$$S_i^a = I \otimes I \otimes I \cdots I \otimes I \otimes S^a \otimes I \otimes \cdots. \quad (B.3)$$

Hence, for two sites i, j we have the commutation rules

$$[S_i^a, S_j^b] = i\delta_{ij}\epsilon_{abc}S_j^c, \quad (B.4)$$

where latin letters label Cartesian directions (e.g., $a = x, y, z$).

Using representation theory we can explain how a spin-1 particle can be decomposed into the symmetric space of two spin-1/2 particles. First, recall that we can decompose the four

B. Spin matrices and representation theory

dimensions of the Hilbert space of two spin-1/2 particles into the *triplet representation*, which is spanned by $|00\rangle, \frac{1}{\sqrt{2}}(|01\rangle + |10\rangle), |11\rangle$, and the *singlet representation* $\frac{1}{\sqrt{2}}(|01\rangle - |10\rangle)$. Viewing the triplet representation as a three-dimensional Hilbert space, these three spin-1/2 pairs have eigenvalues $s_z = 1, 0, -1$ respectively, and so we can view them as a representation of a spin-1.

In general, the tensor product of the Hilbert space of two spins, s_1 and s_2 , can be decomposed into the representations with spins $|s_1 - s_2|, |s_1 - s_2| + 1, \dots, s_1 + s_2$. We can then express the triplet and singlet decomposition for two spin-1/2 particles as

$$(1/2) \otimes (1/2) = (0) \oplus (1), \quad (\text{B.5})$$

which is sometimes called a *fusion rule*. For two spin-1 particles we get using this rule

$$(1) \otimes (1) = (0) \oplus (1) \oplus (2). \quad (\text{B.6})$$

Note that the only way to get (2) is from (1) \otimes (1). We can use of this property to find the ground state of the AKLT Hamiltonian by expressing the Hamiltonian as a sum of projectors onto the $s = 2$ subspace.

A projector $P^{(s)}$ has eigenvalue 1 when applied to a state with spin s and zero otherwise. A projector into m spins of total spin s can be built from products of the operator $\hat{O}_j = (\sum_i^m \vec{S}_i) \cdot (\sum_i^m \vec{S}_i) - j(j+1)$ where $j \neq s$. This can be seen by noticing that $S^2 |s, s_z\rangle = s(s+1) |s, s_z\rangle$, and thus \hat{O}_j returns zero when applied to a state with total spin j .

For two ($m = 2$) spin-1 particles, the projector to $s = 2$ is constructed by projecting out the $s = 0$ and $s = 1$ subspaces (choosing $j = 0, 1$)

$$\begin{aligned} P^{(2)}(\vec{S}_1, \vec{S}_2) &= \lambda \hat{O}_0(\vec{S}_1, \vec{S}_2) \hat{O}_1(\vec{S}_1, \vec{S}_2) \\ &= \lambda [(\vec{S}_1 + \vec{S}_2)^2 - 0(0+1)][(\vec{S}_1 + \vec{S}_2)^2 - 1(1+1)]. \end{aligned} \quad (\text{B.7})$$

The projector $P^{(2)}$ onto spin-2 annihilates any state with total spin s equal to 0 or 1, i.e. $P^{(2)} |s = 1, s_z\rangle = P^{(2)} |s = 0, s_z\rangle = 0$, where s_z denotes the eigenvalue of the state for S^z . The coefficient λ is fixed by the requirement that $P^{(2)} |s = 2, s_z\rangle = |s = 2, s_z\rangle$ which results in $1/\lambda = [2(2+1) -$

B. Spin matrices and representation theory

$0][2(2+1) - 1(1+1)] = 24$. By using that $(\vec{S}_1 + \vec{S}_2)^2 = \vec{S}_1^2 + \vec{S}_2^2 + 2\vec{S}_1 \cdot \vec{S}_2$ and that $\vec{S}_1^2 = \vec{S}_2^2 = 2$ for spin-1 we have

$$\begin{aligned} P^{(2)}(\vec{S}_1, \vec{S}_2) &= \frac{1}{24}[4 + 2\vec{S}_1 \cdot \vec{S}_2][2 + 2\vec{S}_1 \cdot \vec{S}_2] \\ &= \frac{1}{6}(\vec{S}_1 \cdot \vec{S}_2)^2 + \frac{1}{2}\vec{S}_1 \cdot \vec{S}_2 + \frac{1}{3}. \end{aligned} \quad (\text{B.8})$$

As a result, the AKLT Hamiltonian can be written as

$$H = \sum_i \vec{S}_i \cdot \vec{S}_{i+1} + \frac{1}{3}(\vec{S}_i \cdot \vec{S}_{i+1})^2 \quad (\text{B.9})$$

$$= 2 \sum_i (P^{(2)}(\vec{S}_i, \vec{S}_{i+1}) - 1/3). \quad (\text{B.10})$$

As we observed below Eq. (B.6), the only way for two spin-1 particles to be in the $s = 2$ subspace is for each to be in $s = 1$ subspace. Since the AKLT Hamiltonian is the sum of projectors onto the spin-2 subspace of neighbouring spins, it annihilates any state where any two of the four neighbouring spin-1/2 degrees of freedom are in a spin-singlet, because such states have total spin $s = 0$.

Lastly, as mentioned in the main text, the AKLT state has a dilute anti-ferromagnetic order (a site with $s_z = \pm 1$ is followed by a site ∓ 1 , with a string of $s_z = 0$ in between), as discussed in the main text. It can be shown that this order is captured by a non-zero string-order parameter [48].

C

Additional diagrammatic proofs

This appendix section is from [33].

C.0.1 Additional proofs for the AKLT Berry Phase calculation

The following proofs are used in Sec. 4.2.2 to derive the Berry phase of the 1D AKLT state. We only use the standard rewrite rules of Figs. 2.1 and 2.2.

$$\begin{array}{ccc}
 \text{(c)} & & \text{(h)} \\
 \text{(f)} & = \frac{1}{2} & \text{(id)} \\
 \text{---} & & \text{---} \\
 \text{---} & & \text{---} \\
 \end{array} \quad (C.1)$$

$$\begin{array}{ccc}
 \text{(2.17)} & & \text{(ho)} \\
 \text{(f)} & = \sqrt{2} & = \frac{1}{\sqrt{2}} \\
 \text{---} & & \text{---} \\
 \text{---} & & \text{---} \\
 \text{(2.18)} & & \text{(ho)} \\
 \text{(b)} & = \sqrt{2} & = \frac{1}{\sqrt{2}} \\
 \text{---} & & \text{---} \\
 \end{array} \quad (C.2)$$

$$\begin{array}{c}
 \text{(c)} \quad = \quad \begin{array}{c} (\pi c) \\ (2.17) \end{array} \quad = \quad \sqrt{2} \quad \text{(C.3)} \\
 \text{(f)} \quad = \quad \sqrt{2} \quad \text{(ho)} \quad = \quad \frac{1}{\sqrt{2}} \quad \text{(2.18)} \quad = \quad \begin{array}{c} (\pi) \\ \text{---} \end{array}
 \end{array}$$

C.0.2 CSWAP POVM calculations

In the main text it was shown that if the E_x operator is applied to a CSWAP, that the CSWAP is absorbed (see (4.54)). In this appendix we will show the same for E_z and E_y . First, with E_z :

$$\begin{array}{c}
 \text{(b)} \propto \text{(f)} = \text{(ho)} \propto \text{(f)} = \text{(ho)} \propto \text{(C.5)} \\
 \text{(ex)} \propto \text{(c)} \stackrel{\frac{1}{\sqrt{2}}}{=} \text{---}
 \end{array}$$

As such:

$$\begin{array}{c} \text{Diagram 1} \\ \hline \text{Diagram 2} \end{array} = \frac{1}{2\sqrt{2}} \quad (C.6)$$

For the analogous derivation with E_y we need a couple more types of rewrites. First, there is a way to commute a π X-phase through an H-box:

$$\begin{array}{c} \text{Diagram 1} \\ \text{Diagram 2} \end{array} = \begin{array}{c} \text{Diagram 3} \end{array} \quad (C.7)$$

C. Additional diagrammatic proofs

This can be proven easily using (f) to unspider the π phase, followed by (hb) and (ab).

Second, there are ways to remove $\frac{\pi}{2}$ -labelled Z-spiders and π -labelled Z-spiders from a diagram, by complementing the connectivity of their neighbours in a suitable way. These were proven in [20]. To write them down clearly we adopt the notation of *Hadamard-edges* from [20]:

$$\text{Diagram on left} := \text{Diagram on right} \quad (\text{C.8})$$

The first rule is known as *local complementation*:

$$\text{Diagram on left} \propto \text{Diagram on right} \quad (\text{C.9})$$

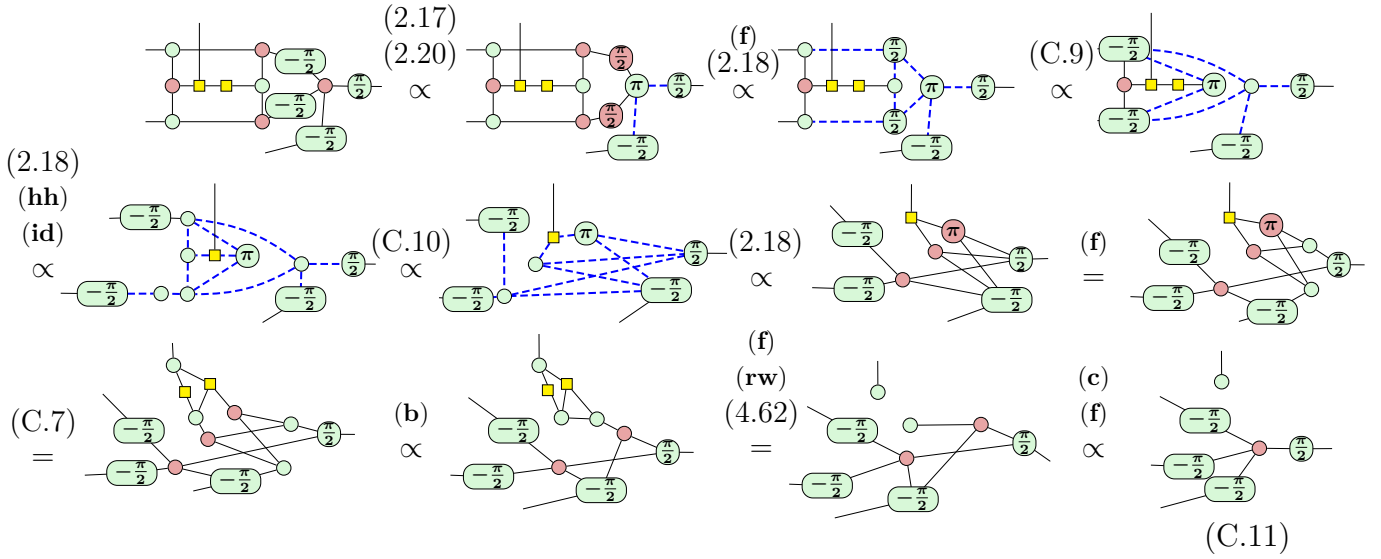
Note that on the right-hand side the middle spider is removed, at the cost of introducing edges between all its neighbours. Because of (4.62), if there was already an edge present between the spiders, the edge is cancelled, hence the name complementation.

The second rule is known as *pivoting*:

$$\text{Diagram on left} \propto \text{Diagram on right} \quad (\text{C.10})$$

Here the connected pair of spiders u and v which have a phase of 0 or π are removed on the right-hand side, at the costs of introducing edges between the exclusive neighbourhood of u , the exclusive neighbourhood of v and the joint neighbourhood, labelled by respectively U , V and W in the diagram.

Now we have all the ingredients we need to prove that E_y applied to the symmetriser reduces to just E_y :



While this derivation is significantly more complicated, note that PyZX still manages to simplify it in an automated way (using a different rewrite strategy).

C.0.3 Removing π phases from a graph state

In the main text it was shown how the π phases from the singlets on the measured 2D AKLT lattice can be moved onto the external wires for the measurement outcome E_z . Here we will demonstrate the same for E_x and E_z .

For an E_x outcome in the bulk of the lattice we have:

$$\begin{array}{ccc}
 \text{Diagram with } \pi \text{ phases on wires} & = & \text{Diagram with } \pi \text{ phases moved to a wire} \\
 \text{C.12}
 \end{array}$$

For an E_y outcome, again in the bulk, we have:

$$\begin{array}{ccc}
 \text{Diagram with } \pi \text{ phases on wires} & = & \text{Diagram with } \pi \text{ phases moved to a wire} \\
 \text{C.13} \\
 \text{Diagram with } \pi \text{ phases on wires} & = & \text{Diagram with } \pi \text{ phases moved to a wire} \\
 \text{Diagram with } \pi \text{ phases on wires} & = & \text{Diagram with } \pi \text{ phases moved to a wire}
 \end{array}$$

D

Overview of graphical rewrite rules

$$\begin{aligned}
 m \left\{ \begin{array}{c} \text{Diagram with } \alpha \text{ in green circle} \\ \vdots \\ \text{Diagram with } \alpha \text{ in red circle} \\ \vdots \\ \text{Diagram with } \alpha \text{ in red circle} \end{array} \right\} n &= \sqrt{2}^{n+m} m \left\{ \begin{array}{c} \text{Diagram with } \alpha \text{ in red circle} \\ \vdots \\ \text{Diagram with } \alpha \text{ in green circle} \\ \vdots \\ \text{Diagram with } \alpha \text{ in green circle} \end{array} \right\} n & \text{Diagram with } \alpha \text{ in green circle} = e^{i\alpha} \text{ (yellow box)} \\
 m \left\{ \begin{array}{c} \text{Diagram with } \alpha \text{ in red circle} \\ \vdots \\ \text{Diagram with } \alpha \text{ in red circle} \\ \vdots \\ \text{Diagram with } \alpha \text{ in red circle} \end{array} \right\} n &= \sqrt{2}^{n+m} m \left\{ \begin{array}{c} \text{Diagram with } \alpha \text{ in green circle} \\ \vdots \\ \text{Diagram with } \alpha \text{ in green circle} \\ \vdots \\ \text{Diagram with } \alpha \text{ in green circle} \end{array} \right\} n & -e^{i\alpha} = \frac{1}{\sqrt{2}} \left(\begin{array}{c} \text{Diagram with } \frac{\alpha}{2} \\ \text{Diagram with } -\frac{\alpha}{2} \end{array} \right)
 \end{aligned}$$

$$\begin{aligned}
 \text{Diagram with } \alpha \text{ in green circle, } \beta \text{ in red circle} &\stackrel{(f)}{=} \text{Diagram with } \alpha + \beta \text{ in green circle} \\
 m \left\{ \begin{array}{c} \text{Diagram with } \alpha \text{ in red circle} \\ \vdots \\ \text{Diagram with } \alpha \text{ in green circle} \\ \vdots \\ \text{Diagram with } \alpha \text{ in green circle} \end{array} \right\} n &\stackrel{(b)}{=} m \left\{ \begin{array}{c} \text{Diagram with } \alpha \text{ in red circle} \\ \vdots \\ \text{Diagram with } \alpha \text{ in green circle} \\ \vdots \\ \text{Diagram with } \alpha \text{ in green circle} \end{array} \right\} n = \frac{1}{(\sqrt{2})^{(n-1)(m-1)}} \\
 \text{Diagram with } \alpha \text{ in green circle} &\stackrel{(\text{id})}{=} \text{Diagram with } \alpha \text{ in red circle} \\
 \text{Diagram with } \alpha \text{ in red circle} &\stackrel{(\pi)}{=} \text{Diagram with } -\alpha \text{ in green circle} \\
 \text{Diagram with } \alpha \text{ in red circle} &\stackrel{(c)}{=} \frac{e^{i\alpha}}{\sqrt{2}^{n-1}} \text{Diagram with } \alpha \text{ in red circle} \\
 \text{Diagram with } \alpha \text{ in green circle} &\stackrel{(\text{ho})}{=} \frac{1}{2} \text{Diagram with } \alpha \text{ in red circle}
 \end{aligned}$$

D. Overview of graphical rewrite rules

E

Sage verification code

This appendix section is originally from [80]

The 3jm symbols were verified via

```
def vertex_ooi(j1,j2,j3):  
    M = matrix([[  
        (-1)^(j3-m3)*wigner_3j(j1,j2,j3,m1,m2,-m3)  
        for m1 in range(-j1,j1+1)  
        for m2 in range(-j2,j2+1) ]  
        for m3 in range(-j3,j3+1) ])  
  
    return M  
  
def vertex_ooo(j1,j2,j3):  
    M = matrix([[  
        wigner_3j(j1,j2,j3,-1*(m1),-1*(m2),-1*(m3))  
        for m3 in range(-j3,j3+1) ]  
        for m1 in range(-j1,j1+1)  
        for m2 in range(-j2,j2+1) ])
```

```
return M
```

The 4jm symbols were verified via

```
def wigner_4jm(j1,j2,j3,j4,m1,m2,m3,m4,j):
    return sum((-1)^(j-m)*wigner_3j(j1,j2,j,m1,m2,m)
               *wigner_3j(j,j3,j4,-m,m3,m4)
               for m in range(-j,j+1))

def vertex_iioo(j1,j2,j3,j4,j):
    M = matrix([
        wigner_4jm(j1,j2,j3,j4,-1*(-m1),-1*(-m2),-1*(m3),-1*(m4),j)
        for m1 in range(-j1,j1+1)
        for m2 in range(-j2,j2+1) ]
        for m3 in range(-j3,j3+1)
        for m4 in range(-j4,j4+1) ])
    return M
```

The 6jm symbols were verified via

```
def sixJ_symbol(j1,j2,j3,j4,j5,j6):
    return sum(sum(sum(sum(sum((-1)^(j1+j2+j3+j4+j5+j6-m1-m2-m3-m4-m5-m6)
                               *wigner_3j(j1,j2,j3,-m1,-m2,-m3)*wigner_3j(j1,j5,j6,m1,-m5,m6)
                               *wigner_3j(j4,j2,j6,m4,m2,-m6)*wigner_3j(j3,j4,j5,m3,-m4,m5)
                               for m1 in range(-j1,j1+1))
                               for m2 in range(-j2,j2+1))
                               for m3 in range(-j3,j3+1))
                               for m4 in range(-j4,j4+1))
                               for m5 in range(-j5,j5+1))
                               for m6 in range(-j6,j6+1))
```

F

Differentiable Manifolds

The differentiable manifold is one of the most general objects on which one can describe calculus. We will here briefly cover the key points, outlining what it is to be a differentiable manifold. For the purposes of this thesis it is enough that the reader is simply comfortable with the subject, an understanding of the nuances particularly regarding some of the more technical topological requirements are not mentioned here, that said the interested reader should see [97].

A manifold is a space almost *Papier – mâché* like in its construction, the newspaper of choice is the \mathbb{R}^n and different parts of it are placed according to certain mappings, choices of position, called *charts* which overall make up an *atlas*. The only additional constraint is a certain common sense agreement that if two bits of \mathbb{R}^n are assigned to the same area by different charts then there should be a mutual path between these charts. Formally we arrive at smooth manifolds through the following set of definitions

Definition 2.

A chart (or n-dimensional chart) for X is an bijective map $\phi : V \rightarrow U$ where V is an open subset of \mathbb{R}^n is an open set in \mathbb{R}^n and $U = \phi(V) \rightarrow X$ is a subset of X .

Definition 3.

Given two charts $(\phi_i : V_i \rightarrow U_i)$ and $(\phi_j : V_j \rightarrow U_j)$ they are *compatible* both $\phi_i^{-1}(U_i \cap U_j) \subset \mathbb{R}^n$ $\phi_j^{-1}(U_i \cap U_j) \subset \mathbb{R}^n$ are open and mutually inverse under changes of coordinates

$$\phi_i^{-1} \circ \phi_j : \phi_j^{-1}(U_i \cap U_j) \rightarrow \phi_i^{-1}(U_i \cap U_j) \quad (\text{F.1})$$

and

$$\phi_j^{-1} \circ \phi_i : \phi_i^{-1}(U_i \cap U_j) \rightarrow \phi_j^{-1}(U_i \cap U_j) \quad (\text{F.2})$$

are given by differentiable smooth functions.

Definition 4.

An atlas $A = (\phi_i : V_i \rightarrow U_i)$ is *smooth* if it consists of pairwise compatible charts.

Definition 5. An *n-dimensional smooth manifold*¹ is a pair (X, A) formed of a set X endowed with a smooth atlas A . Where n is the dimension of X .

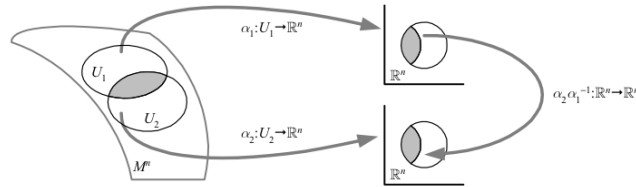


Figure F.1: A depiction of charts[?].

Manifolds are rarely considered in isolation as such it is important to consider the maps between them which is the subject of our final definitions

If we have two manifolds M and N , with respective charts $\phi_\alpha^M : V_\alpha^M \rightarrow M$ and $\phi_\mu^N : V_\mu^N \rightarrow N$.

Let $F : M \rightarrow N$ be a map between them.

Consider the subset $F^{-1}(U_\mu^N) \cap U_\alpha^M$ presuming it is not empty. Then F maps it to U_μ^N . Furthermore consider the pre-image $(\phi_\alpha^M)^{-1}(F^{-1}(U_\mu^N) \cap U_\alpha^M) = (F \circ \phi_\alpha^M)^{-1}(U_\mu^N) \subset V_\alpha^M$. We have a map

$$(\phi_\mu^N)^{-1} \circ F \circ \phi_\alpha^M : (F \circ \phi_\alpha^M)^{-1}(U_\mu^N) \rightarrow V_\mu^N \quad (\text{F.3})$$

¹This definition and all those leading up to it are exactly the same for a topological manifold except there is no requirement for anything to be smooth.

F. Differentiable Manifolds

A map $F : M \rightarrow N$ is smooth if all $(F \circ \phi_\alpha^M)^{-1}(U_\mu^N)$ are open and the above map $(\phi_\mu^N)^{-1} \circ F \circ \phi_\alpha^M$ is a smooth map (from an open set of \mathbb{R}^M to an open set \mathbb{R}^N) for all α and μ .

G

A brief note on curvature and its link to the Einstein field equations

In what follows we will make use of indices in the manner common to general relativity, Greek indices, such as ‘ μ ’ and ‘ ν ’, will indicate an indexing $\{0, 1, 2, 3\}$ while indexing over Roman letters, such as ‘ a ’ and ‘ b ’, will imply an indexing over $\{1, 2, 3\}$ excluding the time-like component. This appendix chapter borrows heavily from [91].

Say we have a metric space with some metric $g_{\mu,\nu}$ and let’s choose some basis $\{e_i\}$ for local coordinates. In this way we talk about an arbitrary vector $V = v_i e^i$, and it’s dual $\tilde{V} = v_i e^i = g_{ij} v_i e^i$.

In a smooth space-time a desirable thing is to know how a thing (vector etc) changes as you move through it. A little more rigorously lets say we want to differentiate a vector along a curve. With a curve parameterised by x^k we can write

$$\frac{d\vec{V}}{dx^k} = \frac{\partial v^j}{\partial x^k} e_j + v^j \frac{\partial e_j}{\partial x^k}$$

where we see that the total derivative has a component that details the change in the basis components and a part that details the change in the local basis itself. To select a particular i^{th} component we apply the dot product with the i^{th} one-form (dual basis vector) and find:

$$\frac{dv^i}{dx^k} = \frac{\partial v^i}{\partial x^k} + v^j \frac{\partial e_j}{\partial x^k} \cdot e^i$$

This is often written in the more intimidating form

$$\nabla_k v^i = \partial_k v^i + v^j \Gamma_{jk}^i$$

having seen its origin we've no need to fear this thing. The is the *covariant derivative* where the first part details the familiar change in the components of a vector and the second, usually more mysterious part, details how the vector will change due to the changes in the basis itself as one moves about - for why should it remain fixed in general? This Γ_{jk}^i in particular is called a Christoffel symbol and is an expression of the '*connection*' written in the local coordinates that are its indices.

One says that a vector has been parallel transported if its covariant derivative is zero. Which in turn implies that the change in the local basis must be exactly cancelling the change in the vector as we travel around the path. The curvature of some enclosed region can be detected by transporting a vector about the enclosing loop. If the space is flat the initial and final vector will be identical, conversely if they are not the same the degree to which they differ provides a measure of the curvature. The measure of how much a loop differs from a flat space is called the *holonomy* of the loop.

With the components we have to hand we can now construct the Riemann curvature tensor. By imagining the covariant derivatives ∇_μ and ∇_ν labelling the derivative going along the paths in direction μ and ν .

$$R_{\mu\nu} = (\nabla_\mu \nabla_\nu - \nabla_\nu \nabla_\mu) = [\nabla_\mu, \nabla_\nu]$$

From which we can obtain the Riemann curvature tensor itself

$$R_{\rho\mu\nu}^\lambda v^\rho = [\nabla_\mu, \nabla_\nu] v^\lambda$$

where v^λ is a vector that's transport along the two different choices of path is compared. If the space is flat in this region then the result will be zero, if the whole space is flat the entire tensor will be zero.

G.1 Einstein's field equations and the Einstein-Hilbert action

Let us first consider the energy-momentum tensor $T^{\mu\nu}$, and define the following derivative quantities from the Riemann curvature, namely: the Ricci tensor $R_{\rho\nu} = R^{\mu}_{\rho\mu\nu}$ and Ricci curvature $R = R^{\nu}_{\nu}$, where we raised an index using the metric. We are then in a position write down the first of Einstein's field equations:

$$R^{\mu\nu} - \frac{1}{2}Rg^{\mu\nu} + \Lambda g^{\mu\nu} = 8\pi\mathcal{G}T^{\mu\nu} \quad (\text{G.1})$$

where G is Newton's constant and Λ is the cosmological constant.

This is often also written as

$$G^{\mu\nu} = 8\pi\mathcal{G}\mathcal{T}^{\mu\nu} - \Lambda g^{\mu\nu} \quad (\text{G.2})$$

where we have the Einstein tensor $G^{\mu\nu} = R^{\mu\nu} - Rg^{\mu\nu}/2$

In general there is no solution to the field equation however in certain cases like a static field with spherical symmetry solutions are derivable. From the perspective of loop quantum gravity we will strive to work backwards from this to a quantisable Hamiltonian structure.

It is often forgotten that the use of Ricci scalar is posited axiomatically in general relativity as a strangely effective guess than thrust on us by necessity. When trying to find a description for space-time it was naturally required that coordinate invariant properties of the manifold were found, and there are a number of these $\{R, R_{\mu\nu}R^{\mu\nu}, R^2, \nabla_{\mu}R\nabla^{\mu}R, \dots\}$. The Ricci scalar is merely the simplest and $R = R_{\mu\nu\alpha\beta}g^{\mu\alpha}g^{\nu\beta}$ and gives the Lagrangian $\sqrt{-g}R$ where $g = \det(g^{\mu\nu})$ which provides the simplest possible Lagrangian that couples to matter

$$S_{\text{EH+M}} = \frac{1}{\kappa} \int d^4x \sqrt{-g}R + \int d^4x \sqrt{-g}\mathcal{L}_{\text{matter}} \quad (\text{G.3})$$

where $\mathcal{L}_{\text{matter}}$ is the Lagrangian for matter fields and κ is a constant. If we ignore the matter term we get the vacuum field equations of GR and we have the Einstein-Hilbert action.

$$S_{\text{EH}} = \frac{1}{\kappa} \int d^4x \sqrt{-g}R \quad (\text{G.4})$$

By minimising this action one can obtain the Einstein field equations. We have now moved from discussions of invariant properties of curved manifolds to a Lagrangian whose minimisation

G.1. Einstein's field equations and the Einstein-Hilbert action

gives the field equations for gravity. The next step in LQG is to move this Lagrangian structure closer to something we can see how to quantise i.e where observables become operators and Poisson bracket constraints to become commutator relations.

H

ADM splitting

In what follows we will make use of indices in the manner common to general relativity, Greek indices, such as ‘ μ ’ and ‘ ν ’, will indicate an indexing $\{0, 1, 2, 3\}$ while indexing over Roman letters, such as ‘ a ’ and ‘ b ’, will imply an indexing over $\{1, 2, 3\}$ excluding the time-like component. It is heavily influenced by the excellent and more complete guide to LQG generally found here [91]. The inclusion of this section at all is to give a sketch guide to how partitioning space-time can lead to a Hamiltonian formulation of GR written in terms of phase space constraints. The Arnowitt-Deser-Misner (ADM hereafter) formalism is precisely the means to define a Hamiltonian (as opposed to Lagrangian) formulation of General relativity that is discussed above. The ADM formalism requires that we foliate space-time into a set of 3D space-like hyper-surfaces, and ordering these by a parameter t that resembles time. Crucially this time parameter choice doesn’t actually affect the dynamics.

Let us take a 4D space-time embedded in a manifold M . We then choose a foliation $\{\Sigma_t, t\}$ of M into space-like 3-manifolds, where Σ_t is the 3D hyper-surface associated to parameter t often referred to as a ‘leaf’. The topology of the overall space-time is then $\Sigma \otimes \mathbb{R}$ with t as a parametrisation of the geodesics orthogonal to Σ_t . At all points we can define a unit time-like vector n^μ where $n^\mu n_\mu = -1$.

With a the metric $g_{\mu\nu}$ on M and the vector field n^μ the foliation is fixed by setting Σ_t of constant ‘time’ are normal n^μ . The diffeomorphism invariance of general relativity tells us there is no

canonical choice of of the time-like vector field¹ $t^\mu : x^\mu \mapsto x'^\mu$ where $x^\mu \in \Sigma_t$ and $x'^\mu \in \Sigma_{t+\delta t}$. This is in fact a gauge symmetry as it can be expressed as a local invariance under the action of a lie group, this tells us we could have chosen *any* time-like vector field t^μ .

Let's now look at the projection of the time-like vector field onto the a leaf of the foliation. This gives the *shift vector* $N^a = t_{||}$ which is tangent to the surface. The normal component denoted *lapse function* $N = t_\perp$ is viewed at the gap between the leaves of the foliation. In this way one can write

$$t^\mu = N n^\mu + N^\mu \quad (\text{H.1})$$

where $N^0 = 0$ in local coordinates. In a sense the time like vector is the composition of the distance to the next foliation and the distance it shifts points relative to the previous foliation.

From this we can show by substitution, and using that $n^\mu n_\mu = -1$ and $N^\mu n_\mu = 0$, that

$$g_{00} = g_{\mu\nu} t^\mu t^\nu = -N^2 + N^\mu N_\mu \quad (\text{H.2})$$

as t^μ is time-like and we are working in the basis $N^\mu = (0, N^a)$, we have $g_{00} = -N^2 + N^a N_a$. To get the other components of the metric we can project along the space-like and time-like directions to see that:

$$g_{\mu\nu} t^\mu N^\nu = N^\mu N_\mu \equiv N^a N_a \quad (\text{H.3})$$

as by its definition $g_{0\nu} = g_{\mu\nu} t^\mu$ and this implies that $g_{0a} = N_a$. This means that by writing the metric in terms of time-like and space-like components then:

$$g_{\mu\nu} = \begin{pmatrix} -N^2 + N^a N_a & N \\ N^T & g_{ab} \end{pmatrix} \quad (\text{H.4})$$

where $a, b \in 1, 2, 3$ and $N := N^a$. Thus the 4D path element is given by

$$ds^2 = g_{\mu\nu} dx^\mu dx^\nu = \left(-N(t)^2 + N^a N_a \right) dt^2 + 2N^a dt dx_a + g_{ab} dx^a dx^b \quad (\text{H.5})$$

with $a, b \in 1, 2, 3$ as the spatial indices of the leaf Σ_t .

This g_{ab} of a metric restricted to a leaf is not the same as the intrinsic metric of the leaf in the foliation. The intrinsic metric takes tensors T defined over the 4D manifold and projects them

¹Recall a vector field is essentially a vector valued function.

H. ADM splitting

onto the leaf. Meanwhile to identify the $T_{||}$ living on the surface Σ_t and T_{\perp} living orthogonal to it, things are different: Given a vector v^μ the orthogonal component is $v_{\perp} = v^\mu n_\mu$ and the orthogonal component is $v_{||} = v^\mu N_\mu$. So a general 4-vector is $v_{\perp} n^\mu + v_{||} \frac{N^\mu}{N^\mu N_\mu}$.

If we then apply the operator $h_{\mu\nu} = g_{\mu\nu} + n_\mu n_\nu$ we find that

$$(g_{\mu\nu} + n_\mu n_\nu) \left(v_{\perp} n^\nu + v_{||} \frac{N^\nu}{N^\mu N_\mu} \right) = v_{\perp} n_\mu (1 + n^\nu n_\nu) + \frac{v_{||}}{N^\mu N_\mu} (N_\mu + n^\nu N_\nu) = v_{||} \frac{N_\mu}{N^\mu N_\mu} \quad (\text{H.6})$$

as $n^\mu n_\mu = -1$ and $n^\nu N_\nu = 0$ we get the the component of v^μ parallel to Σ_t . In this way then $h_{\mu\nu} = g_{\mu\nu} + n_\mu n_\nu$ is the projection operator. This corresponds to the intrinsic 3D metric on Σ_t induced by its embedding in M :

$$h_{ab} = g_{ab} + n_a n_b \quad (\text{H.7})$$

noting that $h_{\mu\nu}$ is only non-zero when contracted with an entirely space-like object and so the restriction to h_{ab} is valid.

As discussed above the Einstein-Hilbert action can be written in terms of the metric $g_{\mu\nu}$ and its derivatives. We are now in a position to use our foliation to describe the Hamiltonian density, the field equivalent of the Hamiltonian. Recall that taking the Legendre transform from the Lagrangian L given coordinates of generalised position q and momentum p .

$$H[p, q] = p \dot{q} - L[q, \dot{q}] \quad \text{where} \quad p = \frac{\partial L}{\partial \dot{q}} \quad (\text{H.8})$$

where p is the generalised momentum to q . The field equivalent of this expression is the following

$$H[\pi, \phi] = \int d^4x \pi \dot{\phi} - L[\phi, \dot{\phi}] \quad (\text{H.9})$$

It can be shown that for GR this can be written as:

$$H[\pi^{\mu\nu}, h_{\mu\nu}] = \int d^3x \pi^{ab} \dot{h}_{ab} - L[h_{ab}, \dot{h}_{ab}] \quad (\text{H.10})$$

Along with intrinsic metric h_{ab} , the hyper-surfaces Σ have another property termed the ‘extrinsic curvature’ given by the spatial projection of the gradient of the normal vectors to the hyper surface

$$k_{ab} = h_a^c h_b^d \nabla_c n_d := D_a n_b \quad (\text{H.11})$$

where D_a is a covariant derivative that only acts on objects with only spatial components. It can also be shown that much like with the intrinsic metric contraction with any object that isn't purely spacial gives zero. The reason to look at this object is that it plays a role similar to that of generalised momentum basis as opposed to the generalised position of the intrinsic metric.

By making two substitutions, writing h for $\det(h^{ab})$ and noting that the 4D volume form $\sqrt{-g} = N\sqrt{h}$ alongside the Gauss-Codazzi equation:

$${}^{(3)}R_{\nu\rho\sigma}^{\mu} = h_{\alpha}^{\mu} h_{\nu}^{\beta} h_{\rho}^{\gamma} h_{\sigma}^{\delta} R_{\beta\gamma\delta}^{\alpha} - k_{\nu\sigma} k_{\rho}^{\mu} - k_{\nu\rho} k_{\sigma}^{\mu} \quad (\text{H.12})$$

then the four-dimensional Ricci curvature scalar R can be written in terms of the 3D Ricci scalar ${}^{(3)}R$ and the extrinsic curvature of Σ :

$$R = {}^{(3)}R + k^{ab} k_{ab} - k^2 \quad (\text{H.13})$$

where $k := k^{ab} h_{ab}$.

This leads to the Einstein-Hilbert action in terms that separate out the component determined only by the leaves of the foliation Σ

$$S_{\text{EH}} = \int dt d^3x N\sqrt{h} \left({}^{(3)}R + k^{ab} k_{ab} - k^2 \right) = \int dt L_{\text{EH}} \quad (\text{H.14})$$

By taking the lie derivative of h_{ab} with respect to the time-like vector field of the foliation one can then obtain the conjugate momentum

$$\pi^{ab} = \frac{\delta L}{\delta \dot{h}_{ab}} = \sqrt{h} \left(k^{ab} - k h^{ab} \right) \quad (\text{H.15})$$

After a certain amount of algebra one can then show that

$$H \left[\pi^{ab}, h_{ab} \right] = \int d^3x N \mathcal{H} - N_a \mathcal{C}^a \quad (\text{H.16})$$

H. ADM splitting

Where

$$\mathcal{H} = \left(-\sqrt{h}^{(3)} R + \frac{1}{\sqrt{h}} \left(\pi^{ab} \pi_{ab} - \frac{1}{2} \pi^2 \right) \right) \text{ (Hamiltonian constraint)} \quad (\text{H.17})$$

$$\mathcal{C}^a = 2D_b \pi^{ab} \text{ (Diffeomorphism constraint)} \quad (\text{H.18})$$

where $\pi = \text{Tr}[\pi^{ab}]$.

The Legendre transform can then be reversed to get the form of the action as

$$S_{EH} = \int dt L_{EH} = \int dt d^3x \left(\pi^{ab} \dot{h}_{ab} - H \left[\pi^{ab}, h_{ab} \right] \right) \quad (\text{H.19})$$

$$= \int dt d^3x \left(\pi^{ab} \dot{h}_{ab} - N \mathcal{H} + N_a \mathcal{C}^a \right) \quad (\text{H.20})$$

From this one can see that the action is a function of the lapse and shift but not its derivative and as such the equations of motion with respect to the lapse and shift are

$$\frac{\delta S_{EH}}{\delta N} = -\mathcal{H} = 0 \quad (\text{H.21})$$

$$\frac{\delta S_{EH}}{\delta N_a} = \mathcal{C}^a = 0 \quad (\text{H.22})$$

Implying that $H = 0$ and $C^a = 0$ are constraints of the phase space. These are known as the Hamiltonian and diffeomorphism constraints respectively.

I

Introduction to $SU(2)$ representation theory

I.1 Introduction to representation theory

Representation theory revolves around the analysis of groups, algebras, and other algebraic structures not discussed here, from the perspective of linear algebra. The motivating idea is that linear algebra is extremely well understood so perhaps by applying relevant homomorphisms to vector spaces.. For a fuller review see [31].

I.1.1 Introductory concepts and Lie groups

The primal definition for us will be the following:

Definition 6. A group is a set G with a map $m : G \times G \rightarrow G$, whose action on elements is denoted $m(a, b) = a \cdot b$ where $a, b \in G$, such that

- $\forall a, b \in G \ a \cdot b \in G$
- $\forall a, b, c \in (a \cdot b) \cdot c = a \cdot (b \cdot c)$
- $\exists I \in G \ s.t \ I \cdot a = a \cdot I = a$
- $\forall a \in G \ \exists a^{-1} \in G \ s.t \ a \cdot b = I$

Of particular importance to us and physics generally is the general linear group. Everything looked at in this thesis regarding representation theory is related to this group. The *general*

linear group over the field F^1 denoted $GL(n; F)$ is the group of all $n \times n$ invertible matrices with entries in F .

The reason for this groups importance is because some of the key symmetries in modern physics are subgroups of the general linear group. For example between the unitary and special unitary groups one has, in rather reductive terms, the entirety of the standard model.

General Unitary group The general unitary group $U(n)$ consists of all matrices A of dimension $n \times n$ such that $A^\dagger A$, where A^\dagger is the hermitian conjugate of A , is a non-zero multiple of the identity matrix, and is just the product of the unitary group with the group of all positive multiples of the identity matrix.

The special unitary group A crucial specialisation of the general unitary group, particularly in the realm of physics, is the special unitary group $SU(n)$. It is the set of $n \times n$ unitary matrices *with determinant 1*. Of particular importance to the notion of quantum mechanical spin is the special unitary group of 2×2 matrices. When $n = 2$ we have $SU(2)$

$$SU(2) = \left\{ \begin{pmatrix} \alpha & -\bar{\beta} \\ \beta & \bar{\alpha} \end{pmatrix} : \alpha, \beta \in \mathbb{C}, |\alpha|^2 + |\beta|^2 = 1 \right\}$$

I.1.2 Lie Groups and Lie Algebras

In physics symmetries are often represented by groups, with the inability of a group to alter a system indicating a symmetry with respect to that group. Symmetry groups however are often ‘continuous’ such as the group of rotations $SO(3)$. The unitary groups and the special subgroups are further examples. When we have such symmetries we can simultaneously see the group as a collection of group elements and also as a smooth manifold (see appendix F). A group that is also a smooth manifold is called a Lie group.

Definition 7. Let G be a smooth manifold which admits a group structure such that the multiplication map $m : G \times G \rightarrow G$ is a smooth map as is the inversion map $inv : G \rightarrow G$ defined $\forall g \in G$ as $inv(g) = g^{-1}$. Then G is a Lie group.

¹This is referencing the mathematical term Field as a set on which addition, subtraction, multiplication, and division are defined and behave as the corresponding operations on rational and real numbers do.

I. Introduction to $SU(2)$ representation theory

At this stage we now want to look at matrices, that is to say the general linear group and its subgroups, with a focus on Lie groups. Before we make this connection it will first be useful to have the notion of a limit sequence of matrices as means to connect the idea of continuity to matrix groups.

Definition 8. A sequence is an Let M_n be a sequence of matrices in $M_n(F)^2$ where F is the field the entries of the matrices belong to. We say that M_n converges to a matrix M if each for each element M_{ij} of this matrix is the limit of the sequences $(M_n)_{ij}$.

Definition 9. A matrix Lie group is a subgroup G of $GL(n; C)$ such that for any sequence of matrices M_n in G , where M_n converges to some matrix M , then either M is in G or M is not invertible³.

It is a foundational result of Lie theory that where there is a Lie group there is a Lie algebra [31]. The interest in the algebra is that it is often a simpler object than the Lie group. While a Lie groups elements action in relation to each other may be relatively complex these can be mapped to elements of an algebra where the the interaction of elements is linear. Indeed it can be shown the Lie algebra completely determines the *local* structure of a lie group. First let us consider a Lie algebra in abstraction unattached to a particular Lie group.

Definition 10. A Lie algebra is a vector space \mathfrak{g} over some field F together with a binary operation $[\cdot, \cdot] : \mathfrak{g} \times \mathfrak{g} \rightarrow \mathfrak{g}$, called the Lie bracket satisfying the following axioms:

- Bilinearity, $[ax + by, z] = a[x, z] + b[y, z]$ $[z, ax + by] = a[z, x] + b[z, y]$ for all scalars a, b in F and all elements x, y, z in \mathfrak{g} .
- Alternativity, $[x, x] = 0$ for all x in \mathfrak{g} .
- The Jacobi identity, $[x, [y, z]] + [z, [x, y]] + [y, [z, x]] = 0$ for all x, y, z in \mathfrak{g} .

Note that the bilinearity and alternativity conditions imply anticommutativity ($[x, y] = -[y, x]$).

²So a function can be seen as a function from an interval of integers to a set of matrices.

³This second point may seem odd. The reason it is there is that though the group of interest is closed in the sense any finite number of applications of the group operation keeps one in the same space, in the limit this is no longer guaranteed. This is essentially the difference between closure under group multiplication and topological closure - there is no reason the presume the limit in this second case should be in the set if all we care about is group structure.

We can now take steps towards connecting matricial Lie groups and algebras. The key technical step is to make use of the exponent of a matrix. Recalling that if X is an $n \times n$ matrix, we define the exponential of X , denoted e^X or $\exp(X)$ by the usual power series

$$e^X = \sum_{m=0}^{\infty} \frac{X^m}{m!} \quad (\text{I.1})$$

where X^0 is defined to be the identity matrix I and where X^m is the repeated matrix product of X with itself. The exponential map shows us how information about the Lie group structure and Lie algebra structure interact.

Definition 11. Let G be a matrix Lie group. The Lie algebra of G , denoted \mathfrak{g} , is the set of all matrices X such that e^{tX} is in G for all $t \in \mathbb{R}$.

It can be shown[31] that if $G \subseteq GL(n; \mathbb{C})$ is a matrix Lie group with Lie algebra \mathfrak{g} then a matrix X is in \mathfrak{g} iff there exists a smooth curve γ in $M_n(\mathbb{C})$ such that:

- $\gamma(t)$ lies in G for all t .
- $\gamma(0) = I$
- $\frac{d\gamma}{dt}|_{t=0} = X$

and so \mathfrak{g} is the tangent space at the identity. We can use this to get the exact form of the groups of primary interest to us, namely the special unitary groups.

Lie algebra of $SU(n)$ The Lie algebra $\mathfrak{su}(n)$ of $SU(n)$ consists of $n \times n$ skew-Hermitian⁴ matrices with trace zero.

This can be shown by taking a smooth curve through the identity of $SU(n)$ which we recall is the set of all $n \times n$ unitary matrices with determinant 1 together with matrix multiplication.

If we let $\gamma : \mathbb{R} \rightarrow SU(n)$ be a smooth matrix-valued function on the reals such that $\gamma(0) = I$ the identity matrix.

Then let us write $\gamma(t) \circ \gamma(t)^{-1} = I_n$ where $\gamma(t)^{-1}$ is the inverse path.

If we then take the tangent of this path we get:

$$\gamma(t) \circ \gamma'(t)^{-1} + \gamma'(t) \circ \gamma(t)^{-1} = 0_n \quad (\text{I.2})$$

⁴A matrix M is equal to the negative of its hermitian conjugate M^\dagger .

I. Introduction to $SU(2)$ representation theory

When $t = 0$ then $\gamma(0) = I$ and we then have

$$\gamma'(0) + \gamma(0)^{-1} = 0_n \quad (\text{I.3})$$

Which tells us that the space of the differentiated matrices at the identity are hermitian and of trace zero.

I.1.3 Representations

For our purposes we consider representations in two contexts: *representations of groups* and *representations of algebras*. The general idea is to look at all the ways the operations and elements of these mathematical objects are modelled by linear operators acting on some space.

Definition 12. A representation of a group G on a vector space V over a field F is a group homomorphism from G to $GL(V)$, the general linear group on V . That is to say a representation is a map:

$$\Pi : G \rightarrow GL(V)$$

such that $\Pi(g_1g_2) = \Pi(g_1)\Pi(g_2)$ for all $g_1, g_2 \in G$.

If Π is a one-to-one homomorphism, the representation is called faithful. When F is \mathbb{R} this is a real representation, when it is \mathbb{C} it is a complex representation.

For a more concrete interpretation of this definition we could say a group representation of a group G is a group homomorphism $\Pi : G \rightarrow GL(V, F)$ for a field F . That is to say a map ϕ that sends $g \in G$ where to a linear map such that $\Pi(g_1g_2) = \Pi(g_1) \circ \Pi(g_2)$ for all $g_1, g_2 \in G$.

Definition 13. If \mathfrak{g} is a Lie algebra, then a representation of \mathfrak{g} on a vector space V over the field F is a Lie algebra homomorphism

$$\pi : \mathfrak{g} \rightarrow \text{gl}(V, F).$$

If π is a one-to-one homomorphism, the representation is called faithful. When F is \mathbb{R} this is a real representation, when it is \mathbb{C} it is a complex representation.

From here on we restrict ourselves to finite representations from which it is possible to understand the original contents of thesis.

Irreducible representations If Π is a finite-dimensional real or complex representation of a matrix Lie group G , acting on a space V . A subspace W of V is called invariant if $\Pi(A)w \in W$ for all $w \in W$ and all $A \in G$. An invariant subspace W is called non-trivial if $W \neq \{0\}$ and $W \neq V$. We say a representation with no non-trivial invariant subspaces is called irreducible. The terms invariant, non-trivial, and irreducible are defined analogously for representations of Lie algebras.

Note that if \mathfrak{g} is a real Lie algebra, we can still consider complex representations of \mathfrak{g} .

Intertwiners A useful concept is the coherent mapping between representations. This can be understood in the sense that the representation of the group element after the representation of some group action on one space is mapped to the representation of the group element after the representation of the same group action on the other space. A similar structure applies to Lie algebras. Imagine that G is a matrix Lie group and Π is a representation of G acting on the space V , where Σ is a representation of G acting on the space W . A linear map $\phi : V \rightarrow W$ is called an intertwining map of representations if

$$\phi(\Pi(A)v) = \Sigma(A)\phi(v) \quad (\text{I.4})$$

for all $A \in G$ and all $v \in V$.

Similarly for a matrix Lie algebra \mathfrak{g} if π is a representation of \mathfrak{g} acting on the space V , and σ is a representation of \mathfrak{g} acting on the space W . A linear map $\phi : V \rightarrow W$ is called an intertwining map of representations if

$$\phi(\Pi(A)v) = \Sigma(A)\phi(v)$$

for all $A \in \mathfrak{g}$ and all $v \in V$.

It can be shown that [31] if G is a matrix Lie group with Lie algebra \mathfrak{g} where Π is a (finite-dimensional real or complex) representation of G , acting on the space V . Then there is a unique representation π of \mathfrak{g} acting on the same space such that

$$\sigma(e^X) = e^{\pi(X)}$$

for all $X \in \mathfrak{g}$. The representation π can then be computed as

$$\pi(X) = \frac{d}{dt} \Pi(e^{tX}) \Big|_{t=0}$$

I. Introduction to $SU(2)$ representation theory

and satisfies

$$\pi(AXA^{-1}) = \Pi(A)\pi(X)\Pi(A)^{-1}$$

for all $X \in \mathfrak{g}$ and all $A \in G$.

One should note that not every representation π of \mathfrak{g} relates to a representation Π of G with the exception of when G is simply connected [97]. Consider the one-dimensional complex vector space \mathbb{C} . For any matrix Lie group G , we can define the trivial representation, $\Pi : G \rightarrow \text{GL}(1; \mathbb{C})$, by the formula

$$\Pi(A) = I$$

for all $A \in G$. Of course, this is an irreducible representation, since \mathbb{C} has no non-trivial subspaces, let alone nontrivial invariant subspaces. If \mathfrak{g} is a Lie algebra, we can also define the trivial representation of \mathfrak{g} , $\pi : \mathfrak{g} \rightarrow \text{gl}(1; \mathbb{C})$, by

$$\pi(X) = 0$$

I.1.4 Compositions of representations

Individual representations are rendered more useful when we can consider how they compose. This dovetails with the idea of a compositional calculus and the interactions of systems based on spin which will prove key in the results of this thesis.

Direct products of representations If we have some matrix Lie group G and $\Pi_1, \Pi_2, \dots, \Pi_m$ are representations of G acting on vector spaces V_1, V_2, \dots, V_m . Then the direct sum of $\Pi_1, \Pi_2, \dots, \Pi_m$ is a representation $\Pi_1 \oplus \dots \oplus \Pi_m$ of G acting on the space $V_1 \oplus \dots \oplus V_m$, defined by

$$[\Pi_1 \oplus \dots \oplus \Pi_m(A)](v_1, \dots, v_m) = (\Pi_1(A)v_1, \dots, \Pi_m(A)v_m)$$

for all $A \in G$.

Similarly, if \mathfrak{g} is a Lie algebra, and $\pi_1, \pi_2, \dots, \pi_m$ are representations of \mathfrak{g} acting on V_1, V_2, \dots, V_m , then we define the direct sum of $\pi_1, \pi_2, \dots, \pi_m$, acting on $V_1 \oplus \dots \oplus V_m$ by

$$[\pi_1 \oplus \dots \oplus \pi_m(X)](v_1, \dots, v_m) = (\pi_1(X)v_1, \dots, \pi_m(X)v_m)$$

for all $X \in \mathfrak{g}$.

Tensor products of representations More important for us is the structure of tensor products of representations which are directly related to the theory of angular momentum when applied to $SU(2)$.

Let us take two matrix lie groups G and H and take Π_1 to be a representation of G acting on a space U and let Π_2 be a representation of H acting on a space V . The tensor product of Π_1 and Π_2 is a representation $\Pi_1 \otimes \Pi_2$ of $G \times H$ acting on $U \otimes V$ defined by

$$(\Pi_1 \otimes \Pi_2)(A, B) = \Pi_1(A) \otimes \Pi_2(B) \quad (\text{I.5})$$

for all $A \in G$ and $B \in H$. It can be shown that this too is itself a representation of $G \times H$ on $U \otimes V$.

An natural question to ask is what this implies for the Lie algebra of the combined representations. We learned above that the Lie algebras of a Lie group can be identified with the tangent space of the Lie group at zero.

If we take $u(t)$ and $v(t)$ as smooth curves on our spaces U and V respectively then we have that

$$\frac{d}{dt}(u(t) \otimes v(t)) = \frac{du}{dt} \otimes v(t) + u(t) \otimes \frac{dv}{dt}.$$

From this we can see the following:

$$\begin{aligned} & (\pi_1 \otimes \pi_2)(X, Y)(u \otimes v) \\ &= \frac{d}{dt}(\Pi_1 \otimes \Pi_2)(e^{tX}u \otimes e^{tY})v \Big|_{t=0} \\ &= \frac{d}{dt}\Pi_1(e^{tX})u \otimes \Pi_2(e^{tY})v \Big|_{t=0} \\ &= \left(\frac{d}{dt}\Pi_1(e^{tX})u \Big|_{t=0}\right) \otimes v + u \otimes \left(\frac{d}{dt}\Pi_2(e^{tY})v \Big|_{t=0}\right) \end{aligned}$$

which is of the form $(\pi_1 \otimes \pi_2)(X, Y)$ on the basis $u \otimes v$ spanning $U \otimes V$. This tells us that if we have $\Pi_1 \otimes \Pi_2$ of $G \times H$. Then when $\pi_1 \otimes \pi_2$ denotes the associated representation of $\mathfrak{g} \otimes \mathfrak{h}$, then

$$(\pi_1 \otimes \pi_2)(X, Y) = \pi_1(X) \otimes I + I \otimes \pi_2(Y) \quad (\text{I.6})$$

for all $X \in \mathfrak{g}$ and $Y \in \mathfrak{h}$.

It will be useful for the purposes of this thesis to restrict ourselves to the action of the tensor product of representations of the same group. Note there is some ambiguity here in separating the action of G from $G \times G$. As a result we can see this situation as the action of the single group G over a tensor product of its representations.

I. Introduction to $SU(2)$ representation theory

With regards to irreducible representation if Π_1 and Π_2 are irreducible representations of a group G , then $\Pi_1 \otimes \Pi_2$ will typically not be irreducible when viewed as a representation of G . One can, then, attempt to decompose $\Pi_1 \otimes \Pi_2$ as a direct sum of irreducible representations. This process, for $SU(2)$, is called the Clebsch-Gordan theory or, in the physics literature, "addition of angular momentum".

I.1.5 Important properties for the representation of $SU(2)$

There are some technical observations about $SU(2)$ that are useful. To understand them we must first talk about simply connected Lie groups. These can be understood as a Lie group where any two points can be connected by a parameterised path (connected) and any two such paths can be smoothly mapped into one another (simple). In a rough, and for our cases sufficient sense, a simply connected space has no holes and is composed of a single connected collection of elements.

Suppose we have a notion of a simply connected space, and matrix Lie groups G and H with Lie algebras \mathfrak{g} and \mathfrak{h} , where $\phi : \mathfrak{g} \rightarrow \mathfrak{h}$ is a Lie algebra homomorphism. If G is simply connected, there exists a unique homomorphism $\Phi : G \rightarrow H$ such that $\Phi(e^X) = e^{\phi(X)}$ for all $X \in \mathfrak{g}$ [31]. In general the inverse map exists so in this instance there is a one-to-one mapping between the irreps of the Lie algebras and the Lie groups, this tells us that it is sufficient to find the irreps for one to get them for the other.

This statement can be seen to apply to our group of interest $SU(2)$. Consider the fact that for any α, β as a pair in \mathbb{C}^2 where $\alpha = a + bi$ and $\beta = c + di$, then the equation $|\alpha|^2 + |\beta|^2 = 1$ that characterises the group $SU(2)$ can be written as $a^2 + b^2 + c^2 + d^2 = 1$. This is the space of the 3-sphere which we know is simply connected. It follows then that as the lie group $SU(2)$ is simply connected there is a one-to-one relation between its irreps and those of its lie algebra.

For our purposes a crucial technical relationship between the irreducible representations of $SU(2)$ is the following:

Proposition I.1.5.1. The n^{th} irreducible representation of $SU(2)$ is equivalent the symmetrised space of n copies of the fundamental representation (where $n = 1$)

Proof. As a simply connected Lie group its irreducible representations are the same as its lie algebra.

Now the fundamental representation of the Lie algebra has the elements $e_1 = \begin{bmatrix} 1 \\ 0 \end{bmatrix}$ and $e_2 = \begin{bmatrix} 0 \\ 1 \end{bmatrix}$ as a basis.

With this in mind we consider J_+, J_- as the raising and lowering maps such that $J_+e_1 = e_2$ and $J_+e_1 = 0$, while $J_-e_1 = 0$ and $J_-e_2 = e_1$.

The symmetrised space of n copies of the fundamental representation then has $\{e_1^n, e_1^{n-1}e_2^n, \dots, e_2^n\}$ as its basis.

Recall that to be an irreducible representation there must be a sub-representation that is closed under the action of the algebra. Consider that J_+ and J_- allow us traverse the spanning basis. For example, $J_+e_1^n = ne_1^{n-1}e_2^n$ and $J_-e_2^n = J_- \circ J_-e_2^n = J_-ne_2^{n-1}e_1 = n(n-1)e_2^{n-2}e_1^2$. In this way we see that there is no closed subrepresentation so these spaces all form irreducible representations of $\mathfrak{su}(2)$. These in turn match the the irreducible representations of $SU(2)$. \square

I.2 Importance of $SU(2)$ in physics

In modern physics one is acutely interested in characterising what a ‘thing’ is via symmetries. At the level of everyday human experience there is a rotational invariance of the fundamental laws. That is to say if you change reference frame to one where we have rotated all the coordinates then Newton’s laws are the same (unlike if we moved to an accelerating one where the laws are not the same). More precisely Newton’s laws are invariant under the action of the group $SO(3)$.

For a quantum mechanical Hilbert space symmetries are represented by unitary operators. Given a group element g in group G there is some unitary U_g . However physical states are rays or equivalence classes of proportional vectors in Hilbert space. The implication of this is that $U(g)$ or $c(g)U(g)$, where $c(g)$ is a complex number of norm 1, are physically identical in their action on a quantum system. As such we write $U(g1)U(g2) = c(g1, g2)U(g1g2)$ for all $g1, g2 \in G$ where $c(g1, g2)$ is a complex number of unit norm. For quantum mechanics proper then symmetries are represented as Projective unitary operators $PU(g)$.

I. Introduction to $SU(2)$ representation theory

Definition 14. The projective unitary group $PU(n)$ is the set of equivalence classes of unitary matrices under multiplication by the diagonal matrix $e^{i\theta} I$.

So a symmetry is described by group G acting on $PU(n)$. In terms of spin and rotation we have the group $SO(3)$ acting via operators on $PU(n)$ where n is the dimension of the system at hand.

Before making use of this like between the symmetries of Hilbert spaces and their correspondence to the physically meaningful projective space we need the notion of a covering group that is also a covering space that is also a group. In short a covering space is space and a map that lays that space over another multiple times such that the map is locally homeomorphic. More formally we can then say that:

Definition 15. Let X be a topological space. A covering space of X is a topological space⁵ C together with a continuous surjective map $p : C \rightarrow X$ such that for every $x \in X$, there exists an open neighbourhood U of x , such that $p^{-1}(U)$ (the pre-image of U under p) is a union of disjoint open sets in C , each of which is mapped homeomorphically onto U by p .

There can be multiple covering spaces but an important one is when the covering space is such that any path between two points can be smoothly deformed into one another i.e it is simply path connected.

Definition 16. A covering space is a universal covering space if it is simply connected.

We are now in a position to bring up the theorem that will link $SU(2)$ and $SO(3)$

Theorem I.2.1. Let $\rho : G \rightarrow PU$ be a continuous homomorphism⁶ which we term a projective representation of G . There is a one-to-one correspondence between the irreducible projective representations of a group G and the irreducible, determinant-one representations of its universal covering group.

Proof. See section 16.7.3 in [98] □

⁵A topological space is an ordered pair (X, τ) , where X is a set and τ is a collection of subsets of X , such that: 1. The empty set and X itself belong to τ . 2. Any arbitrary (finite or infinite) union of members of τ belongs to τ . 3. The intersection of any finite number of members of τ belongs to τ .

⁶i.e $\rho(a) * \rho(b) = \rho(a * b)$.

I.2. Importance of $SU(2)$ in physics

As the universal covering group of $SO(3)$ is $SU(2)$ we arrive at the conclusion that the fundamental elements determining a quantum systems relationship with rotational invariance are the irreducible representations of $SU(2)$. Thus the interest in spin in physics at large.

“I didn’t choose the thug life, the thug life chose me.”

— Tupac Shakur

“I should like to be a horse.”

— Queen Elizabeth II

Bibliography

- [1] A. P. Yutsis, I. B. Levinson, and V. V. Vanagas. *Mathematical Apparatus of the Theory of Angular Momentum*. Israel Program for Scientific Translations, 1962.
- [2] R. P. Feynman. Space-Time Approach to Quantum Electrodynamics. *76(6):769–789*, 1949.
- [3] Bob Coecke and Ross Duncan. Interacting quantum observables. In *International Colloquium on Automata, Languages, and Programming*, pages 298–310. Springer, 2008.
- [4] Bob Coecke and Ross Duncan. Interacting quantum observables: categorical algebra and diagrammatics. *New Journal of Physics*, 13(4):043016, 2011.
- [5] Renaud Vilmart. A Near-Minimal Axiomatisation of ZX-Calculus for Pure Qubit Quantum Mechanics. In *2019 34th Annual ACM/IEEE Symposium on Logic in Computer Science (LICS)*, pages 1–10, 2019.
- [6] Ross Duncan and Simon Perdrix. Rewriting measurement-based quantum computations with generalised flow. In *International Colloquium on Automata, Languages, and Programming*, pages 285–296. Springer, 2010.
- [7] Miriam Backens, Hector Miller-Bakewell, Giovanni de Felice, Leo Lobski, and John van de Wetering. There and back again: A circuit extraction tale. *Quantum*, 5:421, 3 2021.
- [8] Aleks Kissinger and John van de Wetering. Universal MBQC with generalised parity-phase interactions and Pauli measurements. *Quantum*, 3, 2019.
- [9] Niel de Beaudrap and Dominic Horsman. The ZX calculus is a language for surface code lattice surgery. *Quantum*, 4, 2020.
- [10] Craig Gidney and Austin G. Fowler. Efficient magic state factories with a catalyzed $|CCZ\rangle$ to $2|T\rangle$ transformation. *Quantum*, 3:135, 4 2019.
- [11] Michael Hanks, Marta P. Estarellas, William J. Munro, and Kae Nemoto. Effective Compression of Quantum Braided Circuits Aided by ZX-Calculus. *Physical Review X*, 10:041030, 2020.
- [12] Niel de Beaudrap, Ross Duncan, Dominic Horsman, and Simon Perdrix. Pauli Fusion: a Computational Model to Realise Quantum Transformations from ZX Terms. In Bob Coecke and Matthew Leifer, editors, *Proceedings 16th International Conference on Quantum Physics and Logic, Chapman University, Orange, CA, USA, 10-14 June 2019*, volume 318 of *Electronic Proceedings in Theoretical Computer Science*, pages 85–105. Open Publishing Association, 2020.
- [13] Nicholas Chancellor, Aleks Kissinger, Joschka Roffe, Stefan Zohren, and Dominic Horsman. Graphical Structures for Design and Verification of Quantum Error Correction. 2016. arXiv: 1611.08012.
- [14] Liam Garvie and Ross Duncan. Verifying the Smallest Interesting Colour Code with Quantomatic. In Bob Coecke and Aleks Kissinger, editors, *Proceedings 14th International Conference on Quantum Physics and Logic, Nijmegen, The Netherlands, 3-7 July 2017*, volume 266 of *Electronic Proceedings in Theoretical Computer Science*, pages 147–163. Open Publishing Association, 2018. arXiv: 1706.02717.

- [15] John van de Wetering. Constructing quantum circuits with global gates. *New Journal of Physics*, 23(4):043015, 4 2021. arXiv: 2012.09061.
- [16] Alexander Cowtan, Silas Dilkes, Ross Duncan, Will Simmons, and Seyon Sivarajah. Phase gadget synthesis for shallow circuits. In Bob Coecke and Matthew Leifer, editors, *Proceedings 16th International Conference on Quantum Physics and Logic*, Chapman University, Orange, CA, USA., 10-14 June 2019, volume 318 of *Electronic Proceedings in Theoretical Computer Science*, pages 213–228. Open Publishing Association, 2020.
- [17] Alexander Cowtan, Will Simmons, and Ross Duncan. A Generic Compilation Strategy for the Unitary Coupled Cluster Ansatz. *arXiv preprint arXiv:2007.10515*, 2020.
- [18] Niel de Beaudrap, Xiaoning Bian, and Quanlong Wang. Fast and effective techniques for T-count reduction via spider nest identities. 2020. arXiv: 2004.05164.
- [19] Aleks Kissinger and John van de Wetering. Reducing the number of non-clifford gates in quantum circuits. *Physical Review A*, Vol.102-2, 102:022406, 8 2020.
- [20] Ross Duncan, Aleks Kissinger, Simon Pedrix, and John van de Wetering. Graph-theoretic Simplification of Quantum Circuits with the ZX-calculus. *Quantum*, 4:279, 6 2020.
- [21] Roger Penrose. Applications of Negative Dimensional Tensors. In D. J. A. Welsh, editor, *Combinatorial Mathematics and Its Applications*. Academic Press, 1971.
- [22] Ian Affleck, Tom Kennedy, Elliott H. Lieb, and Hal Tasaki. Rigorous results on valence-bond ground states in antiferromagnets. *Phys. Rev. Lett.*, 59:799–802, Aug 1987.
- [23] Michael Victor Berry. Quantal phase factors accompanying adiabatic changes. *Proceedings of the Royal Society of London. A. Mathematical and Physical Sciences*, 392(1802):45–57, 1984.
- [24] Tzu-Chieh Wei, Ian Affleck, and Robert Raussendorf. Affleck-Kennedy-Lieb-Tasaki state on a honeycomb lattice is a universal quantum computational resource. *Physical review letters*, 106(7):070501, 2011.
- [25] Pierre Martin-Dussaud. A primer of group theory for loop quantum gravity and spin-foams. *General Relativity and Gravitation*, 51(9):110, 2019.
- [26] Carlo Rovelli and Francesca Vidotto. *Covariant loop quantum gravity: an elementary introduction to quantum gravity and spinfoam theory*. Cambridge University Press, 2015.
- [27] Miriam Backens and Aleks Kissinger. ZH: A Complete Graphical Calculus for Quantum Computations Involving Classical Non-linearity. In Peter Selinger and Giulio Chiribella, editors, *Proceedings of the 15th International Conference on Quantum Physics and Logic, Halifax, Canada, 3-7th June 2018*, volume 287 of *Electronic Proceedings in Theoretical Computer Science*, pages 23–42. Open Publishing Association, 2019.
- [28] Stach Kuijpers, John van de Wetering, and Aleks Kissinger. Graphical fourier theory and the cost of quantum addition. *arXiv preprint arXiv:1904.07551*, 2019.
- [29] Aleks Kissinger and John van de Wetering. PyZX: Large Scale Automated Diagrammatic Reasoning. In Bob Coecke and Matthew Leifer, editors, *Proceedings 16th International Conference on Quantum Physics and Logic*, Chapman University, Orange, CA, USA., 10-14 June 2019, volume 318 of *Electronic Proceedings in Theoretical Computer Science*, pages 229–241. Open Publishing Association, 2020.
- [30] Niel de Beaudrap. Well-tempered ZX and ZH calculi. *arXiv preprint arXiv:2006.02557*, 2020.
- [31] Brian Hall. *Lie groups, Lie algebras, and representations: an elementary introduction*, volume 222. Springer, 2015.

Bibliography

- [32] Pierre Martin-Dussaud. A Primer of Group Theory for Loop Quantum Gravity and Spin-foams. *Gen Relativ Gravit*, 51(9):110, September 2019.
- [33] Richard DP East, John van de Wetering, Nicholas Chancellor, and Adolfo G Grushin. Aklt-states as zx-diagrams: diagrammatic reasoning for quantum states. *arXiv preprint arXiv:2012.01219*, 2020.
- [34] Lev Davidovich Landau. On the theory of phase transitions. i. *Zh. Eksp. Teor. Fiz.*, 11:19, 1937.
- [35] Xiao-Gang Wen. Topological orders in rigid states. *International Journal of Modern Physics B*, 4(02):239–271, 1990.
- [36] Frank Pollmann, Erez Berg, Ari M Turner, and Masaki Oshikawa. Symmetry protection of topological phases in one-dimensional quantum spin systems. *Physical review b*, 85(7):075125, 2012.
- [37] Y Hatsugai. Quantized berry phases for a local characterization of spin liquids in frustrated spin systems. *Journal of Physics: Condensed Matter*, 19(14):145209, mar 2007.
- [38] Steven R. White. Density-matrix algorithms for quantum renormalization groups. *Phys. Rev. B*, 48:10345–10356, Oct 1993.
- [39] Jutho Haegeman and Frank Verstraete. Diagonalizing transfer matrices and matrix product operators: a medley of exact and computational methods. *Annual Review of Condensed Matter Physics*, 8:355–406, 2017.
- [40] Roman Orus and Guifre Vidal. Infinite time-evolving block decimation algorithm beyond unitary evolution. *Physical Review B*, 78(15):155117, 2008.
- [41] Michael Lubasch, J Ignacio Cirac, and Mari-Carmen Banuls. Algorithms for finite projected entangled pair states. *Physical Review B*, 90(6):064425, 2014.
- [42] F. Verstraete and J. I. Cirac. Renormalization algorithms for Quantum-Many Body Systems in two and higher dimensions. *arXiv e-prints*, pages cond-mat/0407066, July 2004.
- [43] Román Orús. A practical introduction to tensor networks: Matrix product states and projected entangled pair states. *Annals of Physics*, 349:117 – 158, 2014.
- [44] T. B. Wahl, H.-H. Tu, N. Schuch, and J. I. Cirac. Projected entangled-pair states can describe chiral topological states. *Phys. Rev. Lett.*, 111:236805, Dec 2013.
- [45] J. Dubail and N. Read. Tensor network trial states for chiral topological phases in two dimensions and a no-go theorem in any dimension. *Phys. Rev. B*, 92:205307, Nov 2015.
- [46] Didier Poilblanc, J. Ignacio Cirac, and Norbert Schuch. Chiral topological spin liquids with projected entangled pair states. *Phys. Rev. B*, 91:224431, Jun 2015.
- [47] Ji-Yao Chen, Sylvain Capponi, Alexander Wietek, Matthieu Mambrini, Norbert Schuch, and Didier Poilblanc. $SU(3)_1$ chiral spin liquid on the square lattice: A view from symmetric projected entangled pair states. *Phys. Rev. Lett.*, 125:017201, Jun 2020.
- [48] Marcel den Nijs and Koos Rommelse. Preroughening transitions in crystal surfaces and valence-bond phases in quantum spin chains. *Phys. Rev. B*, 40:4709–4734, Sep 1989.
- [49] Zheng-Cheng Gu and Xiao-Gang Wen. Tensor-entanglement-filtering renormalization approach and symmetry-protected topological order. *Phys. Rev. B*, 80:155131, Oct 2009.
- [50] Frank Pollmann, Ari M. Turner, Erez Berg, and Masaki Oshikawa. Entanglement spectrum of a topological phase in one dimension. *Phys. Rev. B*, 81:064439, Feb 2010.
- [51] Y Hatsugai. Quantized Berry Phases as a Local Order Parameter of a Quantum Liquid. *Journal of the Physical Society of Japan*, 11 2006.

- [52] Eugene H. Kim, G. Fáth, J. Sólyom, and D. J. Scalapino. Phase transitions between topologically distinct gapped phases in isotropic spin ladders. *Phys. Rev. B*, 62:14965–14974, Dec 2000.
- [53] P.W. Anderson. Resonating valence bonds: A new kind of insulator? *Materials Research Bulletin*, 8(2):153 – 160, 1973.
- [54] Roman Orus. Tensor networks for complex quantum systems. *Nature Reviews Physics*, 1(9):538–550, 2019.
- [55] Ian Affleck, Tom Kennedy, Elliott H Lieb, and Hal Tasaki. Valence bond ground states in isotropic quantum antiferromagnets. *Communications in Mathematical Physics*, 115(3):477–528, September 1988.
- [56] Sanjay Moudgalya, Nicolas Regnault, and B. Andrei Bernevig. Entanglement of exact excited states of Affleck-Kennedy-Lieb-Tasaki models: Exact results, many-body scars, and violation of the strong eigenstate thermalization hypothesis. *Physical Review B*, 98(23):235156, 2018.
- [57] Frank Pollmann, Erez Berg, Ari M Turner, and Masaki Oshikawa. Symmetry protection of topological phases in one-dimensional quantum spin systems. *Physical Review B*, 85(7):401, February 2012.
- [58] Quanlong Wang and Xiaoning Bian. Qutrit dichromatic calculus and its universality. *Electronic Proceedings in Theoretical Computer Science*, 2014.
- [59] Quanlong Wang. Qutrit zx-calculus is complete for stabilizer quantum mechanics. In Bob Coecke and Aleks Kissinger, editors, *Proceedings 14th International Conference on Quantum Physics and Logic, Nijmegen, The Netherlands, 3-7 July 2017*, volume 266 of *Electronic Proceedings in Theoretical Computer Science*, pages 58–70. Open Publishing Association, 2018.
- [60] Guangyue Ji and Junren Shi. Berry phase in the composite fermi liquid. *Phys. Rev. Research*, 2:033329, Aug 2020.
- [61] Chen Zhao and Xiao-Shan Gao. Analyzing the barren plateau phenomenon in training quantum neural network with the ZX-calculus. *arXiv preprint arXiv:2102.01828*, 2021.
- [62] Alexis Toumi, Richie Yeung, and Giovanni de Felice. Diagrammatic Differentiation for Quantum Machine Learning. *arXiv preprint arXiv:2103.07960*, 2021.
- [63] Ulrich Schollwock. The density-matrix renormalization group in the age of matrix product states. *Annals of Physics*, 326(1):96 – 192, 2011. January 2011 Special Issue.
- [64] Maarten Van den Nest, Akimasa Miyake, Wolfgang Dür, and Hans J Briegel. Universal resources for measurement-based quantum computation. *Physical review letters*, 97(15):150504, 2006.
- [65] Akimasa Miyake. Quantum computational capability of a 2d valence bond solid phase. *Annals of Physics*, 326(7):1656–1671, 2011.
- [66] Michael A Nielsen and Isaac Chuang. Quantum computation and quantum information, 2002.
- [67] B. Coecke and A. Kissinger. *Picturing Quantum Processes: A First Course in Quantum Theory and Diagrammatic Reasoning*. Cambridge University Press, 2017.
- [68] Miriam Backens. The ZX-calculus is complete for stabilizer quantum mechanics. *New Journal of Physics*, 16(9):093021, 2014.
- [69] Matthew B Elliott, Bryan Eastin, and Carlton M Caves. Graphical description of the action of Clifford operators on stabilizer states. *Physical Review A*, 77(4):042307, 2008.

Bibliography

- [70] Daniel E Browne, Matthew B Elliott, Steven T Flammia, Seth T Merkel, Akimasa Miyake, and Anthony J Short. Phase transition of computational power in the resource states for one-way quantum computation. *New Journal of Physics*, 10(2):023010, 2008.
- [71] Ching-Kai Chiu, Jeffrey C Y Teo, Andreas P Schnyder, and Shinsei Ryu. Classification of topological quantum matter with symmetries. *Reviews of Modern Physics*, 88(3):035005, August 2016.
- [72] Norbert Schuch, David Pérez-García, and Ignacio Cirac. Classifying quantum phases using matrix product states and projected entangled pair states. *Phys. Rev. B*, 84:165139, Oct 2011.
- [73] Xie Chen, Zheng-Xin Liu, and Xiao-Gang Wen. Two-dimensional symmetry-protected topological orders and their protected gapless edge excitations. *Phys. Rev. B*, 84:235141, Dec 2011.
- [74] T. Senthil. Symmetry-protected topological phases of quantum matter. *Annual Review of Condensed Matter Physics*, 6(1):299–324, 2015.
- [75] Quantized electric multipole insulators. *Science*, 357(6346):61 – 66, 07 2017.
- [76] Vladimir A Benalcazar, B Andrei Bernevig, and Taylor L Hughes. Electric multipole moments, topological multipole moment pumping, and chiral hinge states in crystalline insulators. *Physical Review B*, 96(24):245115, 12 2017.
- [77] Zhida Song, Zhong Fang, and Chen Fang. (d-2)-Dimensional Edge States of Rotation Symmetry Protected Topological States. *Physical Review Letters*, 119(24):246402, 12 2017.
- [78] Frank Schindler, Ashley M Cook, Maia G Vergniory, Zhijun Wang, Stuart S P Parkin, B Andrei Bernevig, and Titus Neupert. Higher-order topological insulators. *Science Advances*, 4(6):eaat0346, 06 2018.
- [79] Frank Schindler, Zhijun Wang, Maia G Vergniory, Ashley M Cook, Anil Murani, Shamashis Sengupta, Alik Yu Kasumov, Richard Deblock, Sangjun Jeon, Ilya Drozdov, Hélène Bouchiat, Sophie Guéron, Ali Yazdani, B Andrei Bernevig, and Titus Neupert. Higher-order topology in bismuth. *Nature Physics*, 14(9):918–924, September 2018.
- [80] Richard D. P. East, Pierre Martin-Dussaud, and John Van de Wetering. Spin-networks in the zx-calculus, 2021.
- [81] Roger Penrose. Angular momentum: An approach to combinatorial spacetime. In T Bastin, editor, *Quantum Theory and Beyond*, pages 151–180. Cambridge University Press, 1971.
- [82] Giorgio Sarno, Simone Speziale, and Gabriele V. Stagno. 2-vertex Lorentzian spin foam amplitudes for dipole transitions. 50(4):43. arXiv: 1801.03771.
- [83] Giorgio Ponzano and Tullio Eugenio Regge. Semiclassical limit of racah coefficients. 1968.
- [84] Justin Roberts. Classical 6j-symbols and the tetrahedron. *Geometry & Topology*, 3(1):21–66, 1999.
- [85] Seth A Major. A spin network primer. *American Journal of Physics*, 67(11):972–980, 1999. arXiv: gr-qc/9905020.
- [86] Carlo Rovelli and Lee Smolin. Spin networks and quantum gravity. *Physical Review D*, 52(10):5743–5759, 1995. arXiv: gr-qc/9709028v2.
- [87] H. T. Johansson and C. Forssén. Fast and accurate evaluation of wigner 3j, 6j, and 9j symbols using prime factorisation and multi-word integer arithmetic. 2015.
- [88] Grzegorz Czelusta and Jakub Mielczarek. Quantum simulations of a qubit of space. *Physical Review D*, 103(4):046001, 2021. arXiv: 2003.13124.

Bibliography

- [89] Jakub Mielczarek. Spin foam vertex amplitudes on quantum computer—preliminary results. *Universe*, 5(8):179, 2019. arXiv: 1810.07100.
- [90] Lior Cohen, Anthony J Brady, Zichang Huang, Hongguang Liu, Dongxue Qu, Jonathan P Dowling, and Muxin Han. Efficient simulation of loop quantum gravity: A scalable linear-optical approach. *Physical Review Letters*, 126(2):020501, 2021. arXiv: 2003.03414.
- [91] Sundance Bilson-Thompson and Deepak Vaid. Lqg for the bewildered. *arXiv preprint arXiv:1402.3586*, 2014.
- [92] Simone Speziale. Boosting wigner’s nj-symbols. *Journal of Mathematical Physics*, 58(3):032501, 2017.
- [93] GA Kerimov and Yi A Verdiev. Clebsch-gordan coefficients of the sl (2, c) group. *Reports on Mathematical Physics*, 13(3):315–326, 1978.
- [94] Kiss.
- [95] M. Hein, J. Eisert, and H. J. Briegel. Multiparty entanglement in graph states. *Phys. Rev. A*, 69:062311, 6 2004.
- [96] Robert Raussendorf and Hans J. Briegel. A One-Way Quantum Computer. *Physical Review Letters*, 86:5188–5191, 5 2001.
- [97] John M Lee. Smooth manifolds. In *Introduction to Smooth Manifolds*, pages 1–31. Springer, 2013.
- [98] Brian C Hall. *Quantum theory for mathematicians*, volume 267. Springer, 2013.